FINAL REPORT

submitted to the NASA Ames Research Center

for

NASA Cooperative Agreement NCC 2-446

Title of Project:

Analysis of Minerals Containing Dissolved Traces of the Fluid Phase Components "Water" and "Carbon Dioxide"

Friedemann Freund
Principal Investigator

SETI INSTITUTE
2035 Landings Dr.
Mountain View, CA 94043

Sept. 1991

Table of Contents

Chapter		Page
I.1	Summary Abstract	1
I.2	Introduction	1
I.3	Fundamental Questions Raised in this Project	2
II	Gases Released from Olivine by Impact Fracture	5
II.1	Abstract	5
II.2	Introduction	6
II.3	Experimental	7
II.4	Samples and Sample Preparation	8
II.5	Results: FEMS Experiments	9
II.6	SALI Experiments	11
II.7	FIMS Experiments	12
II.8	Discussion	14
II.9	Possible In Situ Contamination	14
II.10	Other Contamination Sources	15
II.11	Fluid Inclusions as a Source for some Emitted Gases	17
II.12	Dissolution Mechanisms of Fluid Phase Components	18
II.13	Gas Evolution from a Supersaturated System	19
II.14	C-N-O-H Precursors and C-N-O-H Molecules	21
II.15	The Role of the O^- States	23
II.16	Metal Vapor Emission	24
II.17	Acknowledgements	24
II.18	References	24
II.19	Legends	28
II.20	Figures 1–8	29

III	Charge Distribution Analysis of Magnesium Oxide	37
III.1	Abstract	37
III.1	Introduction	38
III.2	Identification of the Problem	39
III.3	Charge Distribution Analysis	44
III.4	Experimental	46
III.5	Results and Discussion	48
III.6	Conclusions	61
III.7	Acknowledgements	61
III.8	References	62
IV	O^- Charge Carriers in Magnesium Oxide	65
IV.1	Abstract	65
IV.2	Introduction	66
IV.3	Experimental	67
IV.4	Results and Discussion	69
IV.5	Infrared Spectroscopy of OH^- Impurities	69
IV.6	Identification of O^- by Magnetic Susceptibility	74
IV.7	Evidence for O^- from Electron Paramagnetic Resonance	76
IV.8	Emission of H_2 Molecules and O Atoms	80
IV.9	Conclusions	87
IV.10	Acknowledgements	89
VI.11	References	90

V	Peroxy in Olivine	93
V.1	Abstract	93
V.2	Introduction	94
V.3	Experimental	96
V.4	Results	98
V.5	Discussion	110
V.6	Acknowledgements	117
V.7	References	118
VI	List of Publications Describing Further Work Performed	121

I.1 Summary Abstract

Substantial progress has been made towards a better understanding of the dissolution of common gas/fluid phase components, notably H_2O and CO_2, in minerals. It has been shown that the dissolution mechanisms are significantly more complex than currently believed by the majority of researchers in the field. By judiciously combining various solid state analytical techniques convincing evidence has been obtained that traces of dissolved gas/fluid phase components undergo, at least in part, a redox conversion by which they split into reduced H_2 and reduced C on one hand and oxidized oxygen, O^-, on the other hand. Analysis for H_2 and C as well as for any organic molecules which may form during the process of co–segregation are still impeded by the omnipresent danger of extraneous contamination. However, the presence of O^-, an unusual oxidized form of oxygen, has been proven beyond reasonable doubt. The presence of O^- testifies to the fact that a redox reaction must have taken place in the solid state involving the dissolved traces of gas/fluid phase components. Detailed information about the techniques used and the results obtained are given in the individual chapters of this Final Report.

I.2 Introduction

The work to be performed under the NASA/SETI Cooperative Agreement NCC 2-446 was concerned with traces of dissolved gases such as H_2O, CO_2 and possibly N_2, in minerals.

H_2O, CO_2 and N_2 are present as gas phase or liquid phase components in all terrestrial magmatic and metamorphic environments where minerals crystallize from melts or recrystallize at high temperatures and pressures under near–equilibrium conditions. The same gas/fluid phase components are present on other rocky solar system bodies or were present during their formation. It can further be said that gases of the C–H–O–N system were prevalent in the solar nebula and therefore in touch with every solid matter which condensed prior to the formation of our planetary system. Finally, it can be said with a high degree of confidence that C–H–O–N gases dominate in the entire known universe wherever star formation processes occur amidst molecular clouds seeded with interstellar dust.

Before this universal background of gas–solid interaction the NCC 2-446 project addressed one fundamental question: How do the gas/fluid phase components H_2O, CO_2 and N_2 interact with solid minerals, in particular oxide and silicate minerals? The main objective of the Project was to improve our understanding of the dissolution mechanisms of these gas/fluid components in relation to possible reaction mechanisms leading to the formation of organic molecules.

In the case of H_2O there is general agreement among researchers that traces of H_2O always dissolve in the matrices of those minerals which crystallize or recrystallize in the presence of H_2O,

either as vapor or fluid. There is also general agreement that the H_2O dissolution mechanism entails the ubiquitous formation of OH^- anions associated with defect sites in the mineral matrices.

However, in the case of CO_2 there is no general agreement whether this common gas/fluid phase component dissolves in the minerals. This is despite the fact that, on the basis of thermodynamic laws, one is forced to expect that every gas, in particular every reactive gas, dissolves in every mineral that forms in their presence. A number of authors whose work will be commented upon below have maintained over the past years that CO_2 does not dissolve in minerals even if they crystallized or recrystallized under high CO_2 pressure. I have been embroiled in a long–standing discussion, even controversy, with those who negate any dissolution of CO_2 in such mineral matrices. One of the objectives of the NASA/SETI Cooperative Agreement NCC 2-446 project was to help clarify some of the fundamental issues involved in this controversy and, if possible, offer solutions which will lead to an unambiguous answer.

These objectives have been met, though along research lines not envisioned at the time of submission of the NASA/SETI Cooperative Agreement NCC 2-446. In the following section I shall briefly review the premisses which formed the basis of this Project. I shall not at this point engage in a detailed discussion which includes literature references to my own earlier work and to the work of others in the field. This detailed discussion is given in some of the papers which have either already been published or are submitted or are being now prepared for publication.

The body of this report consists of reprints, preprints and as yet unpublished manuscripts. There are arranged according to the subtopics which they address. For the sake of uniformity of presentation all sections are formatted in the same way, e.g. even in cases where printed papers are available their texts are included here in manuscript form. The appropriate references for identification are given in the headers of each section.

I.3 Outline of the Fundamental Questions Raised in this Project

The work to be performed under the NASA/SETI Cooperative Agreement NCC 2-446 relates to low–z element impurities, in particular H and C, in minerals which have grown in the presence of the common gases or fluids H_2O and CO_2. Contrary to widely held belief there were strong indications* that structurally dissolved gases, specifically H_2O and CO_2, in minerals undergo (at least in part) a redox conversion by which they split into reduced H_2 plus C and oxygen that is oxidized from the 2– to the 1– oxidation state. This redox conversion is independent of changing transition metal oxidation states but may be coupled to them in as yet to be determined ways. If generally true and applicable to a wide range of mineral phases, such a redox conversion would have far–reaching implications for many areas of scientific endeavor.

---

* From the P.I.'s earlier work as described in the enclosed reprints and preprints and from other researchers.

(i) Since any mineral dissolving gaseous components at high temperatures is likely to become supersaturated upon cooling, the diffusively mobile H_2 plus C are expected to segregate to the crystal surface, thereby producing conditions where solute H_2 would react with solute C to give organic molecules or precursors thereof.

(ii) After segregation of the reduced moieties H_2 and C the bulk of the minerals would still contain the oxidized oxygen as a "memory" of the redox conversion.

The interest of this work to NASA's Origin of Life program rests with the fact that the processes summarily described in (i)–(ii) represent an new and potentially important avenue towards the synthesis of organic molecules, in particular complex molecules. The hypothesis can be advanced that such processes might have played a role on the prebiotic Earth. As a result of tectonic and volcanic activities that have been a characteristic feature of the Earth since her earliest geologically recorded history huge amounts of minerals and rocks have passed through the global cycles: Rocks have solidified and crystallized at great depth, in the presence of the ubiquitous gas/fluid components H_2O and CO_2, and have been uplifted to the surface to be subjected to weathering. If these rocks released organic molecules as part of their weathering, they would have represented an untapped source of complex organic molecules.

The NCC 2-446 project started with an attempt to characterize step (i), e.g. the formation of organic molecules produced by the segregation of solute H_2 and solute C from within selected minerals. The work performed concentrated on single crystals of olivine, the dominant mineral phase in the upper mantle, ideally $(Mg,Fe)_2\ SiO_4$ with the Mg:Fe ratio approximately equal to the solar abundances. Since the upper mantle is a region where high temperatures and high pressures prevail — with CO_2 being the dominant fluid phase component followed by H_2O and other quantitatively less important gases — the choice seemed rational. However, the difficulties confronting the attempt of reliable analyses of solute H_2 and C are horrendous. Any laboratory study of organic molecules on mineral surfaces has to first demonstrate that these organic molecules are <u>not</u> the result of contamination by C–bearing gases from the environment. Given the omnipresence of C–bearing gases in natural and laboratory environments and given the extreme sensitivity with which the analyses for organic molecules have to be performed, it is a daunting task to establish proof beyond reasonable doubt of the absence of contamination. The only reasonable approach would be to prepare minerals in the presence of isotopically labelled gases, e.g. D_2O and $^{13}CO_2$, and then search specifically for isotopically labelled organic molecules. This task was not part of the NCC 2-446 project**.

In this Report I present as yet unpublished manuscripts describing experiments that were carried out as part of the NCC 2-446 project. The publication of the complex gas evolution observed upon impact fracture of mantle–derived olivine crystals (Chapter II) has been delayed due to objections raised by annonymous reviewers who seem to subscribe to the notion that the

** I have meanwhile submitted a Proposal to NASA's Life Science Division for carrying out such a new project.

postulated redox conversion of dissolved fluid phase components does not take place and that CO_2 does not dissolve in the solid state.

I have therefore turned to step (ii) outlined above: The search for oxygen in the unusual (higher) oxidation state 1–. The rationale was that, if oxidized oxygen can be shown to be present in minerals crystallized in an overall reducing H_2O/CO_2 atmosphere, this was by itself a valid proof for the above–mentioned redox conversion. Because of the fundamental nature of this reaction the effort was focussed on a structurally and chemically simple compound: Magnesium oxide. MgO crystals are available in high purity grades, e.g. transition metal free, grown by a process known as carbon arc fusion from a melt (at 2800°C) that is saturated with the highly reducing atmosphere of an electric carbon arc. According to fundamental thermodynamic laws such crystals should carry a "memory" of the viciously reducing conditions that prevailed during their synthesis. The least that one would expect to find in them is oxygen in an oxidized state, e.g. O^-, because such O^- is the hallmark of highly oxidizing synthesis conditions.

The major difficulty with respect to O^- (in contrast to O^{2-}) was that nobody had ever tried to search for this unusual oxidation state of oxygen, except in the context of radiation damage of solids. Prior to the project NCC 2-446 no technique was known which could be used for investigating O^- *in situ* in mineral matrices. Therefore I have embarked on an additional project to develop analytical tools to study O^-. This effort led to the discovery of a new physical technique now known as *Charge Distribution Analysis*. CDA takes advantage of the fact that the O^- represent mobile electric charge carriers, so–called positive holes, which occupy shallow acceptor levels near the valence band of wide band gap insulators. In essence, CDA consists of measuring contact–free the dielectric response in an electric field gradient at the limit of 0 Hertz. Since its inception in 1989 CDA has proven to be an extremely valuable and versatile technique. It has been thoroughly tested and demonstrated its applicability in a detailed study of MgO single crystals. CDA has been applied to a variety of materials, synthetic and natural, single crystalline, polycrystalline and glassy, as is documented in the collection of reprints and preprints which are assembled at the end of this Report.

I have also pursued another diagnostic property of the O^-, namely the fact that O^- is paramagnetic (while O^{2-} is diamagnetic). By measuring the anomalous paramagnetism associated with the formation of O^- in transition metal free MgO single crystals the conclusions drawn from the CDA data have been substantiated. It can safely be stated that the presence of O^- in carbon arc fusion grown MgO single crystals has now been established by two fully independent physical techniques of which one, the paramagnetic measurements, gives a unique response which cannot be otherwise interpreted. In this sense the existence of O^- in the crystals under study has been unambiguously proven. Thus, returning to the above two premisses, it can be firmly stated that with (ii) proven to hold, (i) must also be true.

Chapter III–V of this Report consist of a three–part manuscript submitted to the Journal of Geophysical Research but not yet available in the open literature.

GASES RELEASED FROM OLIVINE BY IMPACT FRACTURE

Friedemann Freund*, Sherwood Chang*, J. Thomas Dickinson**,

and Minoru M. Freund***

* NASA Ames Research Center, MS 239-4, Moffett Field, CA 94035

** Dept. of Physics, Washington State University, Pullman, WA 99164

*** SETI Institute, Los Altos, CA 94022;
now at: Dept. of Physics, University of California, Berkeley, CA 94120

Abstract

Mantle-derived olivine crystals from San Carlos, AZ, USA, were fractured and the gas emission was monitored by three techniques: fracto-emission mass spectroscopy (FEMS), surface analysis by laser ionization (SALI) and field ionization mass spectrometry (FIMS). The spontaneous emission of neutrals, measured for 1.5 sec after fracture, includes H_2, H_2O, CO/N_2 and CO_2, organic molecules producing fragments at 63, 65, 77, 91 and 105 amu plus Mg vapor at 24 amu. The emission of H_2O and CO_2 is often less intense than that of complex organic molecules. After fracture in air, followed by introduction into UHV and heating to 500°C, the crystals continue to release complex C-H, C-O-H and probably C-N-O-H molecules. The following compounds have been tentatively identified: benzene, toluene, benzaldehyde/xylene, naphthalene/azulene, biphenylene, fluorene, diphenylmethane, phenanthrene/anthracene, pyrene, chrysene, perylene/ benzopyrene, coronene, benzopyrelene/dibenzopyrene. Contamination from external sources is unlikely. The results are interpreted assuming that, under upper mantle conditions, the fluid phase components H_2O, CO/N_2 and CO_2 enter into dilute solid solution with olivine, forming H_2 and reduced C- and/or N-bearing solute entities besides oxidized (peroxy) entities. Supersaturation during cooling and decompression leads to preferrential segregation of reduced solutes (H_2,C and N) to dislocations, subgrain boundaries etc. The observed organic molecules are believed to derive from precursor entities formed at those segregation sites with preformed C-C, C-H and possibly C-N bonds, including aromatic and polyaromatic precursors. Oxygen is consumed at the fracture surface for forming $H_2O/CO_2/O_2$ through oxidative reactions which involve O^- states. Mg^{2+} cations which become coordinatively unsaturated are converted to Mg^0 and lead to the observed Mg vapor emission.

Introduction

The fluid phase in the upper mantle is part of the geodynamic cycle of volatiles. It is best described as C-N-O-H system with minor additions of sulfur and halides (e.g. Burnham 1979; Eggler and Baker 1982). The major component is CO_2 with H_2O a distant second and occasional N_2, plus CO and CH_4 (Wyllie 1978; Arculus et al. 1984; Bergman and Dubessy 1984). The amonunt of N_2 remains uncertain and may be as low as 1 ppm as measured by fusion extraction (Becker and Clayton 1977; Sakai et al. 1984) or as high as ≈20 ppm as measured by neutron activation analysis (Norris and Schaefer 1982).

Besides filling the intergranular space the fluid phase components may be consumed to form carbonates, hydrous minerals such as micas, amphiboles, humite minerals and possibly brucite. Nitride or oxynitride minerals have not yet been reported.

C-N-O-H compounds also occur in fluid inclusions which are held to represent samples of the free fluid phase trapped in microcracks during deformation and subsequent healing (Roedder 1972, 1984; Murck 1978; Bergman and Dubessy 1984).

A third possibility to store C-N-O-H in the mantle is by forming solid solutions. Evidence for solid solution with H_2O is provided by the ubiquitous occurrence of OH^- in olivine (Wilkins and Sabine 1973; Beran and Putnis 1983; Freund and Oberheuser 1986; Miller et al. 1987) and other nominally anhydrous minerals. The characteristic infrared (IR) absorption bands of OH^- lie in a spectral region where silicate minerals have little or no intrinsic absorption. Hence, they are easily detected.

CO_2-related solute species are more difficult to ascertain spectroscopically. such as carbonate anions, CO_3^{2-}, are more difficult to ascertain. Different C-bearing oxyanion complexes, unknown from bulk minerals, must also be considered. Yet, the possibility of solid solution formation between CO/CO_2 and olivine has been questioned (Mathez et al. 1984; Tsong et al. 1985; Mathez 1987), while in quenched high pressure silicate glasses carbonate anions are believed to exist besides molecular CO_2 (Mysen and Virgo 1980; Fine and Stolper 1985).

Unfortunately most techniques by which carbon in minerals may be analyzed such as photoelectron spectroscopy and secondary ion mass spectroscopy are very sensitive to surface contamination (Oberheuser et al. 1983; Tsong et al. 1985; Freund 1986). Also the $^{12}C(d,p)^{13}C$ nuclear reaction, a less contamination-sensitive technique (Wengeler et al. 1982; Oberheuser et al. 1983), has been critisized (Tsong et al. 1985; Mathez 1987). Shevabreyeva et al. (1987) used a combination of two nuclear reaction, $^{12}C(d,p)^{13}C$ and $^{12}C(d,n)^{13}N$, of which the latter is a bulk technique, and concluded that carbon exists in olivine at the level of several hundred ppm as reported earlier by Oberheuser et al. (1983).

In the present study we pursue our quest for methods and techniques which enable us to obtain more information about fluid phase components in olivine. The method of choice is the on-line measurement of gases and vapors released upon impact fracture in ultrahigh vacuum and during subsequent heating.

Dickinson et al. (1982, 1985) showed that fracture of brittle materials is accompanied by the emission of electrons, of ions, of excited and neutral atoms or molecules, and of electromagnetic radiation from ultraviolet to radio frequencies. Some emissions occur only during crack formation and decay rapidly. Others last longer or be delayed.

Experimental

Three separate experiments were performed: (i) Fracto-Emission Mass Spectrometry (FEMS), (ii) Surface Analysis by Laser Ionization (SALI), and (iii) Field Ionization Mass Spectroscopy (FIMS).

FEMS involves the measurement of the gas emission upon fracturing a single crystal as shown schematically in **Fig. 1** and as described by Dickinson et al. (1986). The crystal was located 12 mm in front of the ionizer (70V) of a fast-scanning UTI 100C quadrupole mass spectrometer. The span of the three point bend fracture device was 2.5 mm. The signal output was digitized at a rate of 100 μsec per channel with a LeCroy Data Acquisition System. Fracture was induced by a stainless steel wedge (0.75 mm radius) advancing at ≈10 cm/sec. The moment of fracture was determined by an acoustic transducer which triggered the data acquisition system. The total pressure change was monitored by a Bayard-Alpert gauge, positioned ≈20 cm from the sample with a 20 msec electronic response time. In most runs the MS was operated in the scanning mode covering a preselected range of atom mass units (1-110 amu) at a rate of 80 msec/scan. While the fracture lasted typically ≈10 μsec, the last residual gas spectrum prior to fracture and the gas emission after fracture were recorded over ≈1.6 sec. Some runs were done in the single mass mode to follow the evolution of one specific gas species with higher time resolution.

The stainless steel ultrahigh vacuum (UHV) system was pumped with a magnetically suspended 400 l/sec turbomolecular pump and a He cryopump giving background pressures in the low 10^{-8} torr range. Simulated runs with no sample in the fracture device were performed to test to what extent the motion of the bellow and mechanical shock led to the release of gases. The observed gas emission was weak and comprised only gases which were already seen in the residual gas spectrum.

The SALI technique has been described by Becker and Gillen (1984). It uses a high intensity (10^8-10^9 W/cm^2) ultraviolet (193 nm) pulsed (20 nsec) eximer laser beam for ionization of gas molecules (except H_2, H_2O, CO, CO_2, N_2 and a few others) by non-resonant multiphoton

processes in conjunction with a time-of-flight mass spectrometer for analysis. The base pressure in the UHV system was in the 10^{-9} torr range. The samples, freshly fractured fragments of 2-4 mm size, were mounted on a heatable carrier plate. The gases analyzed freely evaporated from the sample surface either at RT or upon heating. The ionizing laser pulses intersected the gas ≈1mm above the sample surface. Depending on the signal strength the data were collected and averaged over 100-200 or more laser pulses.

FIMS is a "soft" ionization technique. It uses the steep electric field gradient at the tip of carbon whiskers generated by 5000 V to field-ionize the gases which emate from a sample contained in a heatable fused silica sample tube. Organic compounds are ionized. The mass spectrometer, a 60° magnetic sector instrument (resolution 1300), was pumped with diffusion pumps to a vacuum in the 10^{-6} torr range.

While FEMS 70 V electron beam ionization and SALI laser multiphoton ionization result in strong fragmentation of the gas molecules analyzed, making the assignment of the observed mass fragments to specific molecules difficult, the "soft" field ionization in the FIMS experiments produces mostly parent molecule ions which renders the assignment relatively easy.

Samples and Sample Preparation

The olivine single crystals used in this study came from the San Carlos Indian Reservation, Arizona, USA. They were rounded, 5-20 mm, dull green and optically slightly turbid. Thin sections show a polygonized substructure of slightly misoriented subgrains separated by dislocation walls, probably formed during mechanical deformation in the mantle (Kohlstedt and Goetze 1974; Poirier 1985). Some crystals showed µm-sized veins, filled with fine-grained material, presumably of metasomatic origin (Lloyd 1987). Though some crystals may have contained fluid inclusions, our fracture experiments rarely produced pressure bursts signaling the cracking of gas-filled inclusions.

The olivine crystals fractured softly, even when visually crack-free. This softness contrasts with the usual brittleness of olivine and is probably due to its pronounced domain substructure. Scanning electron microscope examination reveales steps and terraces which appear to indicate subgrain boundaries along which the fracture would preferrentially occur. Fractures may have also occasionally followed cracks containing alteration products. The observations reported below are typical of a fracture behavior which creates fresh fracture surfaces presumably cutting through intact crystal volume.

For FEMS olivine crystals of the appropriate size were cut in halves with a diamond saw, mounted with acetone-soluble resin and ground under water to 1-2 mm thickness. The unpolished slices were removed from the support, cleaned ultrasonically in acetone and H_2CCl_2 or $H_3C_2Cl_3$,

degassed in vacuum ($\approx 10^{-6}$ torr) at RT for 8-12 hrs. Thereafter they were spring-loaded in batches of 20 into the sample carousel and re-evacuated ($<10^{-8}$ torr) for several hours prior to fracturing.

FEMS was tested extensively using different materials, including glass microscope slides, high purity fused silica and synthetic MgO single crystals (Dickinson et al., 1986, 1987). Blank runs with fused silica (Hereaus-Amersil Suprasil™) produced a short-lived gas pulse during fracture and a slight increase of the mass 28 (CO/N_2). No other gases were observed.

For SALI selected olivine crystals were ultrasonically cleaned with hot water, acetone and H_2CCl_2 and rapidly dried. The crystals were crushed in air. 2-4 mm sized pieces were hand-picked with stainless steel tweezers, mounted beneath a fine W mesh or a stainless steel washer on a heatable plate and introduced into the UHV (10^{-9} torr range) within 2-4 min. The gas evolution was monitored at ambient temperature and during heating to 450°C. Procedural blanks with fused silica and pyrex glass showed no gas emission.

For FIMS selected olivine crystals were ultrasonically cleaned in water, acetone and H_2CCl_2, dried and gently crushed in air in an alumina mortar under a laminar flow hood. The coarse powder (40-80 mg) was loaded into the fused silica capillary sample tube, evacuated for 30 min at 50°C to the 10^{-5} torr range and then heated linearily at 6°C/min to 500°C. The mass data (24-500 amu) were averaged over 4 min intervals.

Results: FEMS Experiments

Fig. 2 shows typical examples of the gas emission from olivine fracture (**a**) five consecutive 80 msec scans covering the first 320 msec out of the total 1.6 sec duration of the experiment and (**b**) six scans of which the first three are consecutive and the remaining three spaced in time. In both cases scans (1) show the residual gas spectrum just before fracture, dominated by H_2, H_2O, CO/N_2 and CO_2. Scans (2) contain the fracture near 60 amu followed by emission at 63, 65, 77, 91 and 105 amu ranging from moderate (**a**) to very strong (**b**). Scan (3) in **Fig. 2a** shows off-scale intensities for 18 amu (H_2O), 24 amu, and 44 amu (CO_2) and nearly off-scale intensity for 28 amu (CO/N_2). Intensities for H_2O, CO/N_2, CO_2 and the signal at 24 amu continue to increase in scans (4) and (5). In **Fig. 2a** the H_2 evolution reaches a maximum in scan (4), decaying slowly thereafter. The run shown in **Fig. 2b** is characterized by a shorter pulse of the H_2 emission and remarkably strong emission at 77, 91 and 105 amu remaining clearly detectable after >1 sec.

Other strong peaks lie at 27, 29, 39, 41, 51 amu. Together with the 63, 65, 77, 91 and 105 amu peaks and others with lesser intensities they generally fit 12, 13 or 14 amu increment sequences, suggesting that these peaks represent fragments of series of complex hydrocarbons. Fragments of chlorinated hydrocarbons were never detected, indicating that no solvent had remained after the pre-experiment evacuation procedure.

Fig. 3 shows another typical FEMS run, $3 \cdot 10^{-8}$ torr full scale, with the intensity data plotted on a logarithmic scale. Fracture occurred just before 60 amu causing a initial, intensive burst of ions, atoms and molecules. After the initial burst has decayed masses 65, 77, 91 and 105 amu are seen to go off scale within <32 msec of the fracture. In the following scan, 40-112 msec after fracture, the intensity at 2 amu (H_2) is up by a factor of nearly ten, the intensities at 18 amu (H_2O), and 51 amu are off scale. Surprisingly the peaks at 28 and 44 amu (CO/N_2 and CO_2 respectively) remain of moderate intensity, indicating little CO/N_2 and CO_2. In fact the amount of CO/CO_2 released in this experiment is less than that of the complex hydrocarbons. Prominent peaks lie at 63, 65, 77, 79, 91 and 105 amu. The remaining scans in **Fig. 3** cover the time interval 120-192 msec and 200-272 msec after fracture. While all peaks decrease in intensity, including those for CO/N_2 and CO_2, the intensity of the H_2 emission increases. Also the 24 amu intensity increases, while that of the 56 amu species decreases slowly. Numerous other peaks, in particular those 63, 65, 77, 91 and 105 amu, remain relatively strong up to ≈1 sec after fracture.

Occasionally intense pressure bursts were observed which shut-off of the ionization source. Such pressure bursts are caused by fluid inclusions. Most of our samples, however, yielded spectra which ressembled those shown in **Figs. 2/3** with sizeable but not excessively large amounts of H_2/H_2O and $N_2/CO/CO_2$ and fragments of complex organic molecules. More often than not the emission intensities of some organic fragments, in particular at 77, 91 and 105 amu, equalled or exceded the intensities of the common gases.

Little intensity was observed beyond 105 amu. This suggests that the cut-off occurs around this molecular weight. One experiment was performed at elevated temperature, at ≈50°C, using the radiation of the ionization filament as a heat source. In this run the range of gases emitted extended to ≈150 amu.

In most experiments the intensity at 24 amu was strong and increased with time, typically for 100-300 msec. This behavior ressembles the 24 amu emission from MgO observed with 100 μsec resolution. The 24 amu emission from MgO increased with time up to after ≈300 msec when it suddenly stopped (Dickinson et al. 1986). The 25 and 26 amu emissions followed the same kinetics. It was concluded that the 24/25/26 amu emission arises from Mg atoms, e.g. ^{25}Mg, ^{25}Mg and ^{26}Mg isotopes, vaporizing from the fracture surface. Though we have not yet performed dedicated olivine fracture experiments with μsec time resolution, the 24 amu emission from olivine depicted in **Figs.2/3** appears also be due to Mg atoms. This assignment is supported by a qualitative assessment (at 80 msec time resolution) of the 25 and 26 amu emission.

Another outstanding mass peak shown in **Figs. 2/3** is that at 56 amu: it often appears with medium intensity, is strongest immediately after fracture and decreases with time. Whether it is due to Fe emission requires confirmation by further experiments.

Occasionally we noticed an enhanced emission at 32 amu, suggesting O_2. In the case of MgO fracture an O_2 emission was unequivocally established. This was surprising because the MgO

crystals had been grown under extremely reducing conditions of a carbon arc (Dickinson et al. 1987). In the case of olivine the O_2 emission is still uncertain, mostly because fragments from many different molecules occur in the low mass range.

From the pressure rise of the Bayard-Alpert gauge and the known volume of the UHV system the total amount of non-condensable gases released at a typical FEMS fracture experiment was estimated to be of the order of 10^{15}-10^{16} molecules/cm^2, equivalent to 1-10 monolayers assuming a smooth fracture surface. Complex "organic" molecules account for a substantial fraction of the total of emitted gases.

SALI Experiments

The purpose of the SALI experiments was to test whether the same gases observed upon impact fracture in UHV can also be observed when the olivine crystal was fractured in air and then introduced into the UHV system. Since nonresonant multiphoton ionization is $\approx 10^4$ more effective than the 70 eV electron ionization used in the FEMS experiments, the high SALI sensitivity allows for the detection of low partial pressures.

Fig. 4 a/b shows the gases detected by SALI from an olivine single crystal fragment prepared and introduced into the UHV system as described above. The SALI spectrum displays many of the same mass peaks which were observed in the FEMS experiments, e.g. at 105, 91, 77, 65, 63 and 51 amu.

The fact that mass peaks 105, 91, 77, 65, 63, 51 etc. are observed in the SALI experiments, e.g. after cleaving the olivine crystal in air and exposure to air for as long as $\approx$4 min, indicates that the compounds which produce these mass peaks are not adversely affected by short exposure to air. On the other hand certain peaks observed in FEMS experiments will obviously not appear in SALI spectra, in particular those due to Mg vapor, e.g. at 24 amu for Mg^+. The strong peak at 24 amu in **Fig. 4a** is not due to Mg^+ but to the C_2^+ fragment which forms when hydrocarbons are ionized by multiphoton ionization. Note that the complete series of skeleton C_n^+ ions, $1<n>6$, can be clearly seen in **Fig. 4a** with peaks at 12, 24, 36, 48, 60 and 72 amu.

Fig. 4b shows the mass range above 110 amu. Many peaks are detected up to $\approx$400 amu, documenting the high sensitivity of the SALI technique. The progression is generally by 13 amu, suggesting the addition and/or removal of CH units. There also seems to be a progression by 50 amu, indicating polycondensed aromatic rings. If the peak at 78 is due to benzene, C_6H_6, then the 128 amu peak could be due to naphthalene and/or azulene, $C_{10}H_8$, and the178 amu peak to anthracene and/or phenanthrene, $C_{14}H_{10}$.

At RT the intensities decrease slowly as a function of time. For instance, if the intensity of the 105 amu peak was 2600 relative units $\approx$1.5 min after introduction into the UHV sample chamber (5-6

min after fracture), it dropped to 1600 and 740 after ≈5 and ≈20 min, respectively. Upon heating the intensities increase, passing through a maximum and decay. The integrated intensities of all "organic" compounds released during heating is estimated to be of the order of 10^{15} cm^{-2} corresponding to approximately one monolayer (Becker et al. 1986).

Fig. 5a compares the intensity of the 105 peak with that of the 106 peak during heating to 360°C: both masses exhibit the same "thermal profile", suggesting that they are related to the same parent molecule. **Fig. 5b** compares the "thermal profiles" of 91, 105 and 165 amu. The 91 amu species is a dominant fragment of toluene, $C_6H_5CH_3$, and a fragment of xylenes, of other benzene derivatives as well as dienes. Since there is no apparant correlation between 91 and 105, 91 appears not to be a fragment of the same compound that produces 105. The thermal profile of mass 91 follows that of mass 165 indicating that 91 is a fragment of or chemically related to 165.

Figs. 5c and **5d** show that 39, 63 and 65 follow the "thermal profile" of 91. By contrast 27, 50 and 51 amu behave differently. Since the peaks at 26 and 27 amu are most like due to the diagnostic N-bearing fragments CN^+ and HCN^+, their correlation with species at 50 and 51 amu suggests that the latter two also arise from N-bearing compounds, possibly nitriles.

Pyrex and fused silica procedural blanks did not produce any detectable gas emission. A fresh fragments of a gem-quality olivine single crystal which we included in our SALI study produced faint signals of some of the higher mass fragments as observed before. The observation indicates that the gem-quality olivine may emit minute traces of the same complex organic molecules as the optically slightly turbid crystals. At the same time the essentially "negative" result with the gem-quality olivine shows that cleavage of the crystal in air and its exposure to the laboratory environment did not lead to the contamination of the olivine surface with organic compounds from the laboratory air. It thus confirms that the strong gas emission from the other set of olivine crystals is genuine.

FIMS Experiments

Fig. 6 shows the sum of the intensities of all mass peaks from 40 to 500 amu accumulated from the 80 mg powder sample between 50-500°C. The four most intensive peaks occur at 302, 43, 106 and 128 amu.

Since FIMS produces predominantly parent molecule ions, an assignment of the observed peaks is much easier than by the other two techniques: many mass peaks can be identified as aromatics. At the same time we note that mass peaks which were strong in the FEMS and SALI experiments are often shifted by one amu to higher values. For instance instead of 105 amu one observes a strong 106 amu peak.

If 106 amu represents a parent molecule ion, it may be benzaldehyde, C_6H_5CHO, or any xylene, $C_6H_4(CH_3)_2$. The choice is narrowed by considering the intensities of toluene, $C_6H_5CH_3$ at 92 amu which is closely related chemically. The accumulated intensity at 92 amu is low. Therefore it is unlikely that the main contribution to 106 amu comes from xylene, $C_6H_4(CH_3)_2$. Thus the106 amu peak is probably due to benzaldehyde.

The "thermal profile" of 107 amu is different from that of 106 amu, indicating that the parent molecule at 107 amu belongs to a different group. It may represent a pyridine derivative substituting N for CH in the aromatic ring.

Other peaks in **Fig. 6** which can be assigned to likely parent molecules are: 78: benzene, 128: naphthalene or azulene, 152: biphenylene, 166: fluorene, 168: diphenylmethane, 178: phenanthrene and anthracene, 202: pyrene, 228: chrysene, 252: perylene or benzopyrene, 300: coronene, 302: benzopyrelene or dibenzopyrene, 350: benzocoronene.

Fig. 7 shows selected FIMS thermal profiles. Some thermal profiles are quite similar indicating that they belong to compounds which are chemically related such as the series 84, 98, 112 (not shown in Fig. 7) and 126. Each is separated from the next one by 14 amu, suggesting the addition of CH_2 units. They rise slowly and reach maximum intensity at or above 300°C. Compound 106 amu (probably benzaldehyde) appears first with its maximum intensity between 150-200°C, followed by the 302 amu compound (benzopyrelene or dibenzopyrene) which passes through a maximum around 200°C.

For a simple distillation process lower molecular weight compounds are expected to appear first during heating, e.g. at lower temperatures. Benzene at 78 amu is observed only at high temperatures, >400°C, with increasing intensity. This suggests that benzene is predominantly a pyrolysis product.

Fig. 7 provides further information about the parentage of the 106 amu compound. Its intensity reaches a maximum around 180°C but displays a second maximum at 450°C. This latter maximum coincides with a maximum for toluene (92 amu) and the increasing intensity of benzene (78 amu). It is tempting to suggest that, while the lower T maximum of 106 amu is probably due to benzaldehyde as indicated above, the higher T maximum may due to xylene pyrolizing to toluene and benzene.

Discussion

The sustained emission of gas molecules during and after impact fracture of mantle-derived olivine as measured by FEMS suggests that the olivine crystals contain gaseous components. The gases include common constituents of the C-N-O-H mantle fluids such as H_2, H_2O, CO/N_2 and CO_2 but also "organic" C-N-O-H gases in the mass range up to ≈110 amu. The emission intensity of

the "organic" compounds often equals or exceeds those of the simple stable gases. Furthermore the FEMS experiments show emission at 24 amu which is probably due to Mg vapor.

According to the SALI experiments the complex C-N-O-H gases continue to be emitted for relatively long time after the crystals were fractured in air and exposed to air for a few minutes. The emission is enhanced by heating, giving rise to distinct "heating profiles". With the high sensitivity afforded by SALI the mass range could be extended to ≈250 amu. There are indications that some of the complex "organic" molecules are N-bearing.

The FIMS experiments finally extend the mass range of the evolved C-N-O-H gases beyond 300 amu and provide clues as to their chemical identity. They suggest that many of the emitted gases are polyaromatic hydrocarbons.

Possible *In Situ* Contamination

The FEMS experiments are designed to minimize, if not exclude, *in situ* contamination of the fresh fracture surface from the residual gas. From the residual gas spectra we know that the UHV system did not contain any of the "organic" molecules observed after fracture, down to a level $\ll 10^{-9}$ torr (see scan 1 in **Fig. 2**).

Because the FEMS data are collected rapidly during and after fracture, within <1.5 sec, residual gas molecues cannot adsorb onto the fresh surface. Gas kinetic theory gives the number of gas molecules which collide with a surface per unit time at a given gas pressure. Even if we assume that each colliding molecule becomes chemisorbed, at $\approx 10^{-9}$ torr their number is so small that it would take ≈1000 sec to form one monolayer. For any potential contaminant at a partial pressure of $\ll 10^{-9}$ torr to form a monolayer would require »1000 sec. Therefore the maximum contamination from the residual gas is $>10^{-3}$ monolayer

This is corraborated by the absence of any noticeable C-N-O-H emission during procedural blank runs and earlier work with MgO (Dickinson et al. 1986, 1987). The procedural SALI blank runs have additionally demonstrated beyond reasonable doubt that the observed C-N-O-H molecules are <u>not</u> contaminants from the ambient laboratory air, adsorbed after fracturing.

Next we address the question whether "organic" C-N-O-H molecules could be synthesized on the fresh fracture by surface-catalyzed Fischer-Tropsch reactions from H_2, CO (and NH_3), if these gases exist in the olivine crystals under study. We have noted above that 1-10 monolayers of "organic" molecules are estimated to be emitted in a typical FEMS experiment. For a surface-catalyzed reaction to produce that much gas within μsec to msec at RT the reactants must first become adsorbed on the surface. Even if H_2 and CO (and NH_3) had been abundantly available in fluid inclusions (for which there is no evidence), before these gas molecules become catalytically reactive they must "stick" to the surface. Barker and Torkelson (1975) have demonstrated that

freshly broken quartz and basalt surfaces, when exposed for several minutes to gases such as CH_4, CO and CO_2 at pressures of several torr, will adsorb only a fraction of a monolayer. Hence, it appears unlikely that Fischer-Tropsch synthesis could produce the observed "organic" molecules under the FEMS conditions, e.g. on a μsec to msec time scale.

Other Contamination Sources

If the "organic" molecules are not products of *in situ* contamination nor synthesis, where, when and how were they introduced into the olivine crystals under study?

The three possibilities are: the organics were formed or acquired either (i) in the mantle, (ii) during ascent with the volcanic magma, or (iii) after emplacement at the surface of the earth.

(i) Fluid inclusions in mantle-derived minerals are generally believed to represent samples of mantle fluids trapped by microcrack formation and subsequent healing (e.g. Roedder 1984). Fluid inclusion studies show CO_2 to be the most abundant component in olivines, generally far in excess of H_2O and only occasionally accompanied by minor components such as CO, SO_2, COS, H_2S, H_2, CH_4 and N_2 (Roedder, 1965; Murck et al., 1978; Bergman and Dubessy, 1984). NH_3 and complex C-H, C-O-H or C-N-O-H molecules have never been reported except for traces of C_2H_4 and C_2H_6 in some mantle-derived chromites (Johan et al., 1983) and light to medium molecular weight hydrocarbons in minerals from a highly alkaline felsic intrusion (Konnerup-Madsen et al. 1979).

(ii) Next we consider the possibility that "organic" molecules were introduced into the olivine crystals during ascent. Mathez et al. (1984) and Mathez (1987) hypothesize that volcanic C-N-O-H fluids penetrate into the olivine crystals along microcracks and become catalytically reduced to carbon which could develop "organic" compounds upon further reactions.

Though no mechanisms have been proposed by which volcanic fluids can be catalytically reduced on olivine surfaces, we concede that reactions by some as yet unknown mechanism may not be entirely ruled out. If they occur, the resulting "organic" molecules would line the walls of existing microcracks.

Infrared spectroscopy (IR) is a sensitive probe for the detection of C-H in olivine which is intrinsically transparent around 3000 cm^{-1}. **Fig. 8** shows the IR spectrum between 3500 - 2000 cm^{-1} of a 6.7 mm thick San Carlos olivine crystal from the same batch of crystals which produced the rich suite of complex "organic" molecules on which report in this paper. Except for a slight ondulation of the background no IR absorption band is detected between 2800-3100 cm^{-1}, the range of the C-H stretching vibrations. This contrasts with MgO single crystals synthetically grown in a slightly moist electric carbon arc atmosphere where a n_{C-H} band was clearly observable consisting of two broad absorption maxima (Freund and Wengeler 1982). The MgO crystals

emitted CH_4 plus several simple hydrocarbons upon fracture (Dickinson et al. 1986). However, this broad IR double band is unlike any band molecular CH_4 and other simple hydrocarbons would generate if trapped in microcracks.

The FEMS and FIMS observations provide yet another argument against organic contaminants in microcracks: when olivine crystals break which contain microcracks, the fracture will preferentially propagate along such cracks. Any "organic" compounds contained therein would become exposed and susceptible to evaporation/distillation. For homologous series such as the polyaromatic hydrocarbons the rate of evaporation will depend on the relative vapor pressures which decrease with increasing molecular weights. Therefore we should see a characteristic time dependence of the emission intensities after fracture and characteristic "thermal profiles".

Within the 80 msec time resolution achieved by FEMS in the scan mode we observe no correlation between the masses of the higher molecular weight fragments, in particular 105, 91, 77 etc. and their emission rates (see **Figs. 2/3**) suggesting that their respective parent molecules do not simply distill off the surface. The FIMS experiments provide additional support: the 302 amu compound, presumably dibenzopyrene, evolves below 200°C, while the 252 amu compound, presumably benzopyrene, comes between 280-380°C and pyrene (202 amu) peaks only at 380°C. Another sequence of molecules with 365-368 amu (not shown in **Fig. 7**) is released at still lower temperatures, around 150°C. Thus the thermal emission of the complex C-N-O-H compounds appears not to be obey the simple law of distillation.

We therefore conclude that contamination by volcanic C-N-O-H fluids which penetrated microcracks and bacame catalytically reduced by some as yet unknown mechanism, can be reasonably ruled out as the source of the observed emission of "organic" molecules during and after fracture.

(iii) Next we consider contamination acquired at the surface of the earth, primarily biogenic contamination.

Obviously, the olivine crystals under study have been exposed for long time to environmental contaminants. Subgrain boundaries formed by dislocation arrays (Poirier 1985) are probably not wide enough for large biogenic molecules to enter. If biogenic contaminants diffused into microcracks and resided therein, their contribution to the observed gas emission can be ruled out on the basis of the same arguments as discussed above under (i) and (ii). Absence of biogenic contamination is also indicated by the paucity of the masses observed such as 302, 106/105, 92/91, 78/77 etc. Typical gas evolution and pyrolysis FIMS patterns of samples with known biogenic contaminants or kerogens tend to be much richer (Becker et al., 1986). Thus we conclude that environmental biogenic contamination is also an improbably source for the "organic" molecules emitted from the olivine crystals under study.

Fluid Inclusions as a Source for some Emitted Gases

We noted in our FEMS experiments that H_2, H_2O, CO/N_2 and CO_2 were generally released over relatively long time, often increasing over ≈200 msec before decaying (see **Fig. 2a**). Such a behavior is contrary to what one would expect, if gases were released from gas/fluid inclusions dissected by the fracture plane. If gas-filled cavities are broken open, the gas volume becomes liberated at once, typically within <10 μsec. The gases then freely expand and reach the ionizer which is located 12 mm away within ≈10 μsec. The gas pulses will dissipate quickly, due to the large volume of the UHV system and to the powerful pumps. On the basis of experience gathered during the FEMS study of cloudy MgO crystals which contain minute cavities (Dickinson et al. 1987), pressure pulses generated by microscopic fluid inclusions will not last longer than ≈30 msec.

The FEMS emission of H_2, CO/N_2 and CO_2 for periods of >100 msec point at a sustained gas supply from within. One possibility is that the gases seep out of a "leaky" reservoir of fluid inclusions connected to the fracture surface by diffusion channels. Though this is broadly in line with the fact that fluid inclusions are preferentially located on healed microcracks which may act as diffusion conduits (Roedder 1984), it also requires that the fluid inclusions lie just far enough beneath the surface to give the observed release kinetics. Our observations do not bear out the prevalence of such special conditions.

Dissolution Mechanisms of Fluid Phase Components

Next we address solid solution formation between C-N-O-H fluid phase components and olivine.

In the system $MgO\text{-}SiO_2\text{-}H_2O$ to which olivine belongs by its Mg-rich end member forsterite, the occurrence of OH^- anions is not limited to regular OH^--bearing phases such brucite, $Mg(OH)_2$, serpentine, $Mg_3[(OH)_4|Si_2O_5]$, talc, $Mg_2[(OH)_2|Si_4O_{10}]$, etc. H_2O also dissolves in the nominally anhydrous phases such as olivine. Together with an appropriate number of cation vacancies the OH^- anions become a part of the structure though their exact location and environment are still disputed (Beran and Putnis 1983; Freund and Oberheuser 1986; Miller et al. 1987).

CO_2 depresses silicate melting points and changes phase relations in multiphase systems in much the same way as H_2O, though the pressures required are higher (e.g. Burnham 1979). The melting point depression is commonly explained by CO_2 dissolution in the liquid, either in form of CO_2 molecules or as carbonate anions, CO_3^{2-} (Mysen and Virgo 1980; Bergman and Spera 1984; Fine and Stolper 1985). The idea that CO_2 may also form a solid solution with olivine first presented by Green and Radcliffe (1975) has been rejected by Mathez et al. (1984) and Mathez (1987).

This rejection cannot be upheld on the basis of fundamental rules of solid solution formation. Any olivine which crystallizes in the system (Mg,Fe)O- SiO_2-CO_2 must be non-stoichiometric and must contain at least a trace of structurally incorporated CO/CO_2 component. Since carbon is a low-z element as a solute it is expected to form oxyanion complexes such as carbonate anions, CO_3^{2-}. Other C-bearing oxyanions, however, cannot be excluded.

Nitrogen which is also a fluid phase component in the upper mantle is generally considered as chemically inert occurring only in the form of N_2, unless NH_4^+ substitutes for K^+ in micas (Hallam and Eugster 1976). Fundamentally, however, nitrogen must also be able to enter into solid solution as the ceramic system Si_3N_4-Si_2N_2O-Mg_2SiO_4 (Hendry et al. 1975; Lange 1979).

In other words, mantle-derived olivines may also contain dissolved nitrogen either as N_2 or in the form of N-bearing oxyanions. Low levels of N have been reported in SiO_2, possibly in form of NO_2^- oxyanions which would be isoelectronic with CO_2^{2-} (Stathis and Kastner 1984). Knobel (1983) and Knobel et al. (1984) reported on N in synthetic MgO and natural olivine. Fusion of basaltic glass and extraction of nitrogen as N_2 gave values in the range of 1 ppm (Becker and Clayton 1977). Exley et al. (1987) found 0.2 - 2.1 ppm N by fusion extraction. Total N analyses by neutron activation tend to give significantly higher values, 22 ppm (Norris and Schaeffer 1982).

Miller et al. (1987) determined the the OH^- content of olivines from different locations and found typical values of the order of 3-20 per 10^6 Si. Freund and Oberheuser (1986) have suggested that OH^- pairs in olivine may be converted to molecular H_2 plus peroxy entities, O_2^{2-} or $Si/^{OO}\backslash Si$. This so-called charge transfer or CT reaction is a redox reaction which oxidizes oxygen to O^- while reducing protons to H_2 (Freund 1985). It has been studied in MgO and CaO (Freund and Wengeler 1982; Freund et al. 1982) where the diagnostic H-H stretching band of molecular H_2 is rather strong. Miller et al. (1987) report not to have found spectroscopic evidence for H_2 and call the validity of the CT reaction in question.

The amount of CO_2 component dissolved and the nature of the C-bearing species are poorly constrained. C concentrations in the range 10-500 ppm have been reported (Tingle and Green 1986; Oberheuser et al. 1983; Shilobreyeva et al. 1987). Based on studies of MgO and CaO (Freund and Wengeler 1982; Wengeler et al. 1982) it has been suggested (Oberheuser et al. 1983) that solute C in olivine occurs in the form of CO_2^{2-} anions associated with divalent cation vacancies and similar to the CO_2^- and CO_2^{2-} complexes in other matrices (Kafafi et al. 1984).

CO_2 dissolution may procede via the "orthocarbonate" anion, CO_4^{4-} which is theoretically predicted to be stable (Johnson and Wasson 1974) or by forming CO_2^{2-} and O_2^{2-} via a CT reaction as in the case of dissolved H_2O. Note that in CO_2^{2-} the carbon is reduced, while in O_2^{2-} the oxygen is oxidized to the formal oxidation state -1.

Gas Evolution from a Supersaturated System.

The next question to be addressed concerns supersaturation. If solid solutions exist between olivine and the components of the C-N-O-H mantle fluid, each low-z element will be present at a specific concentration governed by the partial pressures (P) and temperature (T). Though the concentrations may not be known, the concentrations must decrease with decreasing T and P, for instance during ascent of the rock to the surface of the Earth.

If equilibrium cannot be constantly adjusted, supersaturation ensues. Supersaturation means that the host mineral matrix will tend to exsolve the low-z "impurity" just like, for instance, Ca^{2+} exsolves from MgO (McCune and Wynblatt 1983; Mackrodt 1987). Dislocations, subgrain and grain boundaries are always preferred impurity exsolution sites.

Naively the exsolution of C-N-O-H components may be thought of as a degassing process whereby the released gases are identical to those originally dissolved under mantle conditions, adjusted for the oxygen fugacity of the system. In other words, the gases released should consist of a mixture of H_2, H_2O, CH_4, CO, CO_2 and/or N_2. Indeed, under near-equilibrium conditions, for instance during a slow diapiric rise, these will be the gases exsolved.

However, when decompression and cooling are rapid such as during a volcanic ascent, we expect extreme non-equilibria. Under these conditions the C-N-O-H compounds which exsolve do not need to be the thermodynamically stable simple gases. This is particularily true, if we have reason to believe that a variety of solute species exist such as H_2 molecules plus C- and N-bearing oxyanions of different redox states. Then the situation may become very complex.

On a microscopic scale the exsolution will be controlled by the diffusion of the different solute entities. It suffices that one subset, for instance the reduced entities, has a higher average mobility. Then the gases or compounds which exsolve will be very different from the naively expected mixture of H_2, H_2O, CH_4, CO, CO_2 and/or N_2.

To further illustrate this point we note that CO_2^{2-} can dissociate into CO^- plus O^-. This dissociation has been postulated as the crucial step in the C diffusion mechanism which allows C atoms to enter interstitial sites and to become mobile. The degree of supersaturation of the solid solution can be reduced by exsolving only C and H_2, while retaining the oxidized entities, probably Si/^{OO}\Si. Whether or not this happens is a question of relative mobilities, for instance the mobility of the C atom diffusing in conjunction with an O^- state as a CO^-. At the exsolution sites, e.g. at dislocations, grain and subgrain boundaries, C-C bonds are predicted to form at the expense of the C-O^- bonds. This eventually leads to the precipitation of C_n (Freund 1986a/b).

$^{12}C(d,p)^{13}C$ nuclear reaction and secondary ion mass spectrometric data have been interpreted to indicate that carbon is subject to surface segregation (Wengeler et al. 1982; Oberheuser et al.

1983; Freund 1986a), while Tsong et al. (1985) and Mathez et al. (1987) have expressed doubts whether carbon can exist in minerals in solid solution.

Tingle and Green (1986) attempted to measure the diffusion of ^{14}C into an olivine single crystal at upper mantle pressure and temperature conditions, using ^{14}C-doped graphite as a source for carbon. Though they observed C diffusion profiles, the carbon solubility in the bulk was less than expected, ≈100 ppm, and apparently independent of P and T. Recrystallized olivine, on the other hand, had a much higher ^{14}C concentration. The apparent difficulty to introduce ^{14}C into an existing olivine single crystal is not in contradiction with the proposed CO_2 solid solution model which requires a readjustement of the overall stoichiometry (Freund 1986a/b). Such an adjustement, however, is possible when the olivine recrystallized and indeed reportedly incorporated much more ^{14}C at the simulated upper mantle conditions (Tingle and Green 1986).

Since there is no consensus as to whether or not olivine can form a solid solution with CO/CO_2, the question is, whether the FEMS, SALI and FIMS experiments reported here can provide us with additional insight. If we assume that CO_2 dissolves by way of a CT reaction as proposed earlier (Freund 1986a), the FEMS, SALI and FIMS observations may provide a portion of the answer.

C-N-O-H Precursors and C-N-O-H Molecules.

The CT dissolution mechanism of CO_2 predicts two types of solutes, one reduced (carbon) and one oxidized (peroxy). If the C-bearing solute entities have a higher mobility, preferrential C segregation occurs. If dislocations, subgrain and grain boundaries are sinks for segregating carbon, they are also the sites where polyatomic C_n entites form through C-C bond formation at the expense of $C\text{-}O^-$ bonds. The same segregation arguments apply to H_2 and to N-bearing solute entities, meaning that the dislocations, subgrain and grain boundaries become enriched in H_2 and N with the ensuing possibility of C-H and C-N bond formation.

A conspicuous feature of the San Carlos olivine crystals used in this study is a dense dislocation network as part of an extended polygonized domain substructure (Kohlstedt and Goetze 1974; Poirier 1985). Assume that, deep in the mantle and prior to eruption, the olivine crystals contained carbon homogeneously dissolved at a concentration C_o. During decompression and cooling the solubility decreases and carbon will segregate. The segregant concentration C(x) at a distance x from such a segregation site is $C(x) = C_o \exp[-U(x)/kT]$ where U(x) is the interaction energy (Lücke and Stüwe 1971). C-C bond formation is predicted to take place at the segregation sites leading to polyatomic C_n entities, plus additional C-H and C-N bonds, with n growing as segregation procedes. A monoatomic segregation layer would correspond to a continuous carbon film with a few C-O, C-H and C-N bonds.

Another potentially important question is that the C_n entities thus formed are expected to be sterically constrained by the 2-dimensional structure of the subgrain boundary similar to an epitaxial overgrowth. C_6 rings, for instance, fit onto O^{2-} anions like a crown. Several C_6 may fuse to polyaromatic structures and C-C sidechains may branch off in a specific way. Other shapes may be discriminated against by the structured environment. The result would be that the number of possible "organic" molecules synthesized by segregation from the solid state would be quite limited as compared to the total number of compounds known from liquid chemistry.

As long as the C_n entities are inside the crystal structure, even if their locus of formation is a defect such as a dislocation or subgrain boundary, they cannot be expected to be fully developed *molecules* . We rather should view them as *precursor* entities, still bonded to the mineral matrix via $C\text{-}O^-$ bonds, possibly resembling the known cyclic CO_x^{n-} oxocarbon anions, where $3< x > 6$ (Eggerding and West 1976; Staedeli et al. 1977). C_6 precursors on a subgrain boundary may resemble a rhodizonic anion, $C_6O_6^{n-}$, with n = 2 or 3, a benzene-like ring with six O substituting for H, formed through condensation of CO molecules on oxide surfaces with transfer of electrons from the oxide onto the adsorbate (Morris and Klabunde 1983).

If we look closely at our FEMS data, the gas emission may actually be controlled by the conversion of precursors sitting on or close to the fracture surface into mature molecules. The conversion can be done by scissoring $C\text{-}O^-$ bonds and replacing them with C-H bonds. For instance benzaldehyde C_6H_5CHO which stands out in the FIMS experiments (as 106 amu molecular ion) and FEMS experiments (as 105 amu $C_6H_5CO^+$ fragment) strikes us as being a molecule which could have formed from a rhodizonite-like anion complex (with one remaining $C\text{-}O^-$ sidechain) using a minimum of H to complete the molecular structure.

Another aspect which may be important for understanding the FEMS results relates to the extreme non-equilibrium condition at the fracture surface. This produces a strong driving force for further segregation from the near-by bulk. , If C diffusion procedes via the CO^- complex, the transport of carbon to the segregation site is coupled to the transport of a positive charge, e.g. O^-. This causes the segregation site to become positively charged and to counteract further carbon segregation, even in a state of supersaturation (Freund 1986a/b). However, during fracture the charge is destroyed due to electron and ion emission during the fracture process. Diffusion of solute C from the near bulk would then be driven by the extreme gradient of the electrochemical potential bringing additional C and H to the fracture surface.

Heating further activates diffusion and, hence, enables segregation. Heating also enhances reactions between segregants and at the same time allows larger molecules to desorb.

This brings us back to the FIMS question (see **Fig. 7**): Why do the heavy 302 amu molecules (probably benzopyrelene or dibenzopyrene, $C_{24}H_{14}$) evolve at a distinctly lower temperature than a number of lighter molecules? Maybe six asymmetrically arranged condensed C_6 rings form a sterically favorable precursor entity which becomes the 302 amu compound. Other smaller entities

require additional segregation or more H relative to the number of C to convert into desorbable molecules. Obviously, at sufficiently high temperatures pyrolysis sets in with benzene C_6H_6 as the main pyrolysis product besides toluene $C_6H_5CH_3$. As shown in **Fig. 7** benzene (78 amu) and toluene (92 amu) rise late in the heating program, suggesting that they are formed by pyrolysis.

We may also draw attention to an interesting similarity between the mass spectra as reported in this paper and some molecular ion spectra detected in ionopause of Comet Halley by the Giotto spacecraft (Mitchell et al. 1987). The ions at 63 and 65 recur with high intensities in both data sets. Outside the Halley ionopause low resolution mass spectra reveal a series of peaks centered at 75, 90 and 105 amu which Heubner (1987) proposed to be due to dissociation products of polyoxymethylenes, derivatives of aldehydes.

Maybe the complex organic molecules from Halley are formed by reations similar to the ones discussed above, e.g. through segregation of solute C and other low-z elements from silicate grains which are constituents of the comet. The appearance of these molecular ions in the Halley ionopause suggests thermal and radiation-induced desorption from dust grains ejected from the Comet's surface, followed by UV ionization.

The Role of the O^- States.

We need to address another puzzling aspect of the FEMS experiments: why do the olivine crystals simultaneously emit oxidized gases (CO_2, H_2O, possibly even O_2) and reduced gases ("organics") plus metal vapor upon fracture? FEMS experiments on MgO have shown that, following fracture, reduced "organic" molecules and Mg vapor are emitted at the same time as CO_2, H_2O and even O_2 (Dickinson et al. 1986). The answer appears to lie in the presence of peroxy entities in the mineral structure. Such peroxy entities are the counterparts of the reduced entities and probably of the form $Si/^{OO}\backslash Si$ (Freund and Oberheuser 1986).

Peroxy entities dissociate by breaking the O-O bond and releasing an O^- state: $O_2^{2-} = O^- + O^-$. An O^- is an electronic defect in the valence band, as radical state, commonly called a positive hole (Henderson and Wertz 1977; Marfunin 1979; King and Freund, 1984). O^- states have several properties which are important in the context of the present study. (i) They move without mass transport through the mineral structure. (ii) They repel each other in the bulk and diffuse to the surface. (iii) They are powerful oxidizing reagents disproportionating into free oxygen: $O^- + O^- = O^{2-} + 1/2\ O_2$.

In some FEMS experiments the 1(H^+), 2 (H_2^+), and 17 (OH^+) amu intensities as a function of time indicate a negative correlation between the emission of H_2 and H_2O. A possible interpretation is that H_2O molecules are formed through oxidation of H_2 molecules by O^- states, if such O^- states flood the surface and scavenge the H_2 molecules before they desorb. With <100 μsec time

resolution, Dickinson et al. (1987) observed erratic variations of the O_2 emission from MgO crystals over periods of ≈300 msec after fracture. They suggested that the oxidizing and reducing character of the fracture surface fluctuates due to rapid variations of the local O^- density.

In the case of the olivine fracture we have not yet carried out similar experiments at higher time resolution. However, the similarity of the olivine data to the MgO results is striking. If the MgO observations also apply to the olivine fracture, areas on the olivine fracture surface with a high O^- density would momentarily become oxidizing, generating H_2O, CO_2 and possibly even O_2, while other areas remain reducing and allow "organic" molecules to evolve.

Metal Vapor Emission.

If H_2O, CO_2 and other O-bearing molecules are formed through oxidation by O^-, the oxygen consumed in such reactions must be supplied the fracture surface. The reason is that O^- states are just electronic defects in the O^{2-} sublattice traveling without mass transport via the valence band (King and Freund 1984). At the surface the O^- can oxidize the solute entities according to the schemes:

$$CO^- + O^- = CO + O^{2-}$$

$$CO_2^{2-} + 2\ O^- = CO_2 + 2\ O^{2-}$$

$$H_2 + 2\ O^- = H_2O + O^{2-}$$

If oxygen is lost from the surface, coordinatively unsaturated cations remain which in turn may be the source of the observed Mg vapor emission: $Mg^{2+} + 2\ O^- = Mg^o + O_2$.

Acknowledgements

This work was supported by the NASA Ames Research Center Director's Discretionary Fund. One of us (F.F.) acknowledges support from the National Research Council. We thank Christopher H. Becker, SRI-International, Menlo Park, CA., for his cooperation during the SALI experiments. L.C. Jensen and M.R. McKay helped with the FEMS experiments. G.A. St. John provided technical assistance during the FIMS measurements. We thank the Surface Science Laboratories, Inc., Mountain View, CA., for the olivine infrared spectrum.

References

Aines R.D. and Rossman G.R. (1984) Water in minerals - a peak in the infrared? J. Geophys. Res. B89, 4059-4071.

Arculus R.J., Dawson J.B., Mitchell R.H., Gust D.A. and Holmes R.D. (1984) Oxidation states of the upper mantle recorded by megacryst ilmenite in kimberlite and type A and B spinel lherzolites. Contrib. Mineral. Petrol 85, 85-94.

Barker C. and Torkelson B.E. (1975) Gas adsorption on crushed quartz and basalt. Geochim. Cosmochim. Acta 39, 212 - 218.

Becker, C.H. and Gillen, K.T. (1984a) Surface analysis by nonresonant multiphoton ionization of desorbed or sputtered species. Anal. Chem. 56, 1671-1674.

Becker, C.H. and Gillen, K.T. (1984b) Nonresonant multiphoton ionization as a sensitive detector of surface concentrations and evaporation rates. Appl. Phys. Lett. 45, 1063-1065.

Becker, C.H., Malhotra, R. and St. John, G.A.:1986, NASA Contract Report A-32685C(VAD), SRI-International Project Nr. PYU 1161 MP 86-046.

Becker R.H. and Clayton R.N. (1977) Nitrogen isotopes in igneous rocks. EOS Trans. Amer. Geophys. Union 58, 536 (abstr.)

Beran A. and Putnis A. (1983) A model of the OH positions in olivine, derived from infrared-spectroscopic investigations. Phys. Chem. Minerals 9, 239-251.

Bergman S.C. and Dubessy J. (1984) Carbon dioxide – carbon monoxide fluid inclusions in a peridotite xenolith: implications for upper mantle fugacity. Contrib. Mineral. Petrol. 85, 1-13.

Burnham D.W. (1979) The importance of volatile constituants. In: *The Evolution of Igneous Rocks Fiftieth Anniversary Perspectives* , H.S. Yoder, ed., Princeton Press, 439-482

Chang S., DesMarais, D., Mack, R., Miller, S.L. and Strathearn: 1083, in: *Earth's Earliest Biosphere* , J.W. Schopf, ed. Princeton Univ. Press, p. 53.

Dickinson J.T., Jensen L.C. and Park M.K. (1982) Time-of-flight measurements of the mass-to-charge ratio of positive ion emission accompanying fracture. J. Mater. Sci. 17, 3173-3178

Dickinson J.T., Dresser M.J. and Jensen L.C. (1985) Time correlation of ion and electron emission from surfaces following fracture. In: Desorption Induced Electronic Transitions (DIET), Springer Ser. Surf. Sci. 4, 281-289

Dickinson, J.T., Jensen, L.C., McKay, M.R. and Freund, F. (1986) The emission of atoms and molecules accompanying fracture of single crystal MgO. J. Vac. Sci. Technol. A4, 1648-1652

Dickinson J.T., Jensen L.C. and McKay, M. (1987) Neutral molecule emission from the fracture of crystalline Mg. J. Vac. Sci. Technol. A5, 1162-1168

Eggerding D. and West R. (1976) Synthesis and properties of deltic acid (dihydroxycyclopropenone) and the deltate ion. J. Amer. Chem. Soc. 98, 3641-3644.

Eggler, DH. and Baker D.R.(1982) Reduced volatiles is the system C-O-H: Implications to mantle melting, fluid formation and diamond genesis. In: Advances in Earth and Planetary Sciences, High

Pressure Reseach in Geophysics, S. Akimoto and M.H Manghnani, eds. 12, 237-250, Center for Academic Publ., Tokyo.

Exley R.A., Boyd S.R., Mattey D.P. and Pillinger C.T. (1986/87) Nitrogen isotope geochemistry of basaltic glasses: implications for mantle degassing and structure? Earth Planet. Sci. Lett. 81, 163-174.

Fine G. and Stolper E. (1985) The speciation of carbon dioxide in sodium aluminate glasses. Contrib. Mineral. Petrol 91, 105-121.

Freund F. (1985) Conversion of dissolved "water" into molecular hydrogen and peroxy linkages. J. Non-Cryst. Solids 71, 195-202.

Freund F. (1986a) Solute carbon and carbon segregation in magnesium oxide single crystals - secondary ion mass spectrocmeter study. Phys. Chem. Minerals **13**, 262-276.

Freund F. (1986b) Carbon in oxides and silicates - dissolution versus exsolution. J. Cryst. Growth 75, 107-121.

Freund F. and Oberheuser G. (1986) Water dissolved in olivine: a single crystal infrared study. J. Geophys. Res. 91, 745-761.

Freund, F. and Wengeler, H. (1982) The infrared spectrum of OH^--compensated defect sites in C-doped MgO and CaO single crystals. J. Phys. Chem. Solids 43, 129-145.

Freund F., Wengeler H. and Martens R. (1982) A hydrogen-deuterium fractionation mechanism in magnesium oxide. Geochim. Cosmochim. Acta 46,1821-1829.

Green H.W. (1972) Carbon dioxide charged asthenosphere. Nature, 238, 2-5.

Green H.W. and Radcliffe, S.V. (1975) Dislocation mechanisms in olivine and flow in the upper mantle. Geol. Soc. Am. Bull. 86, 846 - 854.

Hallam M. and Eugster H.P. (1976) Ammonium silicate stability relations. Contrib. Mineral. Petrol. 57, 227-238

Henderson B. & Wertz J.E. (1977) Defects in the Alkaline Earth Oxides. Taylor & Francis, London.

Hendry A., Perera D.S., Thompson D.P. and Jack K.H. (1975) Phase relations in the magnesium oxide-silicon nitride-aluminum oxide system. Spec. Ceram. 6, 321-331.

Heubner W.F. (1987) First polymer in space identified in Comet Halley. Science 237, 628-630

Johan Z., Dunlop H., Le Bel L., Robert J.J. and Volfinger M. (1983) Fort. Mineral. 61, 105-114.

Johnson D. K. and Wasson J.R. (1974) On the existence of NS_3^-, NS_4^{3-}, NO_4^{3-} CO_4^{4-} and CS_4^{4-} anions - semiempirical molecular orbital calculations. Inorg. Nucl. Chem. Lett. 10, 891-894.

Kafafi Z.K., Hauge R.H., Billups W.E. and Margrave J.L. (1984) Carbon dioxide activation by alkali metals. 2. Infrared spectra of $M^+CO_2^-$ and $M^{2+}CO_2^{2-}$ in argon and nitrogen matrices. Inorgan. Chem. 23, 177-183.

King B.V. and Freund F. (1984) Surface charges and subsurface space charge distribution in magnesium oxide containing dissolved traces of water. Phys. Rev. B29, 5814-5824.

Knobel R.M. (1983) H-C-N-O gases from MgO and silicate surfaces. Ph.D. Thesis Univ. Cologne.

Knobel R.M., Breuer H. and Freund F. (1984) Abiotic synthesis of organic molecules from minerals containing traces of dissolved H_2O, CO_2 and N_2. Part II: Experimental data. Origin of Life Proc. 7th Int. Conf., K. Dose, A.W. Schwarz, W.H.P. Tieman, eds., Reidel Publ., Dodrecht, 197-202 (1984)

Kohlstedt D.L. and Goetze C. (1974) Low-stress, high temperature creep in olivine single crystals. J. Geophys. Res. 79, 2045-2051;

Konnerup-Madsen J., Carson E. and Rose-Hansen J. (1979) Hydrocarbon-rich fluid inclusions in minerals from the alikaline Ilimaussaq intrusion, South Greenland. Bull. Minéral. 102, 642-653.

Lange F.F. (1979) Eutectic studies in the system silicon nitride - silicon oxynitride - magnesium silicate (Si_3N_4-Si_2N_2O-Mg_2SiO_4). J. Amer. Cerma. Soc. 62, 617-619.

Lloyd F.E. (1987) Characterization of mantle metasomatic fluids in spinel lherzolites ad alkali clinopyroxenites from the West Eifel and South West Uganda. In: Mantle Metasomatism. M.A. Menzies and C.J Hawkesworth, eds. Academic Press 91-124.

Marfunin A.S. (1979) Spectroscopy, Luminescence and Radiation Centers in Minerals. Springer Verlag, New York.

Martens R., Gentsch H. and Freund F. (1976) Hydrogen release during the thermal decomposition of magnesiium hydroxide to magnesium oxide. J. Catalysis 44, 366-372.

Mathez, E.A., Dietrich, V.J. and Irving, A.J. (1984) The geochemistry of carbon in mantle peridotites. Geochim. Cosmochim. Acta 48, 1849-1859.

Mathez, E.A., Blacic J.D., Berry J, Maggiore, C. and Hollander M. (1987) Carbon in olivine: results from nuclear reaction analysis. J. Geophys. Res. 92, 3500-3506.

McCune R.C. and Wynblatt P. (1983) Calcium segregation to a magnesium oxide (100) surface. J. Amer. Ceram. Soc. 66, 111-117.

Melton C.E. and Giardini A.A. (1974) The composition and significance of gas released from natural diamonds from Africa and Brazil. Amer. Mineral. 58, 775-782.

Melton C.E. and Giardini A.A. (1975) Experimental resultsa and a theoretical interpretation of gaseous inclusions found in Arkansas natural diamonds. Amer. Mineral. 60, 413-417.

Melton C.E. and Giardini A.A. (1981) The nature and significance of occluded fluids in three Indian diamonds. Amer. Mineral. 66, 746-750.

Mitchell D.L., Lin R.P., Anderson K.A., Carlson C.W., Curtis D.W., Korth A, Rème H., Sauvaud J.A., d'Uston C. and Mendis D.A. (1987) Evidence for chain molecules enriched in carbon, hydrogen and oxygen in Comet Halley. Science, 237, 626-628.

Miller G.H., Rossman G.R. and Harlow G.E. (1987) The natural occurrence of hydroxide in olivine. Phys. Chem. Minerals 14, 461-472.

Morris R.M. and Klabunde K.J. (1983) Formation of paramagnetic adsorbed molecules on thermally activated magnesium and calcium oxides. Further studies on carbon monoxide. J. Amer. Chem. Soc. 105, 2633-2639.

Murck, B.W., Burruss, R.C. and Hollister, L.S.: 1978, Amer. Mineral. 63, 40.

Mysen B.O. and Virgo D. (1980) Solubility mechanisms of carbon dioxide in silicate melts: a Raman spectroscopic study. Amer. Mineral. 65, 885-899

Norris T.L. and Schaeffer O.A. (1982) Total nitrogen content of deep sea basalts. Geochim. Cosmochim. Acta 46, 371-379.

Nakamura A. and Schmalzried H. (1983) On the non-stoichiometry and point defects of olivine. Phys. Chem. Minerals, 10, 27-37.

Poirier J.-P. (1985) Creep of Crystals: High Temperature Deformation Processes in Metals, Ceramics and Minerals. Cambridge Univ. Press.

Roedder, E.: 1965, Amer. Mineral. 50, 1746.

Roedder, E.: 1984, Fluid Inclusions, Reviews in Mineralogy, 12, p. 503 Mineral. Soc. Amer., Washington.

Sakai H., Des Marais D.J., Ueda A. and Moore J.G. (1984) Concentrations and isotope ratios of carbon, nitrogen and sulfur in ocean-floor basalts. Geochim. Cosmochim. Acta 48, 2433-2441.

Staedeli W., Hollenstein R. and Von Philipsborn W. (1977) Carbon-13 nmr spectroscopy XVII C-13 nmr spectra, structure and reactivity of cyclic oxocarbons. Helv. Chim. Acta 60, 948-958.

Stathis J.H. and Kastner M.A. (1984) Photoinduced paramagnetic defects in amorphous silicon dioxide. Phys. Rev. B29, 7079-7081.

Shilobreyeva S.N., Kadik A.A., Minaya V.M. Kazakov S.S. and Kuz'min L.Y. (1987) Analysis of carbon in olivine crystals of deep origin. Doklady Acad. Nauk USSR Mineralogiya 297, 457-461.

Stolper E. (1982a) Water in silicate glasses: in infrared study. Contrib. Mineral. Petrol. 81, 1-17.

Stolper E. (1982b) The speciation of water in silicate melts. Geo. Cosmochim. Acta 46, 2609-2620.

Tingle T.N. and Green H.W. (1986) Carbon solubility in olivine: implications for upper mantle evolution. Geology, 15, 324-326.

Tsong, I.S.T., Knipping, U., Loxton, C.M., Magee, C.W. and Arnold, G.W. (1985) Carbon on surfaces of magnesium oxide and solivine sinkgle crystals - diffusion from the bulk or surface contamination? Phys. Chem. Minerals 12, 261-270.

Wengeler H., Knobel R., Kathrein H., Freund F., Demortier G. and Wolff G. (1982) Atomic carbon in magnesium oxide single crystals - depth profiling, temperture- and time-dependent behavior. J. Phys. Chem. Solids 43, 59-71

Wilkins R.W.T. and Sabine W. (1973) Water content of some nominally anhydrous silicates. Amer. Mineral. 58, 508-516

Wyllie, P.J. (1978) Mantle fluid compositions buffered in peridotite- CO_2, with H_2O by carbonates, amphibole and phlogopite. J. Geology 86, 687-713.

Legends

Fig. 1 Schematic view of the fracture device used in the FEMS experiments.

Fig. 2 Five consecutive 80 msec FEMS scans of a San Carlos olivine crystal. Scan (1): residual gas spectrum; scan (2)-(5): the next 320 msec including the fracture near 60 amu in scan (2). Besides H_2/H_2O, CO/CO_2 a number of complex H-C-N-O molecules are emitted.

Fig. 3 Similar data as in Fig. 3, plotted on a logarithmic scale.

Fig. 4 Typical SALI mass spectrum from the gases thermally released from an olivine fragment after cleavage in air and introduction into UHV.

Fig. 5a/d "Thermal profiles" of gases released during heating in the SALI instrument.

Fig. 6 Gases emitted from crushed olivine single crystal powder sample in the FIMS experiment, accumulated over the temperature range up to 500°C.

Fig. 7 Intensities of selected mass peaks in the FIMS experiment. Note the high intensity of the 302 peak which reaches its maximum at a lower temperature than several lower molecular weight compounds.

Fig. 8 Infrared absorption spectrum of a San Carlos olivine crystal of the type used in this study. Note the near absence of any O-H stretching bands and the occurrence of a broad double band in the region of the C-H stretching absorption.

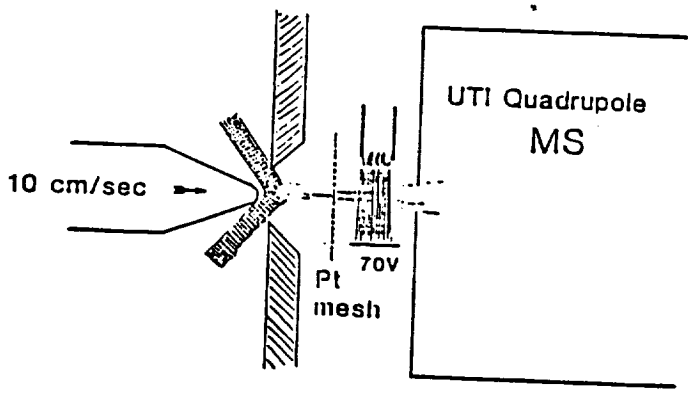

Fig. 1

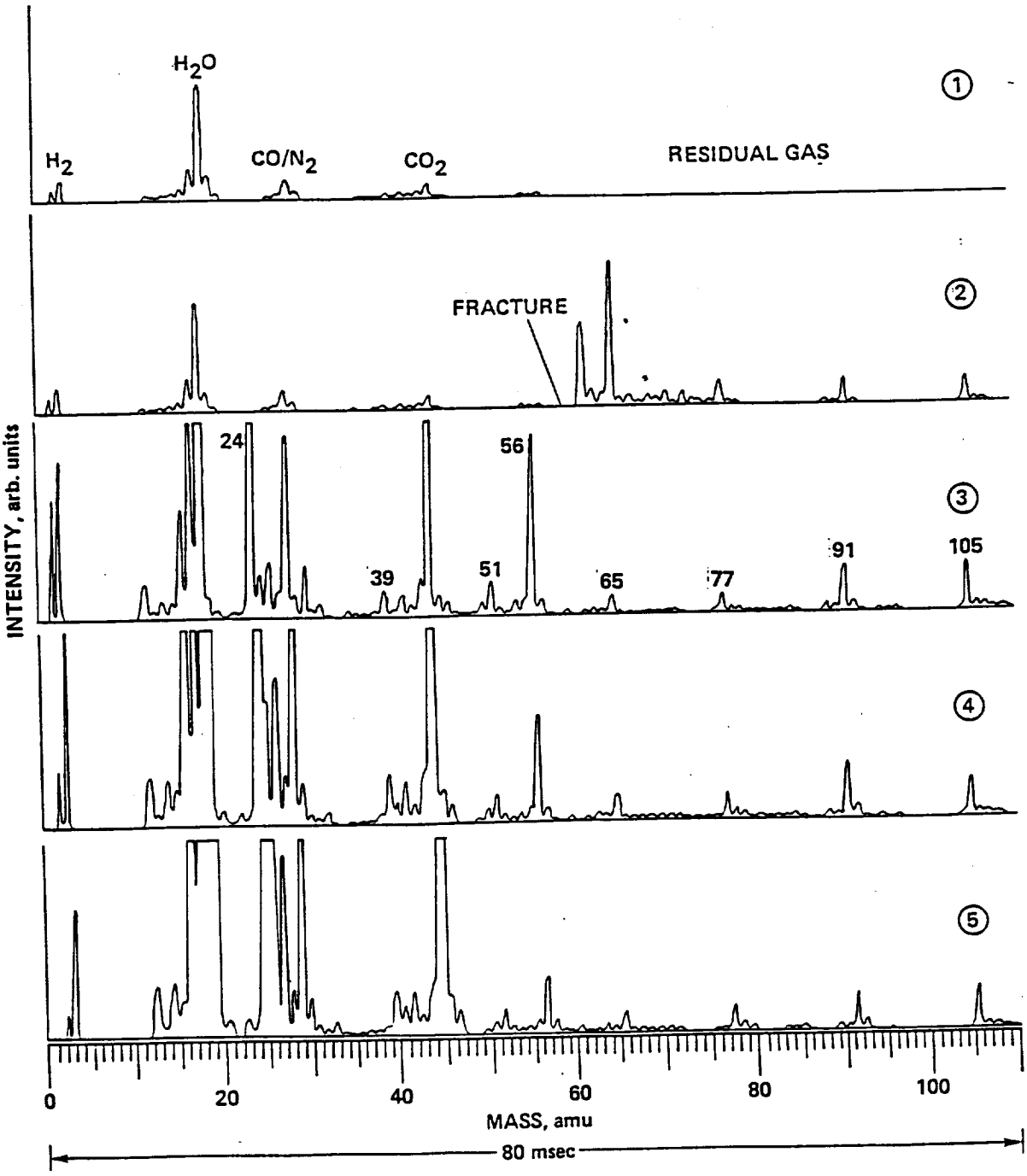
SAN CARLOS OLIVINE IMPACT FRACTURE MS
H_2O
H_2
CO/N_2
CO_2
RESIDUAL GAS
FRACTURE
24
56
39
51
65
77
91
105
INTENSITY, arb. units
0
20
40
60
80
100
MASS, amu
80 msec

Fig. 2

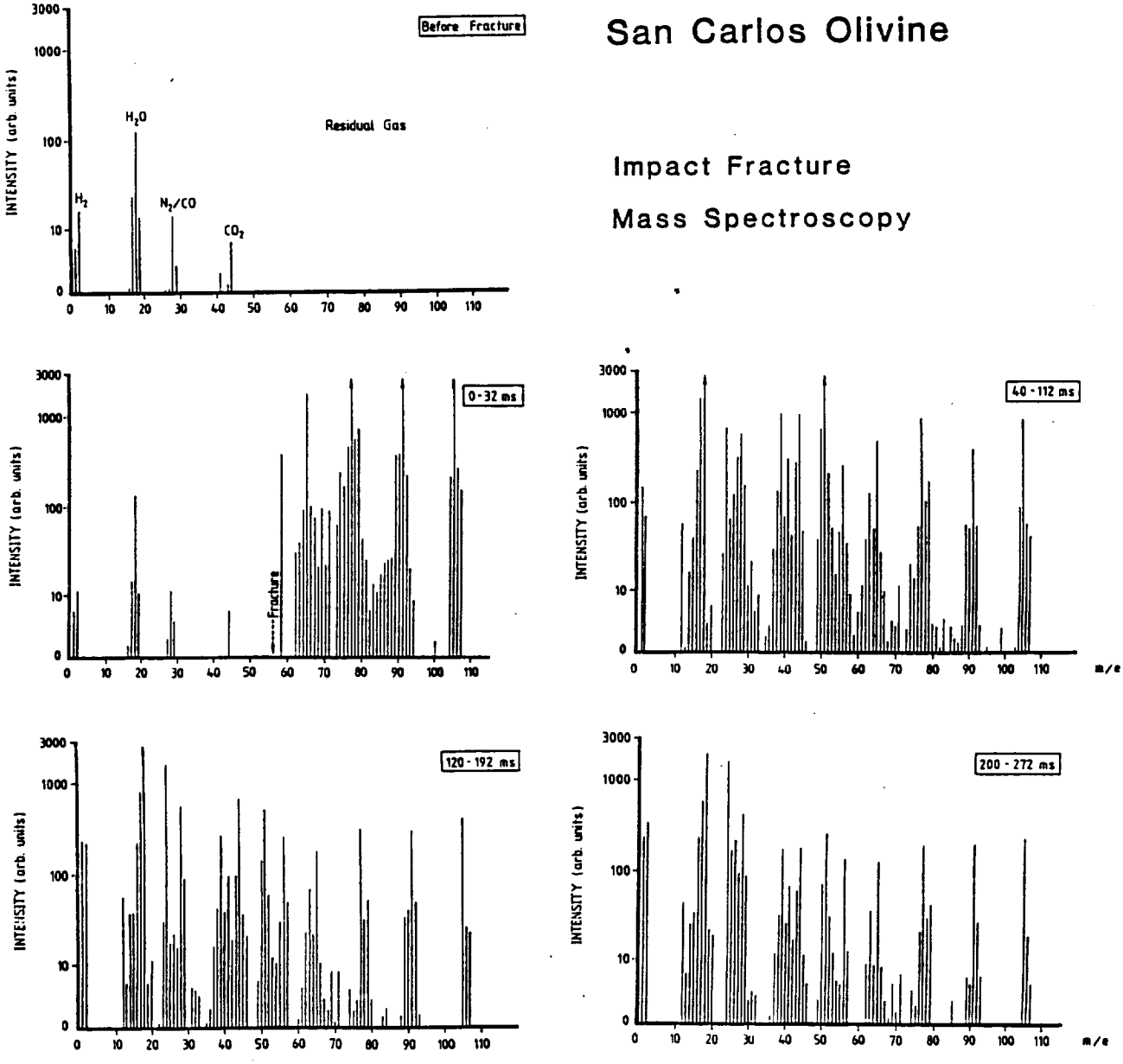
San Carlos Olivine
Impact Fracture
Mass Spectroscopy
Before Fracture
Residual Gas
H_2
H_2O
N_2/CO
CO_2
0 - 32 ms
Fracture
40 - 112 ms
120 - 192 ms
200 - 272 ms
INTENSITY (arb. units)
m/e

Fig. 3

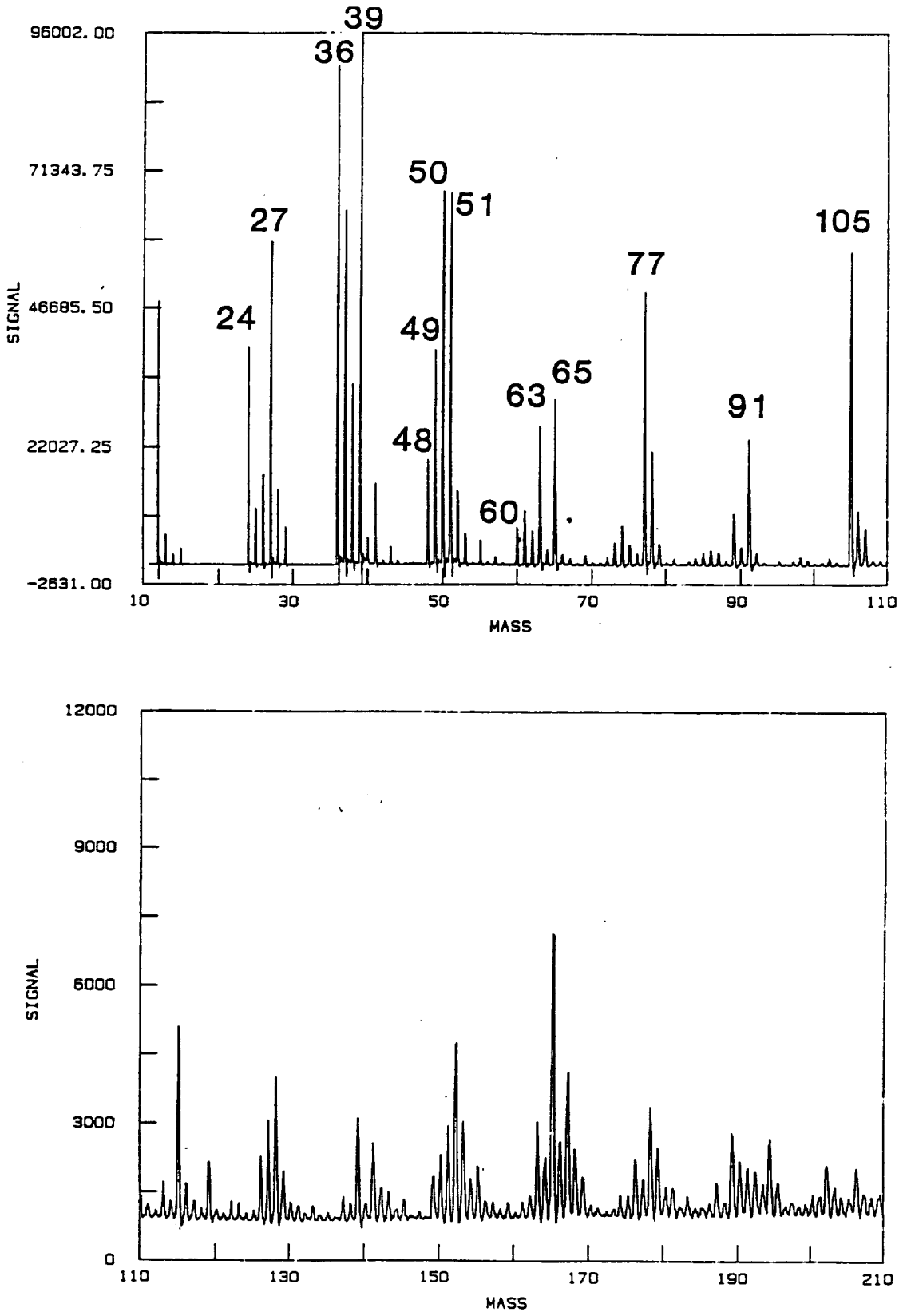
96002.00
71343.75
46685.50
22027.25
-2631.00
SIGNAL
10
30
50
70
90
110
MASS
39
36
50
51
27
105
77
24
49
65
63
91
48
60
12000
9000
6000
3000
0
SIGNAL
110
130
150
170
190
210
MASS

Fig. 4

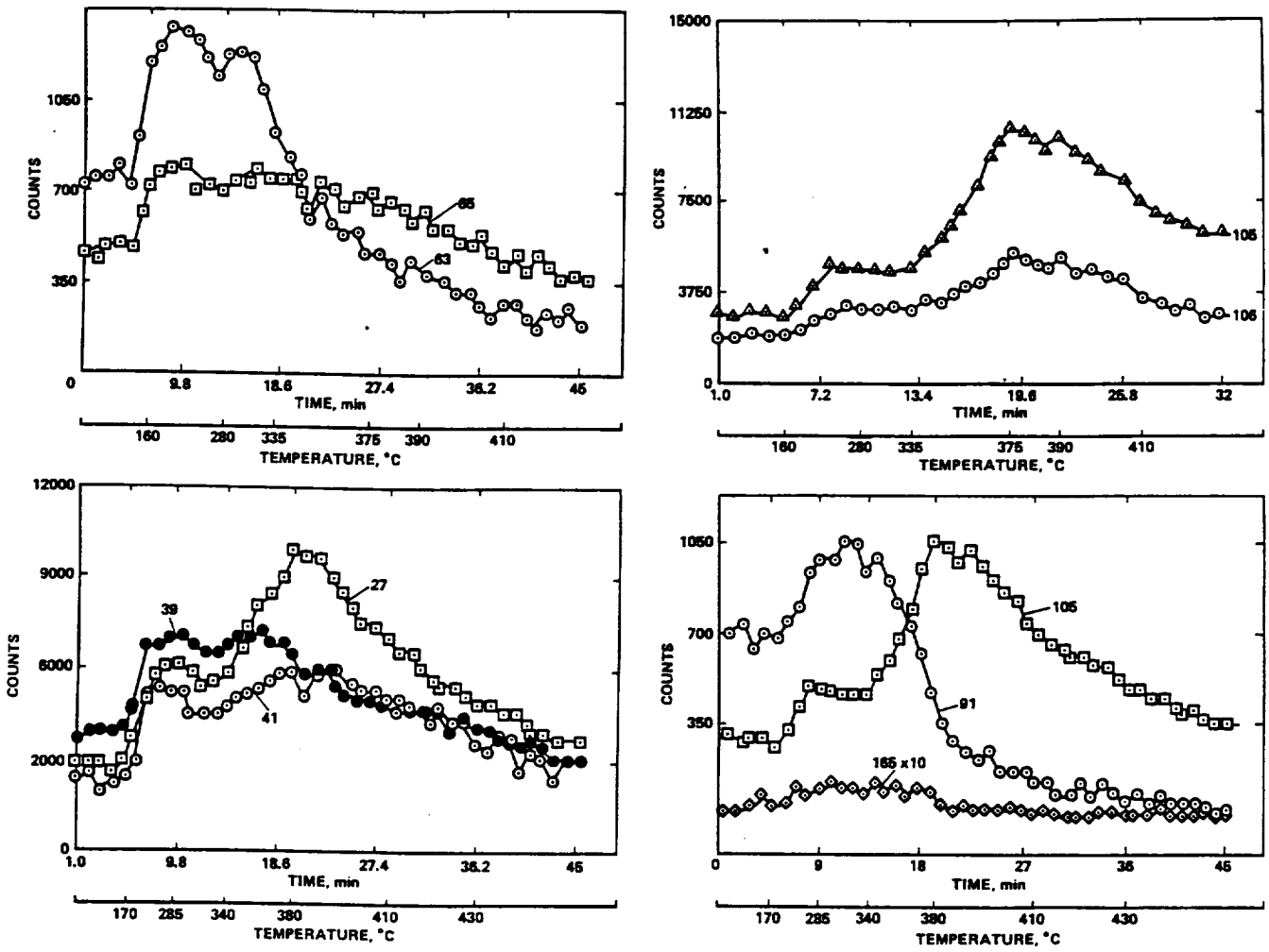
COUNTS
1050
700
350
0
9.8
18.6
27.4
36.2
45
TIME, min
160
280
335
375
390
410
TEMPERATURE, °C
65
63
15000
11250
7500
3750
1.0
7.2
13.4
19.6
25.8
32
105
106
12000
9000
6000
2000
39
27
41
170
285
340
380
410
430
91
165 x10

Fig. 5

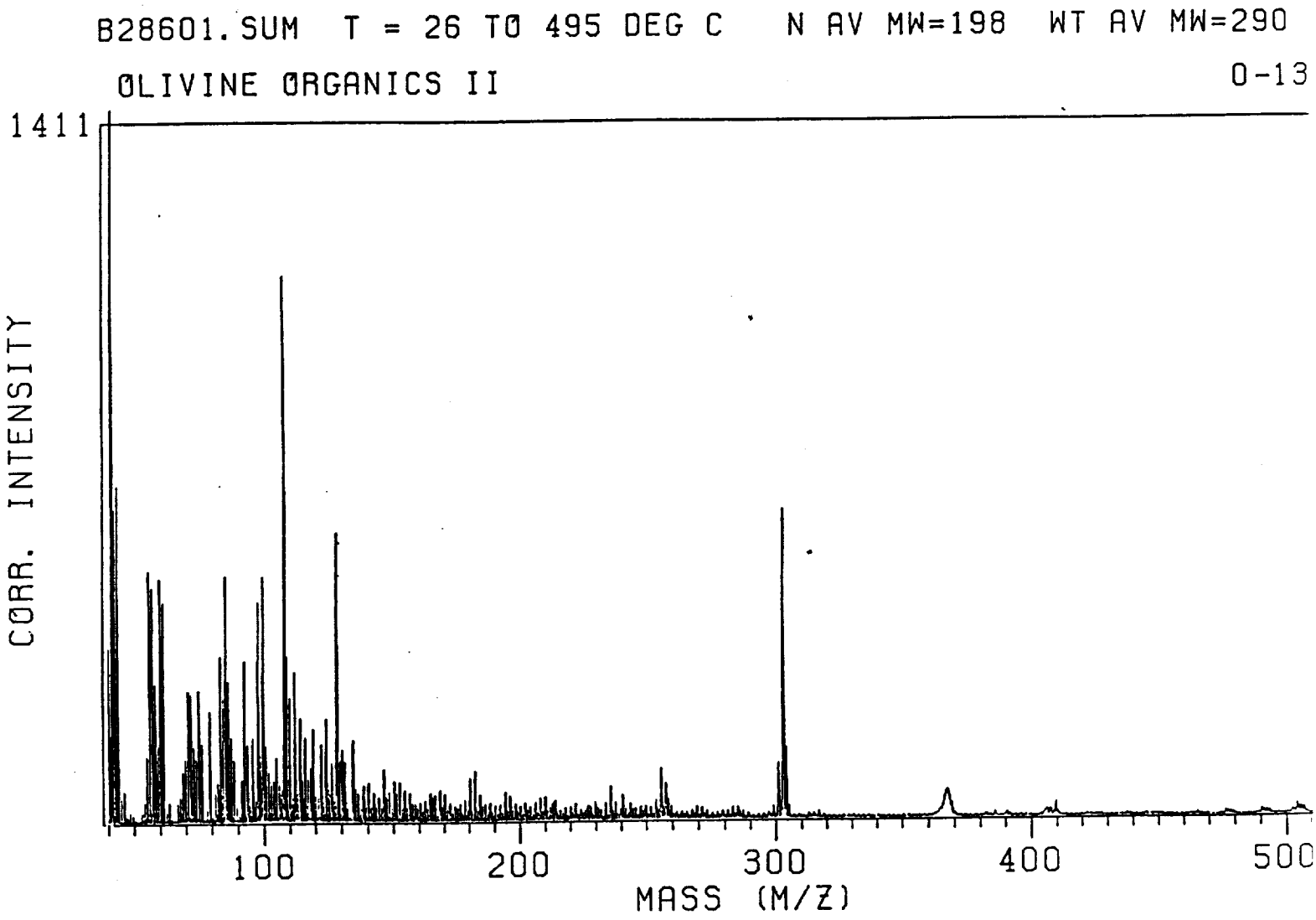
B28601.SUM T = 26 TO 495 DEG C N AV MW=198 WT AV MW=290
OLIVINE ORGANICS II
0-13
1411
CORR. INTENSITY
100
200
300
400
500
MASS (M/Z)

Fig. 6

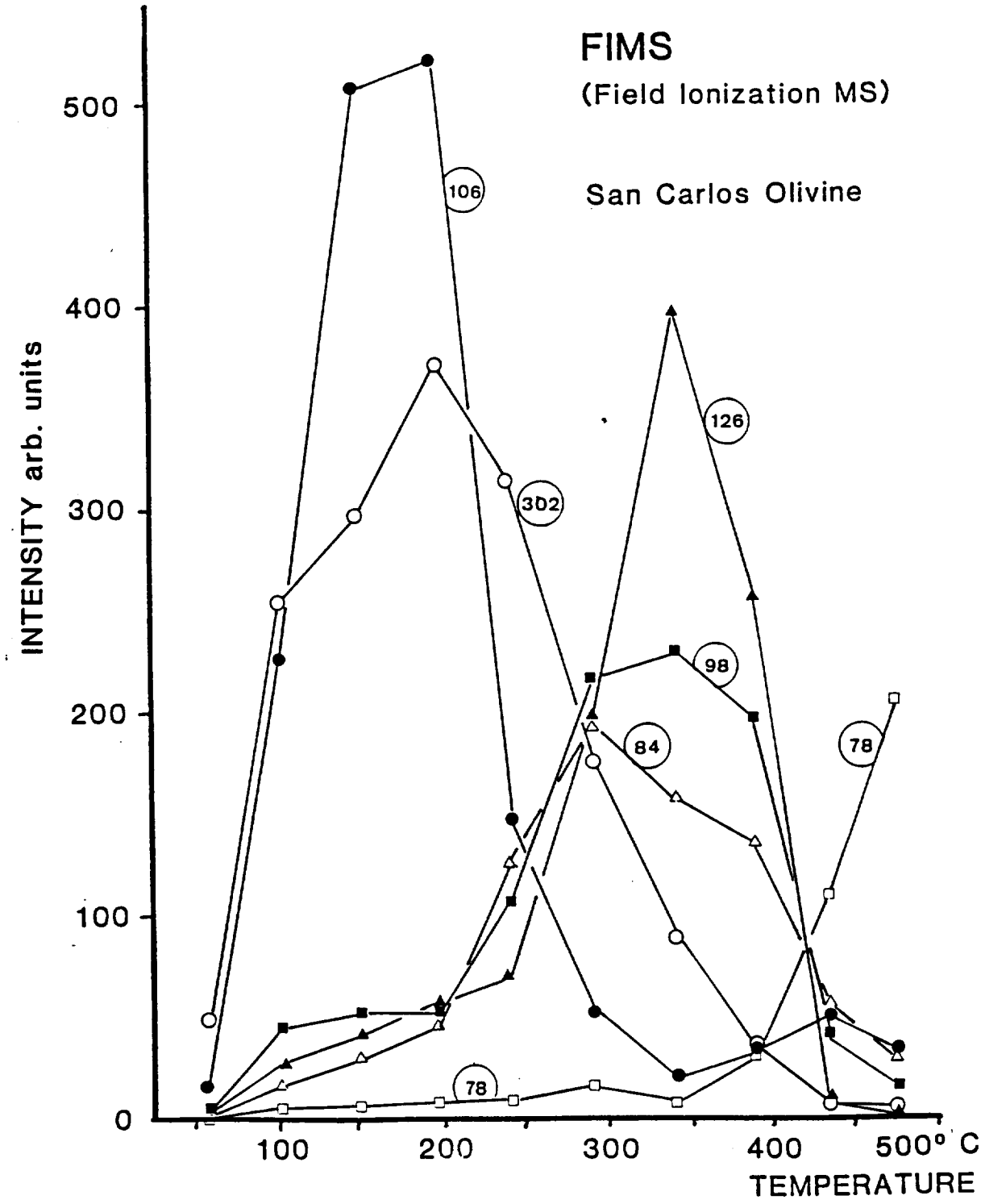
FIMS
(Field Ionization MS)
San Carlos Olivine
INTENSITY arb. units
500
400
300
200
100
0
106
302
126
98
84
78
78
100
200
300
400
500° C
TEMPERATURE

Fig. 7

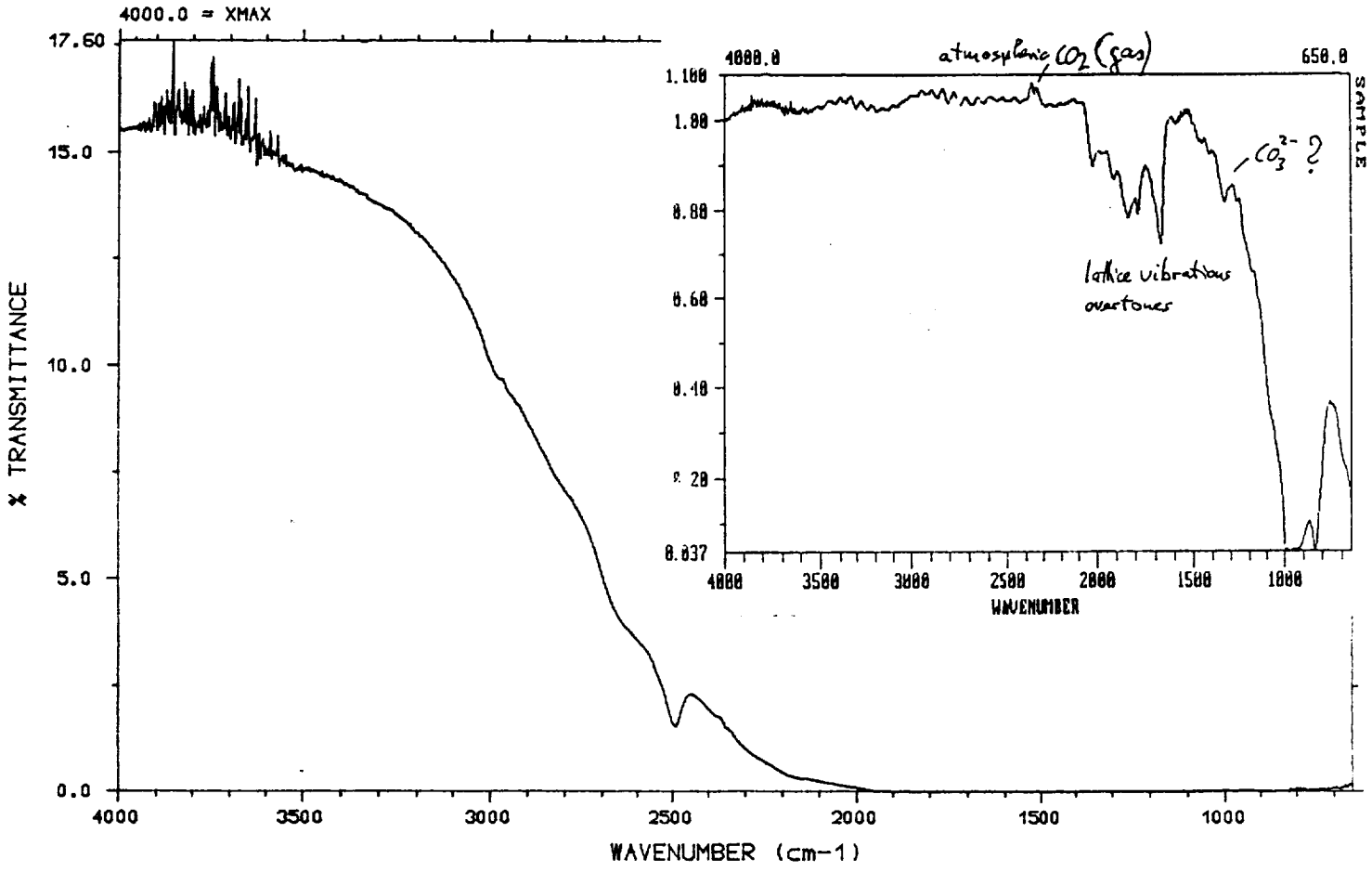

SURFACE SCIENCE
LABORATORIES
INC.

IR/30S MCT

SAMPLE NAME : OLIVINE ROCK BLOCK
SAMPLE FORM : MICROSCOPE/TRANSMITTANCE
OPERATOR : HEG AP2902
APODIZATION : TRIANGULAR
CREATED : 5/05/87 6:26:28

RESOLUTION : 4 CM -1
SCANS : 1024

Fig. 8

Electrical Conductivity Measurements under Minimum Perturbation Conditions Part I: Charge Distribution Analysis of Magnesium Oxide

Friedemann Freund[++], Minoru M. Freund[+] and François Batllo[°]

Department of Physics, San Jose State University, San Jose, CA 95192

Abstract

A new technique, Charge Distribution Analysis, has been developed which measures electric and dielectric properties contact–free at the limiting case of 0 Hz under minimum perturbation conditions. CDA allows to determine surface charges and their associated internal electric fields. This unique feature and a high sensitivity make CDA particularly suitable to study electron and hole conductivity in otherwise highly insulating minerals. Positive charge carriers have been identified in nominally high purity MgO single crystals between 200–400°C where the electrical conductivity is in the 10^{-12}–10^{-14} S/m range, and between 500–800°C where it rises to 10^{-4}–10^{-5} S/m. The charge carriers reversibly appear and disappear during repetitive heating/cooling cycles. Because of their pronounced tendancy to diffuse to the surface and cause a high surface conductivity, these charge carriers have been misinterpreted as sign of contamination. The internal electric field associated with the surface charge indicates that the charges are not due to contamination but are generated in the bulk and that their diffusion to the surface is an internally controlled process.

[++] also at the SETI Institute, c/o NASA Ames Research Center, MS 239-4, Moffett Field, CA 94035.
[+] Department of Physics, Swiss Institute of Technology, CH-8097 Zürich, Switzerland
now at the Department of Physics, University of California, Berkeley, CA 94720.
[°] Permanent address: Réactivité des Solides, Université de Bourgogne, 21004 Dijon, France.

Introduction

Most minerals are insulators. If they carry an electric current, they do so because ions become mobile at elevated temperatures or because they contain electronic charge carriers that can move in response to an externally applied field. Ions hop from lattice site to lattice site either interstitially or via a vacancy mechanism. Electronic charge carriers may also be visualized as hopping from site to site or delocalize via orbital overlap. The important physical information that can be gained from electrical conductivity measurements pertains to the nature of the charge carriers and to the way they conduct current by moving through the mineral structure or through a rock at given temperatures, pressures and gas or fluid environments.

Olivine, the major mineral of upper mantle rocks, has been studied extensively. Most conductivity measurements have been carried out under "simulated" upper mantle conditions [*Constable and Duba, 1990; Schock and Duba, 1985; Schock et al., 1977; Schock, Duba and Shankland, 1989; Sockel, 1974*], above 1000°C at ambient pressure (0.1 MPa) in H_2:CO_2 or CO:CO_2 gas mixtures for controlling the oxygen fugacity, f(O_2) [*Ballhaus et al., 1990*]. Measurements under high pressures have also been performed [*Bradley et al. 1964; Shankland 1969; Duba 1972; Duba and Nicholls 1973; Duba et al. 1974; Omura et al., 1989*] though not in the presence of the H–C–O fluids believed to exist in the upper mantle. The reason for not using high pressure H–C–O fluids is that these fluids tend to have a high electrolytic conductivity which drowns the typically much smaller solid state conductivity of the minerals to be studied. On the other hand H–C–O gases and fluids are known to be important components of the earth's interior and it may make a difference whether they are present at 0.1 MPa or at realistic upper mantle pressures. When fluid phase components dissolve in the minerals – even on a trace level – they give rise to defects and impurities which may profoundly affect the electrical conductivity. H_2O dissolves in olivine, forming OH^- associated with different defect sites [*Beran and Putnis, 1983; Freund and Oberheuser, 1986; Miller et al., 1987; Wilkins and Sabine, 1973*]. The ubiquitous occurrence of OH^- in olivine has led to a recent surge of interest in the possibility that hydrogen – more exactly protons – may act as charge carriers and make a significant contribution to the conductivity of the upper mantle [*Hirsch, 1990; Karato, 1990*].

Against the background of decades of intense study one may be inclined to think that all potentially important charge carriers and conduction mechanisms in olivine should have been identified. However, there is one peculiarity in the electric response of olivine at 0.1 MPa for which no compelling explanation has been offered so far: the enhancement of the conductivity by many orders of magnitude whenever mantle–derived olivine crystals are heated in the laboratory for the first time. The anomaly is restricted to relatively low temperatures – below about 700°C – and generally disappears while the samples are slowly heated in the reducing H_2:CO_2 or CO:CO_2 gas mixtures. The cause of this conductivity peculiarity is unknown, but since it disappears readily between 700–800°C it has not raised much concern. Most researchers have been satisfied

with the assumption that the observed conductivity anomaly of olivine is a laboratory–induced artefact, a "dirt effect" which does not need to be taken seriously.

In this study we examine the validity of this assumption. Recognizing that olivine crystals from the upper mantle are enormously complex – crystallographically and with respect to defects and impurities – we first turn to a model system with less variables. A suitable model system is MgO crystallizing in the simple face–centered cubic structure. Synthetic MgO crystals of nominally highest purity grade are available. As we shall show below they exhibit a strikingly similar electrical conductivity anomaly as mantle–derived olivine crystals. In Part I we describe a novel technique, Charge Distribution Analysis (CDA) which allows us to obtain information about the charge carriers that is unavailable through conventional conductivity measurements [*Freund et al., 1989*]. In Part II we show how supplementary physical techniques can help us to identify the nature of the charge carriers responsible for the conductivity anomaly. Finally, in Part III, using the knowledge gained by studying MgO we shall apply CDA to mantle–derived olivine crystals and draw conclusions about their charge carriers.

Identification of the Problem

Electrical conductivity measurements serve to detect charge carriers that can move in response to an externally applied electric field. The conductivity σ is usually given in units of reciprocal Ohm·centimeter, $\Omega^{-1}cm^{-1}$, or Siemens per meter, S/m. It can be written as sum of contributions from charge i,j: $\sigma_{i,j} = \sum_{i,j} \sigma_0 \exp [-E/kT]$, where σ_0, E, k and T are, respectively, pre-exponential factors, activation energies, the Boltzmann constant and the absolute temperature. Conductivity data are conveniently presented as Arrhenius plots, e.g. log σ vs $1/T$.

In predominantly ionic solids all charge carriers fall into two categories: ionic and electronic. Ions commonly move via a vacancy hopping mechanism or interstitially. Their diffusion involves mass transport. In refractory oxides and silicates ionic diffusion is generally restricted to high temperatures, typically >800°C. Electronic charge carriers can be electrons or holes. Neither involves mass transport.

Electrons are negative charges. Their movement may be visualized as localized hopping or as due to orbital overlap between nearby ions with partially filled shells such as transition metal cations which results in delocalized states. Holes are defect electrons with respect to the perfect structure. They are positive charges, often symbolized by $h^{\cdot}$. Their diffusion can take place either on the cation or the anion sublattice or on a combination of both. Holes are commonly associated with transition metal cations undergoing transient oxidation, for instance $Fe^{2+} \Leftrightarrow Fe^{3+} + h^{\cdot}$. However, holes do not need to be confinced to the cation sublattice. They can also reside on and move via the O^{2-} sublattice. In this case they are called "positive holes" or "oxygen associated holes" and represent O^{-} radicals [*Griscom, 1990; Henderson and Wertz, 1977*]. Such O^{-} radicals have been identified in many natural minerals exposed to ionizing radiation [*Marfunin, 1979*].

Radiation–induced O^- irreversibly disappear upon annealing. Questions which need clarification are (i) what role do such O^- play in the electrical conductivity at higher temperatures, and (ii) where in the mineral matrix are the O^- located or stored when they are not, or not yet, mobile charge carriers?

Electrical conductivity measurements of minerals, either with direct currents (d.c.) or with alternate currents (a.c.), are commonly carried out with metal electrodes in direct contact with the samples. The electrodes are deposited by evaporation or pasted onto the sample surfaces or mechanically pressed against them to make the best possible contacts. Unfortunately metal–to–insulator contacts are also sources of concern. To detect the charge carriers which move through the sample they have to be converted into electrons at the interfaces. If the carriers are electrons or holes, their Fermi levels have to adjust across the metal–to–insulator contacts. If they are ions, the conversion to electrons needed to drive the external measuring circuit requires electrochemical reactions at the interface. In all cases the contact potentials may become perturbed by the accumulation of space charges or by chemical reactions in the near–electrode region. In extreme cases the flow of charge carriers can be totally interrupted due to electrode passivation. Another concern with conventional techniques relates to surface and grain boundary conductivity. Surfaces, grain boundaries and subgrain boundaries represent extended 2–dimensional defects where intrinsic valence and conduction bands are shifted on the energy scale, where additional defect levels are introduced and activation energies for many diffusional processes lowered. Lastly there is the possibility of surface contamination during sample handling or in the course of measurements.

Fig. 1 illustrates an Arrhenius plot, log σ vs 1/T [K], for olivine and olivine–rich rocks compiled from data reported by Duba and coworkers [*Constable and Duba, 1990; Duba et al, 1974; Shankland and Duba, 1990*]. The high temperature (HT) branch is represented by open and solid triangles and small solid squares. In the HT region the conductivity is fairly reproducible for given oxygen fugacities and is caused by cation diffusion [*Buening and Busek, 1973; Morin et al., 1977a,b; Smyth and Stocker, 1975*], possibly enhanced by hole diffusion via the cation sublattice, transiently trapped on Fe^{2+} sites to generate Fe^{3+} [*Schock et al., 1989*]. For synthetic forsterite a mixed HT mechanism has been proposed combining predominantly electronic conduction in the crystallographic a and b directions and cation diffusion via vacancy hopping in the c direction [*Schock et al., 1989*]. Upon cooling the HT branch never extends very far below 800°C, but changes more or less abruptly into a low temperature (LT) extension with a distinctly smaller activation energy. The conduction mechanism in the LT region is seldom discussed. Two LT extensions are depicted in **Fig. 1** by the small solid and open squares.

The anomalously high conductivity which is typically observed below approximately 700°C during initial heating is delineated in **Fig. 1** by large open squares. In the example selected here a fresh sample was heated in a 1:1 CO/CO_2 mixture at 0.1 MPa pressure at 1°C/min [*Constable and Duba, 1990*]. Up to about 700°C the conductivity was many orders of magnitude higher than the downwardly extrapolated HT branch and several orders of magnitude above any of the LT

extensions measured during cooling. The anomaly ended around 700°C when the conductivity decreased precipitously, joining the HT branch above 800°C.

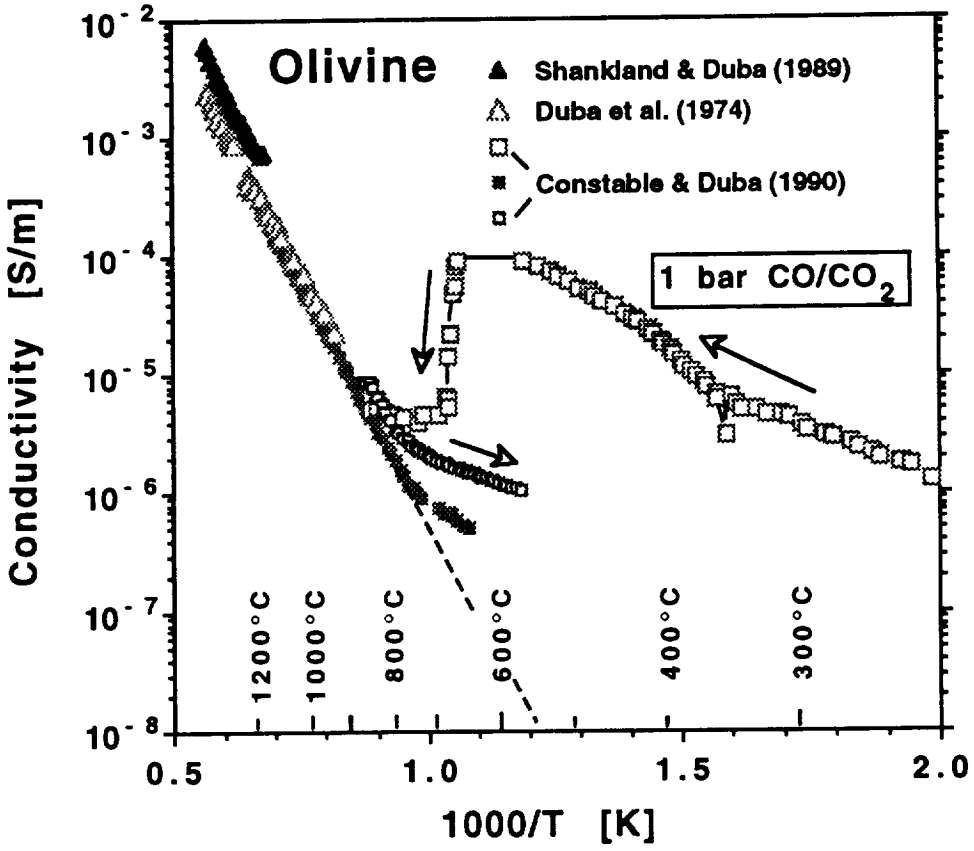

Fig. 1 Electrical conductivity of olivine single crystal and dunite samples under simulated upper mantle conditions (P = 1 bar) compiled from data by Duba and coworkers [*Constable and Duba, 1990; Duba et al., 1974; Shankland and Duba, 1990*]. During initial heating an anomalously high conductivity is observed, variously assigned to "dirt" on the sample surface or to amorphous carbon precipitating out of the $CO:CO_2$ gas mixtures at low temperatures in the stability field of graphite.

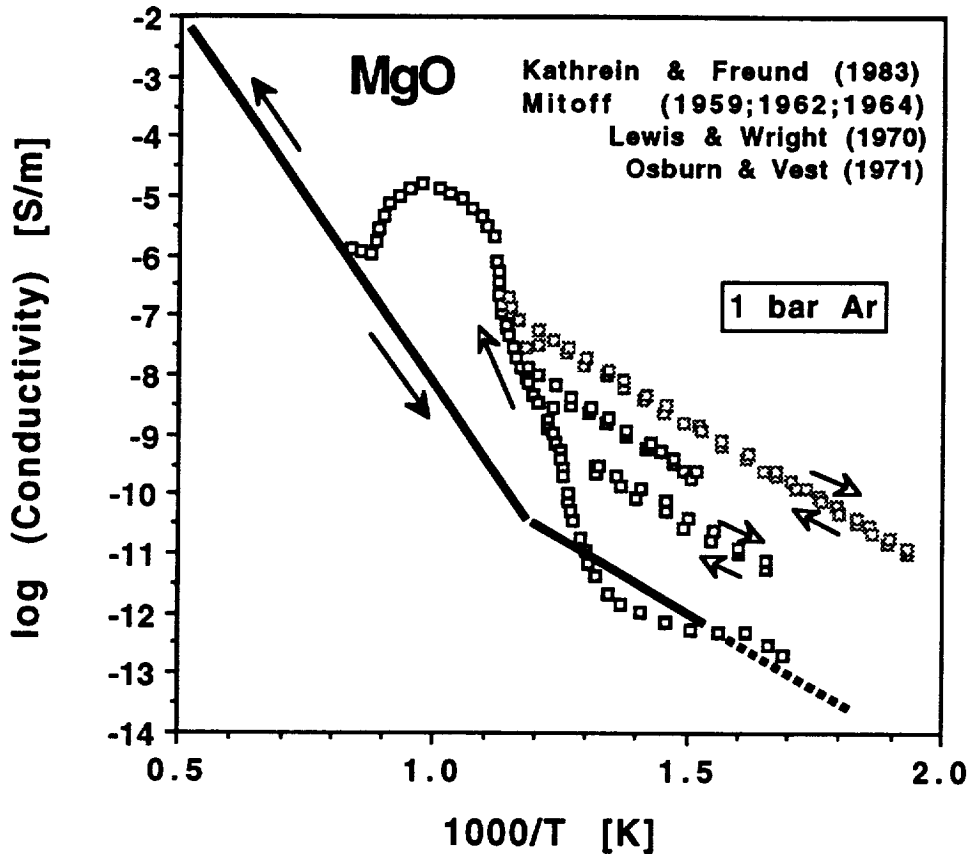

Fig. 2 Typical electrical conductivity behavior of high purity, arc–fusion grown MgO single crystals heated in high purity Ar. The data represented by open squares are adopted from *Kathrein and Freund (1983)*. The small maximum below 400°C (1000/T > 1.5) was confirmed by *Kathrein et al. (1980)*. The steep section of the solid line delineates the high temperature Arrhenius branch as reported by many authors including *Mitoff (1959, 1962, 1964)*, *Lewis and Wright (1970)* and *Osburn and Vest (1971)*. The less steep section and dashed extension is adopted from graphical representations given by *Lewis and Wright (1970)* and from work by *Kathrein and Freund (1983)*.

Surface contamination or structural disorder within a surface layer of unspecified thickness have long been thought to cause the conductivity anomaly in olivine [*Duba, 1972; Duba et al., 1974; Duba et al., 1988; Duba and Shankland, 1982*] and pyroxene [*Duba et al., 1973*]. Recently, Constable and Duba [*1990*] suggested that CO_2 undergoes disproportionation in the stability field of graphite, $CO_2 = C + O_2$, precipitating a layer of amorphous carbon onto the sample surface. Assuming that thermodynamic equilibrium can be achieved around 700°C the precipitated carbon

layer would react with gas phase CO_2 as soon as the CO/CO_2 mixture leaves the stability field of graphite and disappear again, revealing the intrinsic conductivity of the olivine sample under study. The fact that a 1:1 CO/CO_2 mixture at 0.1 MPa leaves the stability field of graphite around 670°C [*Deines, et al., 1974*] the end of the conductivity anomaly around this temperature (see **Fig. 1**) is quoted as supporting evidence for the gas phase CO_2 disproportionation reaction [*Constable and Duba, 1990*]. If this were true, the same conductive carbon layer should form on any substrate heated in a 1:1 CO/CO_2 mixture to any temperature below 670°C. Conversely, no carbon layer and, hence, no electrical conductivity anomaly, should be observed in any CO/CO_2–free gas or gas mixture.

Fig. 2 shows the d.c. conductivity of synthetic MgO single crystals measured in pure Ar at 0.1 MPa pressure, e.g. in a CO/CO_2–free atmosphere. The MgO crystals were of the nominally highest purity grades, 4N or 99.99% with <50 ppm transition metal impurities. They were grown by the carbon arc fusion technique [*Butler et al., 1971*]. The bold line in **Fig. 2** depicts the HT branch with its high activation energy, 2.4 eV, as reported by many authors [*Osburn and Vest, 1971; Sempolinski and Kingery, 1980; Sempolinski et al., 1980*] and a typical LT extension, characterized by a lower activation energy, ≈1 eV. As in the case of olivine, the LT branch is observed during cooling whenever the sample has undergone extensive heating and equilibration at higher temperatures. The open squares represent a conductivity anomaly that closely resembles that of olivine for which Constable and Duba [*Constable and Duba, 1990*] invoked carbon precipitation from the gas phase. When this anomaly was studied in greater detail [*Kathrein and Freund, 1983*], it became clear that it was reversible with a characteristic hysteresis behavior. It could be shown that there in fact are two distinct temperature regions where the conductivity is anomalously high, 300–400°C where the conductivity is in the 10^{-12}–10^{-13} S/m range [*Kathrein et al., 1980*] and 500–800°C. Application of guard electrodes is not fully effective, indicating that the charge carriers may not be confined to the outermost surface [*Kathrein and Freund, 1983*]. Both conductivity anomalies are reversible. In the experiment depicted in **Fig. 2** the heating of the MgO crystal (previously subjected to several temperature cycles up to 800°C) was interrupted by three cooling and reheating cycles at 10°C/min. Three branches were obtained with the same slope as the LT extension from the HT region. Since this measurement was conducted in Ar, the anomaly cannot be blamed on carbon precipitation from a CO_2–containing gas phase.

The similarity between the anomalous conductivity of olivine in CO/CO_2 mixtures and of MgO in pure Ar gas leads us to wonder whether this behavior can really be caused by extraneous surface contamination or by carbon that has precipitated from the gas phase. Maybe both, mantle–derived olivine and synthetic MgO crystals, contain some indigenous charge carriers which are responsible for this peculiar anomaly but which have not yet been correctly identified.

Conventional techniques use electrodes in direct contact with the samples. However, metal–to–insulator contacts often lead to serious perturbations at the interfaces. In addition, conventional techniques are notoriously inept to differentiate between surface and bulk conductivities. We have recently reported on a new non–contacting technique to measure mobile charge carriers in highly

insulating samples under minimum perturbation conditions [*Freund et al., 1990, 1989*]. We shall discuss this new technique in the next chapter and illustrate its application with data of nominally high purity MgO single crystals. Application to natural olivine single crystals and the discussion of possible geophysical implications will be deferred to Part III.

A. Charge Distribution Analysis

In essence, conductivity measurements determine whether or not charge carriers exist in a given sample that can diffuse in an externally applied electric field. Conventionally these measurements are carried out with electrodes in direct contact with the samples. However, the same information can be obtained contact–free by measuring the dielectric response [*Freund, 1990*].

When a dielectric is placed in an electric field $\mathbf{E}_{ext}$ it polarizes. Its polarization $\mathbf{P}$ is given as:

$$\mathbf{P} = \frac{\varepsilon_0(\varepsilon-1)}{4\pi}\,\mathbf{E}_{ext} \qquad (1)$$

where ε_0 is the permitivity of vacuum and ε the dielectric constant. The polarization depends on the frequency at which it is measured and the term "dielectric constant" has been applied to the entire range from optical frequencies, 10^{14}–10^{16} Hz, to 0 Hz [*Kittel, 1980*]. The so–called "static" dielectric constant is usually measured at 10^3–10^6 Hz and extrapolated to 0 Hz.

In a homogeneous electric field the dielectric experiences no net acceleration. However, when placed in an electric field gradient along a direction z, a force $\mathbf{F}_z$ acts on the sample which draws it towards the region of higher field density. In the case of an ideal dielectric the force is independent of the polarity: $\mathbf{F}_z^{\pm} = \mathbf{F}_z^{+}(\mathbf{E}_{ext}) = \mathbf{F}_z^{-}(-\mathbf{E}_{ext})$. Using Maxwell's equations $\mathbf{F}_z$ is given by:

$$\mathbf{F}_z = \int_V \nabla(\mathbf{P}\cdot\mathbf{E}_{ext})\,dV \qquad (2)$$

where the volume integral must include the sample but not the sources of the field.

In the case of a real dielectric, e.g. a material containing various defects and impurities, this force is generally <u>not</u> independent of the polarity, $\mathbf{F}_z^{+}(\mathbf{E}_{ext}) \neq \mathbf{F}_z^{-}(-\mathbf{E}_{ext})$. For the purpose of the present paper we break the polarization down into five contributions, $\mathbf{P}_{el} + \mathbf{P}_{ion} + \mathbf{P}_{local} + \mathbf{P}_{space} + \mathbf{P}_{surface}$. The first two contributions refer to the ideal structure [*Ashcroft and Mermin, 1976*]. $\mathbf{P}_{el}$ represents the electronic polarization of the electronic shells of atoms and ions which can follow fields that oscillate at frequencies up to 10^{14}–10^{16} Hz. $\mathbf{P}_{ion}$ represents the ionic polarization due to the field–induced displacement of atoms and ions which have typical response times of the order of 10^{-9}–10^{-12} sec. The last three contributions arise from defects or impurities and generally have longer relaxation times. $\mathbf{P}_{local}$ contains contributions from local dipoles which may rotate in the electric field but not diffuse over macroscopic distances. $\mathbf{P}_{space}$, the space charge polarization, is caused by charges which can diffuse over macroscopic distances. Space

charge polarization can also occur in the absence of externally applied electric fields. Surface charges occur because (i) the free energies of formation of cation and anion vacancies in ionic crystals in the bulk differ from those near the surface and thus create an imbalance [*Kliewer and Koehler, 1965; Lehovec, 1953*], (ii) the energy levels in the valence and conduction bands as well as in impurity levels are shifted [*Kittel, 1980*], and (iii) if charge carriers of one sign have a significantly higher mobility than the compensating charge carriers of the opposite sign, a charge layer forms at the surface together with a subsurface depletion zone [*Sze, 1969*]. We combine (i) to (iii) into the $\mathbf{P}_{surface}$ term and refer to it summarily as the "surface charge".

$\mathbf{P}_{el}$ and $\mathbf{P}_{ion}$ weakly dependent upon temperature (T) [*Thorp et al., 1986*]. $\mathbf{P}_{local}$ may be T–dependent to the extent that local defects with a dipole moment are subject to thermally activated reorientation in the applied electric field. Their dipole moments, $\mu = d \cdot e$, are small because d, the separation between the charges e, is of the order of interatomic distances, 10^{-8} cm. Hence, $\mathbf{P}_{local}$ is not expected to make a large contribution. By contrast, $\mathbf{P}_{space}$ can be large, if charges diffuse over large distances. At the limit d may be the size of the crystal in field direction, say 10^{-1} cm, and dipole moments stemming from diffusing mobile charges may make a contribution $\approx 10^7$ times larger than that from rotating local dipoles.

$\mathbf{P}_{el}$, $\mathbf{P}_{ion}$, $\mathbf{P}_{local}$, and $\mathbf{P}_{space}$ are invariant to the reversal of the field gradient. By contrast $\mathbf{P}_{surface}$ contributions are variant to field gradient reversal. This means that a dielectric with a surface charge will be either attracted to or repelled from the region of higher electric field density, depending on the sign of the charge and the polarity. Assuming that bulk and surface terms are independent of each other we can separate field–invariant and field–variant contributions by forming the linear combinations:

$$\mathbf{F}_\Sigma \equiv \frac{1}{2}(\mathbf{F}^- + \mathbf{F}^+) = \frac{\varepsilon_o(\varepsilon\text{-}1)}{4\pi} \int_V \nabla[(\mathbf{P}_{el} + \mathbf{P}_{ion} + \mathbf{P}_{local} + \mathbf{P}_{space})]\mathbf{E}_{ext}\, dV \qquad (3)$$

$$\mathbf{F}_\Delta \equiv \frac{1}{2}(\mathbf{F}^- - \mathbf{F}^+) = \int_V \nabla(\mathbf{P}_{surface} \cdot \mathbf{E}_{ext})\, dV \qquad (4)$$

Eqs. (3) and (4) reveal an important feature of the CDA technique: its capacity to determine the sign of a surface charge and, hence, the sign of the majority carriers. This information is normally not available through conductivity measurements, but only through Seebeck coefficient (thermopotential) and Hall measurements [*Ashcroft and Mermin, 1976; Kittel, 1980; Sze, 1969*].

To evaluate $\mathbf{F}_\Sigma$ and $\mathbf{F}_\Delta$ we subtract $a_\pm U^2$ from $\mathbf{F}^\pm$ where U is the voltage and $a_\pm$ are constants:

$$\mathbf{F}^\pm = \mathbf{F}_0^\pm + a_\pm U^2 \qquad (5)$$

The $a_\pm U^2$ term with $a_- = a_+$ describes the ideal dielectric, while $\mathbf{F}_0^\pm$ arises from the charge at the surface which acts as an electrostatic mirror. With this approximation $\mathbf{F}_\Sigma$ and $\mathbf{F}_\Delta$ become:

$$\mathbf{F}_\Sigma = \frac{1}{2}(\mathbf{F}_0^- + \mathbf{F}_0^+) + \frac{1}{2}(a_- + a_+)\, U^2 \qquad (6)$$

$$\mathbf{F}_\Delta = \frac{1}{2}(\mathbf{F}_0^- - \mathbf{F}_0^+) + \frac{1}{2}(a_- - a_+)\, U^2 \qquad (7)$$

At low voltages we can set $\mathbf{F}_0^+ = \mathbf{F}_0^- + \delta\mathbf{F}$, and $a_- = a_+ + \delta a$, where $\delta\mathbf{F} \ll \mathbf{F}_0^\pm$ and $\delta a \ll a_\pm$. This corresponds to a small perturbation of the $\mathbf{P}_{surface}$ contribution representing the electrostatic mirror. At high voltages the $\mathbf{F}_0^\pm$ terms become negligible and $a_\pm = 1/2\,(a_+ + a_-)$. We can thus define $\mathbf{F}_\Sigma$ and $\mathbf{F}_\Delta$ through their high and low voltage limits, respectively:

$$\mathbf{F}_\Sigma \approx \tfrac{1}{2}(a_- + a_+)\,U^2 \equiv a\,U^2 \qquad \text{; for high U} \qquad (8)$$

$$\mathbf{F}_\Delta \approx \tfrac{1}{2}(\mathbf{F}_0^- - \mathbf{F}_0^+) \qquad \text{; for low U} \qquad (9)$$

Experimental

For the CDA measurements a PERKIN-ELMER Thermogravimetric Analyzer TGS-2 was modified by the introduction of a circular Au bias electrode (3 mm diameter) at the bottom of the cup–shaped Pt furnace (10 mm internal diameter, 18 mm height), and of an annular Au counterelectrode (12 mm high) on the inside wall of the furnace reaching from its upper rim downwards. Thus the electric field lines were symmetrical to the cylinder axis, emerging vertically from the bias electrode at the bottom fanning out upwards and ending horizontally in the counterelectrode. The bias electrode and counterelectrode were connected to the ± output and ground respectively, of a KEITHLEY 240A digital voltage source (±1100V). The Pt windings of the furnace were bifilar and a.c. operated using one half period of the sine wave for power and the other for measuring the resistance and, hence, the temperature. The sample rested at four points on a Pt stirrup (0.1 wire, 6 mm diameter loop) suspended from a fused silica fiber, well insulated from ground. The Pt stirrup gave no contribution to the CDA measurements except for a constant off–set that was independent of temperature. The distance between the lower sample surface and the bias electrode was chosen at different values, generally at 150 ± 20 μm. In its most sensitive range the balance can detect forces equivalent to an apparent weight change of $<10^{-7}$ g.

The samples were nominally high purity MgO single crystals, grown from a CO/CO_2–saturated melt in a carbon arc fusion furnace [*Butler et al., 1971*] by W. & C. Spicer, Ltd., England. The crystals were rated 4N with less than 100 ppm cationic impurities, typically ≈10 ppm of Cr, Mn, and Ni, <30 ppm Fe, and <50 ppm (Al + Si). In addition they contain OH^- in the range of 10–100 at.–ppm, due to the presence of adsorbed H_2O in the MgO powder starting material [*Chen, et al., 1975; Freund and Wengeler, 1982*]. The crystals came as large (3-10 cm^3) cubes or "as grown" thumb–sized forms bordered by pitted, irregular growth surfaces. The crystals were slightly yellowish–brown, due to color centers not related to transition metal impurities. Except for a clear rim of 2–4 mm thickness adjacent to the growth surfaces, the crystals were typically cloudy in the center, due to a network of curved subgrain boundaries decorated by μm–sized cavities. For the CDA experiments pieces (approximately 6 x 6 x 2 mm) were obtained by cleavage. To approximate a cylindrical shape the four edges were rounded on SiC sanding paper. The crystals were cleaned in acetone and methanol, dried in air, and subjected at least one *in situ* heating and cooling cycle up to 800–900°C.

All measurements were performed in high purity, dry Ar at a flow rate of about 10 ml/min with no additional control of the oxygen fugacity. Heating between temperatures (25 or 50°C increments) was at 20°C/min. After reaching the maximum temperature the crystals were cooled to 25°C or 100–150°C at 1°C/min. During heating the samples were allowed to thermally equilibrate at each step prior to the application of the bias voltages. An equilibrium time of about 5 min was generally found sufficient. The positive and negative bias was applied in 2, 5, 10, 20, 50 or 100 V increments, depending upon the experiment. After each sequence the dielectric polarization of the sample was allowed to relax under 0 V bias for several minutes while the temperature was raised to the next step. At some temperatures "creeping" occurred, e.g. the dielectric polarization increased over several minutes to an hour. The creeping was not due to slow thermal equilibration of the sample under study but to the appearance of charges which diffused in the electric field gradient. Creeping under positive bias was, as a rule, slower than creeping under negative bias at the same temperature, indicating that the diffusion of charge carriers within the sample was not symmetrical. Whenever the creeping rates differed markedly under positive and negative bias, a surface charge developed, indicating that the asymmetry in the charge carrier diffusion process is caused by the filling of surface states. Occasionally, to test the reproducibility, the sequence of positive and negative bias application was reversed. Except for the temperature intervals marked by "creeping" and except for cases where insufficient time was given for relaxation of the sample under 0 V bias, the reproducibility was typically better than ±10%, independent of whether the sample was first polarized under positive or under negative bias.

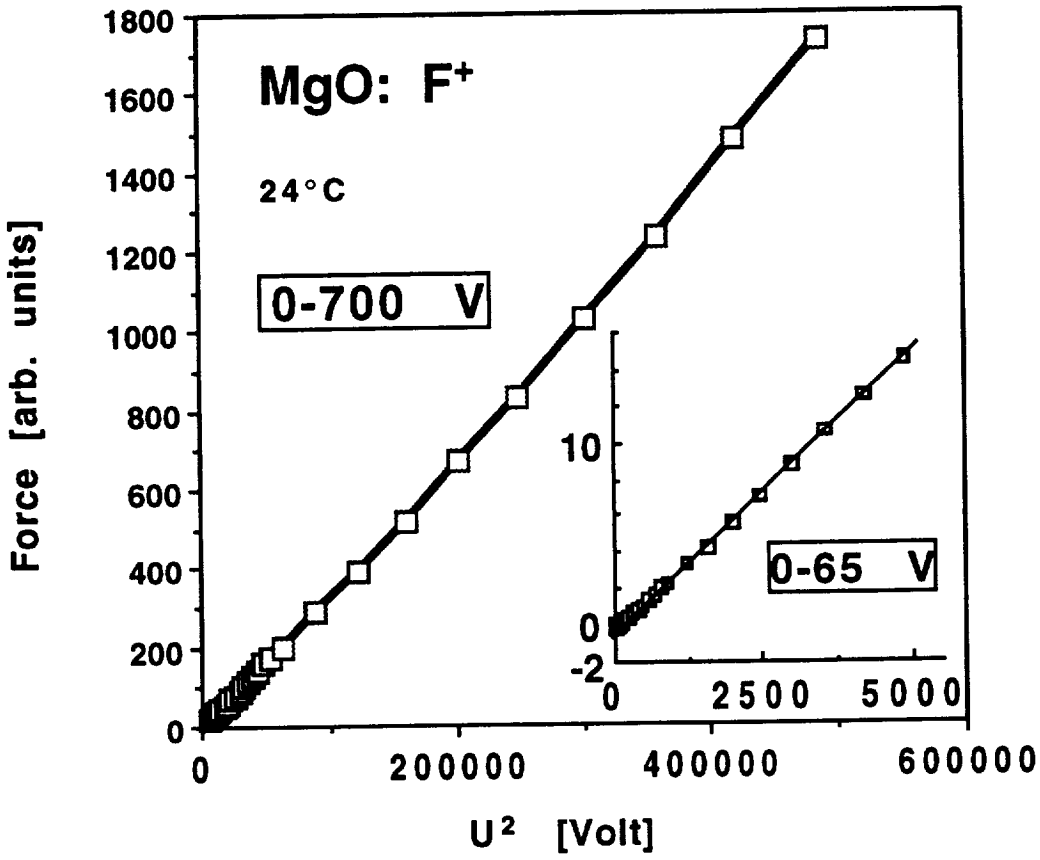

Fig. 3 Plot of F^+ versus U^2 at 24°C over the voltage range 0-700 V showing that, except for a slight deviation at low voltages (inset) a parabolic straight line is obtained, indicating that MgO behaves as a near–perfect dielectric material. The slope of the line is proportional to the dielectric susceptibility, $\chi = \varepsilon - 1$, where ε is the dielectric constant. The intersect with the ordinate at –0.75 V indicates a weak positive surface charge.

Results and Discussion

At ambient temperature the MgO crystal responded as a nearly ideal dielectric material: immediately after application of the field gradient a force was measured which remained constant with time. The force was proportional to the square of the applied voltage, $F^+ \propto U^2$, as shown in **Fig. 3**, giving a near–perfect straight line over the range 0–700V. Its slope is proportional to the dielectric susceptibility ($\varepsilon - 1$) where ε is the dielectric constant, 9.6 for MgO [*Gourley and Runciman, 1973*]. At low voltages a small deviation is noted (inset in **Fig. 3**), indicating an

intersect with the ordinate at about –0.75 force units. This repulsion under positive bias is due to a weak $\mathbf{P}_{surface}$ term, suggesting a weak positive surface charge on the MgO crystal under study.

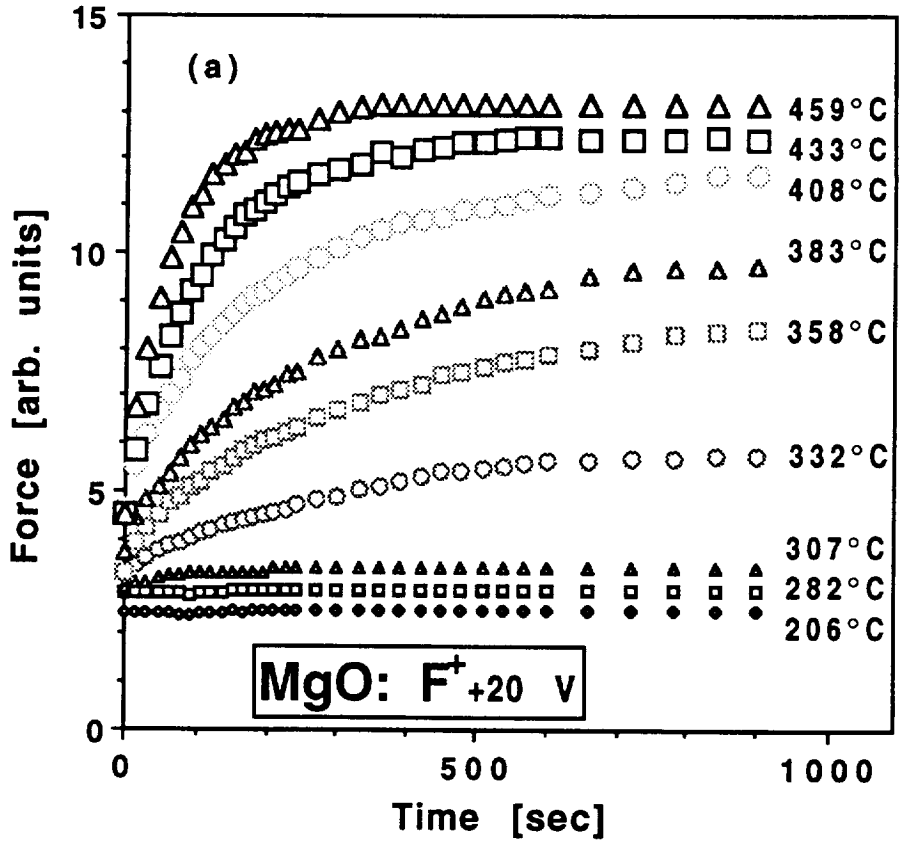

Fig. 4a F^+ measured as a function of time at +20 V between 200-585°C. Note "creeping" above 300°C.

Normally one would not expect any drastic change of the dielectric polarization with temperature (T) because the T dependence of the $\mathbf{P}_{el}$ and $\mathbf{P}_{ion}$ terms, characteristic of any ideal dielectric, is of the order of the volume thermal expansion coefficient. This expectation, however, is not fulfilled at $T \geq 300$°C as illustrated by **Fig. 4**. In (**a**) we show that $\mathbf{F}^+$, measured as a function of time (t) at +20 V, remains nearly constant below 282°C. At 282°C and more clearly at 307°C $\mathbf{F}^+(t)$ increases slightly during the first 200 sec. At 332°C the "creeping" extends over at least 900 sec, becoming progressively faster with increasing T and reaching a steady state at 459°C after about 300 sec, about 5 times larger than $\mathbf{F}^+$ at 200°C. At higher T the kinetics further change as shown in (**b**). At 484°C and 510°C the creeping is slow lasting for over 1500 sec. At 534°C a steady

state is reached within ≈600 sec. This time shortens to <90 sec at 585°C. At 585°C, the steady state F^+ value is ≈15 times larger than F^+ around 200°C. This time–dependent increase in the dielectric response suggests the appearance of mobile charge carriers in the MgO crystal under study.

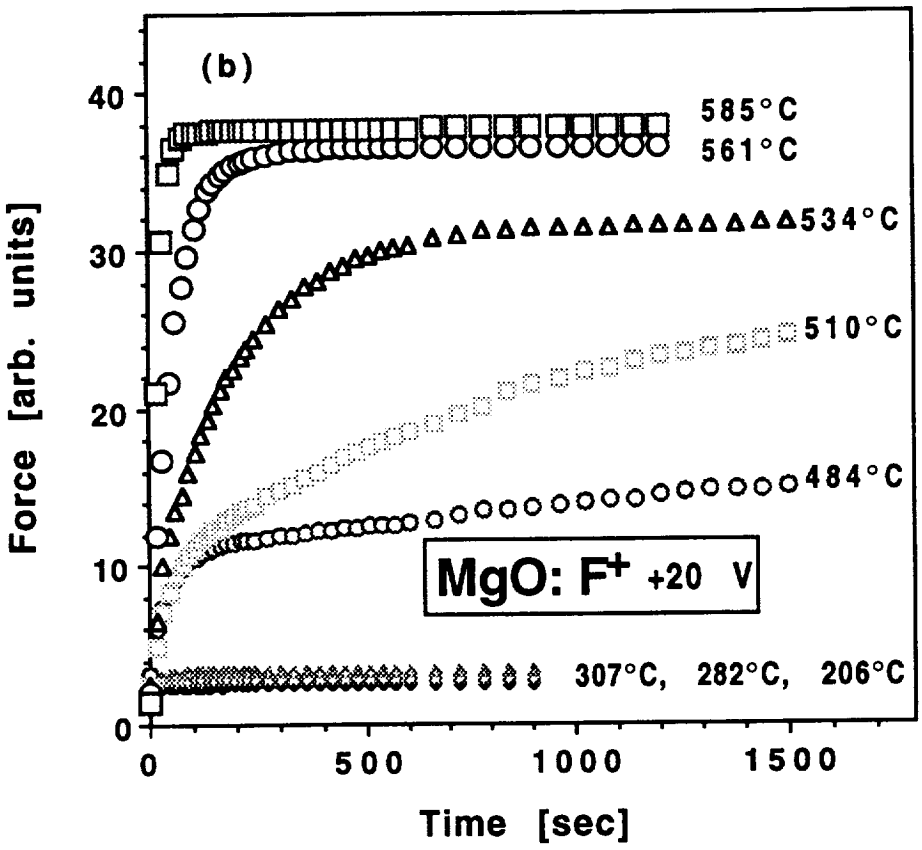

Fig. 4a/b F^+ measured as a function of time at +20 V (a) between 200-585°C and (b) up to 585°C. Note the different ordinate scales and the extended "creeping" above 300°C.

In order to study the surface charge contribution, $P_{surface}$, we measured F^+ and F^- under otherwise identical conditions but at higher bias voltages of ±50 V. The higher bias voltage increases the electric field gradient and thus not only increases F^+ but also increases the charge carrier diffusion. In **Fig. 5** we show the result of the measurements below 425°C when the d.c. conductivity of the same purity–grade MgO crystal (**Fig. 2**) displayed a shallow maximum*. The CDA measurements were carried out at follows: The crystal was first heated in Ar to 800°C, then

* In this and the next figures $F^{\pm}$, F_{Σ} and/or F_{Δ} are plotted versus T [°C], not 1/T [K].

cooled at 10°C/min to 150°C and annealed overnight in Ar. It was cooled further to 75°C and reheated in a stepwise fashion at 20°C/min in small 5–10°C increments to a series of temperatures between 75–410°C. After 4–5 min equilibration at each temperature –50 and +50 V were applied. $F^+(t)$ and $F^-(t)$ were measured at 2 sec resolution over about 60 sec. Between reversals from +50 V to –50 V the crystal was allowed to relax at 0 V for 2–5 min, depending upon the rate of creeping.

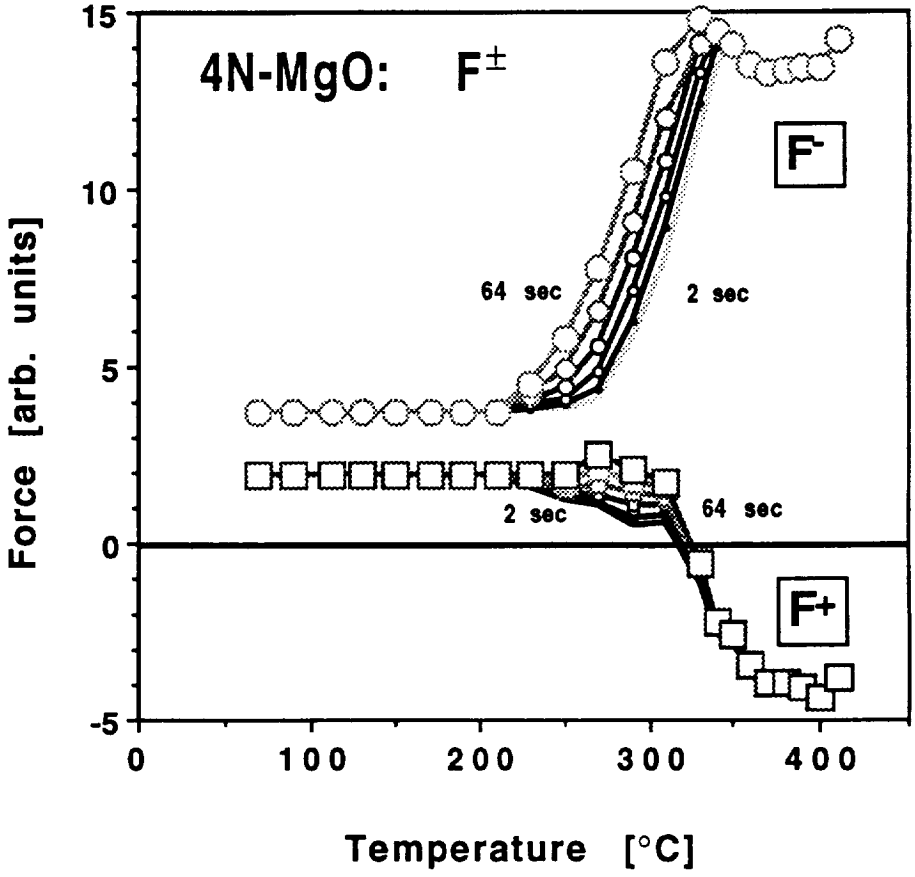

Fig. 5 CDA response of MgO under ±50 V below 425°C, indicating the appearance of mobile charges above 225°C and an enhancement of the positive surface charge.

Over the entire temperature interval F^- was larger than F^+, e.g. $F_\Delta > 0$, indicating a positive $P_{surface}$ contribution. Below 220°C both F^- and F^+ are constant. Between 225–325°C, F^- increased about three– to fourfold, reaching a small maximum around 325°C. F^+ decreased above 300°C and became repulsive above 325°C, indicating a positive $P_{surface}$ contribution strong

enough to repel the sample from the bias electrode, e.g. from the region of higher electric field density.

It is instructive to compare the CDA response as shown in **Fig, 5** with the d.c. conductivity of MgO as measured by conventional techniques over same temperature interval, 100–425°C [*Kathrein and Freund, 1983*]. As is apparent from **Fig. 2** the conductivity is extremely low, $10^{-12} - 10^{-14}$ S/m, equivalent to $10^{-14} - 10^{-16}\ \Omega^{-1}cm^{-1}$, meaning that only 10^2–10^4 charge carriers pass through 1 cm^2 sample cross section per volt·second. In order to measure such low conductivities special efforts have to be made to minimize electric stray fields, electrostatic charging, surface conduction and thermopotentials. In **Fig. 6** we show the results of a d.c. conductivity measurement of an MgO disk of 14 mm diameter, 1 mm thickness with two circular Pt electrodes (7 mm effective diameter) and an annular guard electrode. The measurements were carried out under highest purity Ar on a fused silica support using shielded leads up to within 1 cm of the electrodes using a furnace with a low voltage SiC heater. The entire apparatus, including the d.c. circuit, was built into a fully enclosed Faraday cage, set on Teflon blocks. Batteries were used as a voltage source (500–1000 V) and the currents were measured in the 10^{-12} amps range by means of a battery–operated KEITHLEY 610C electrometer during slow (2–5°C/min) heating/cooling cycles. The response was ohmic between 500–1000 V. Curve 1 represents the current measured after annealing the MgO crystal at 25°C for >12 hrs. Upon cooling the current fell into the $<10^{-13}$ amps range and eventually reversed sign, due to thermopotentials or electrode–related depolarization currents. Curves 2 and 3 were obtained upon reheating after 2–6 hrs of annealing at 100°C.

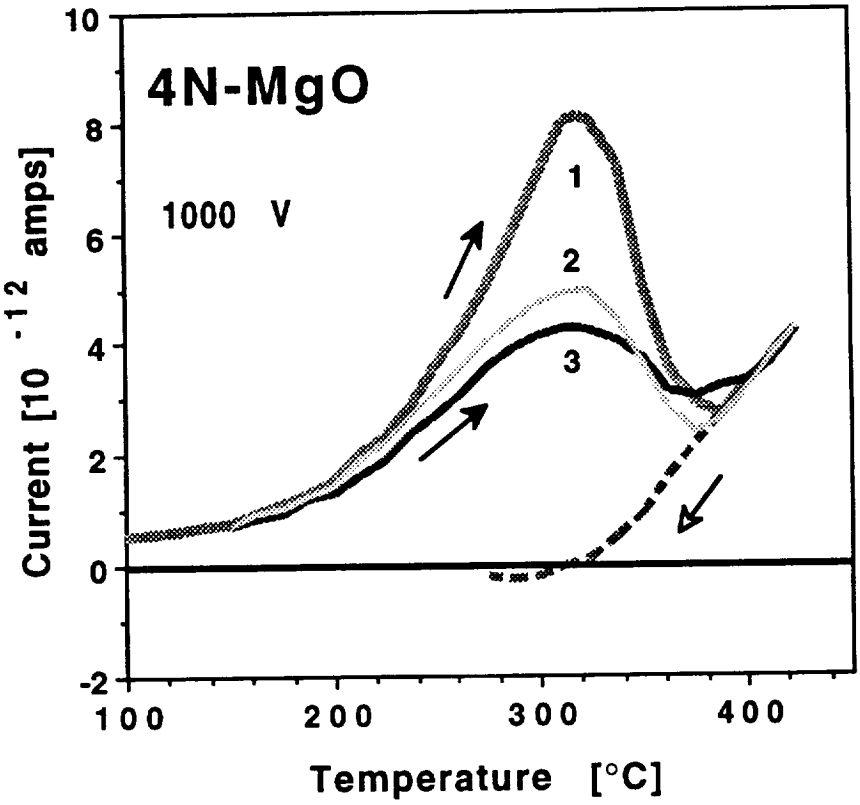

Fig. 6 D.c. Conductivity of MgO measured with a 3–electrode configuration and a high field between 100–425°C. Curves 1, 2 and 3 reflect various heating cooling cycles with increasingly shorter annealing times at room temperature or 100°C (after [*Kathrein et al., 1980*]).

The conductivity maxima around 300–400°C and the hysteresis behavior which depended upon the annealing time were reproducible. When these measurements were reported several years ago [*Kathrein et al., 1980*] the nature of the charge carriers was still uncertain. On the basis of the CDA measurements depicted in **Fig. 5** we can now say that the 200–400°C conductivity anomaly in the MgO crystals is not a "dirt" effect caused by the high d.c. voltages or due to an extraneous surface contamination. Furthermore, we now know that the charge carriers are positive and that they are capable of building up a strong internal field within the crystal.

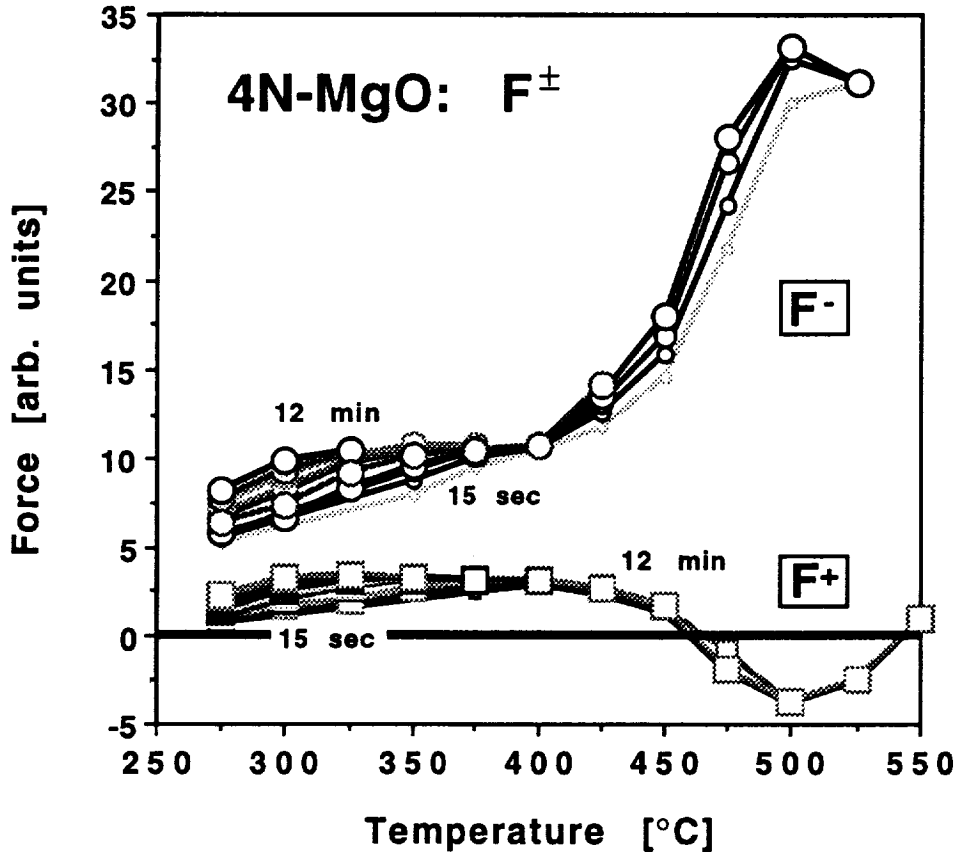

Fig. 7 CDA response at the on–set of the large d.c. conductivity anomaly depicted in **Fig. 2.** The stepwise increase of F^+ above 400°C signals the appearance of mobile charges. The fact that $F^- > F^+$ indicates that the charges are positive and lead to a strong positive surface charge on the MgO crystal.

Fig. 7 shows F^- and F^+ between 275–550°C. At each temperature F^- was measured first, followed by 2-3 min relaxation at 0 V, and F^+ measurement. F^- remained larger than F^+, indicating a continuation of the positive surface charge. Above 400°C F^- increased rapidly while F^+ decreased and eventually became repulsive around 475°C, indicating an enhancement of the positive surface charge. Creeping became prominent for F^- between 400–525°C but was nearly absent from F^+. This was in disagreement with the pronounced creeping under positive bias shown in **Fig. 4b** probably because, after application of the negative bias, the system was given only relatively short time (2-3 min) to relax under 0 V before the positive bias was applied. Because a negative bias tends to attract positive charges to the surface, the subsequent application of the positive bias encountered a surface that was already in a saturated state.

The appearance of the strong positive surface charge (F_Δ) between 450–500°C, coincident with the stepwise increase of the field–invariant dielectric polarization (F_Σ) and the concomitant sharp rise of the d.c. conductivity, does not support the notion of surface contamination [*Freund, 1990; Freund et al., 1989*]. Surface contamination cannot give rise to any surface charge that is maintained by an internal electric field.

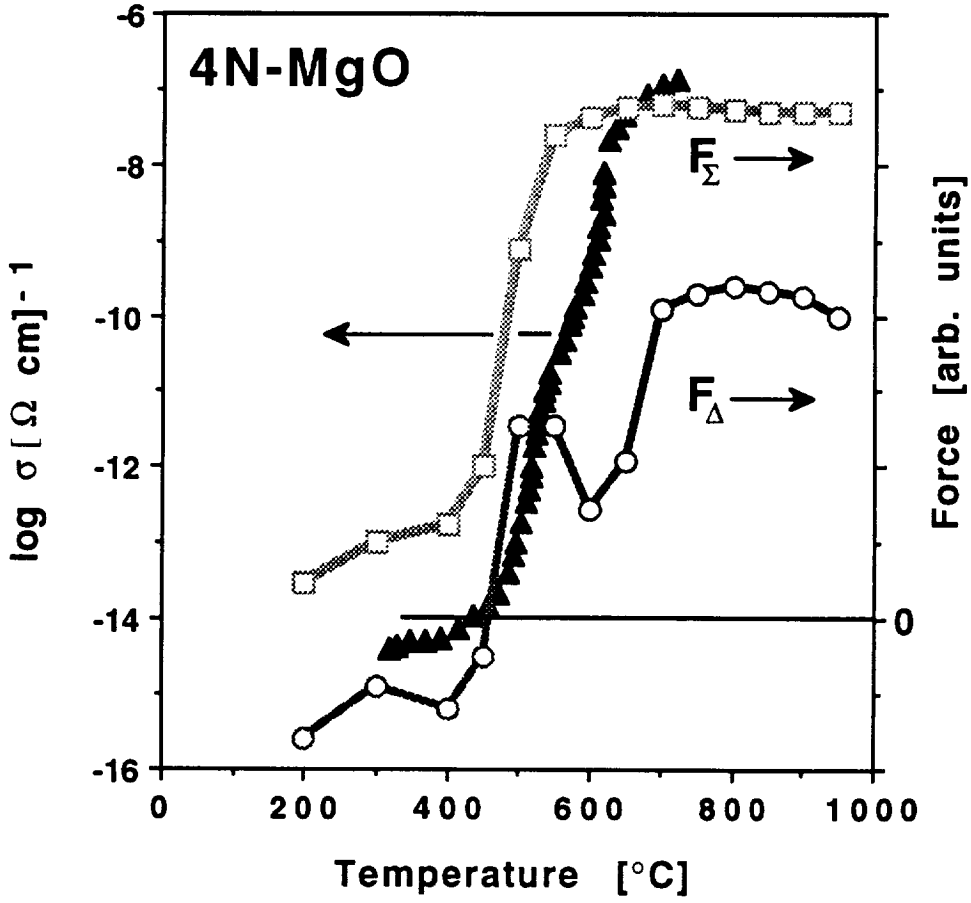

Fig. 8 Portion of the d.c. conductivity curve between 300–700°C (solid triangles) from **Fig. 2** (left scale) plotted together with F_Σ (open squares) and F_Δ (open circles) from a CDA experiment using a very slowly cooled MgO crystal.

In **Fig. 8** we plot $F_\Sigma(T)$ and $F_\Delta(T)$ from a different run together with the 300–700°C section of the d.c. conductivity rise towards the anomaly from **Fig. 2**. $F_\Sigma(T)$, the sum of the field–invariant contributions, shows the large step–wise increase between 400–500°C that coincides

with the increase in the d.c. conductivity and an essentially flat portion above 600°C. Despite a small maximum towards positive values at 300°C $\mathbf{F}_\Delta(T)$ was found to be weakly negative below 425°C — a behavior which seemed to be typical of very slowly cooled MgO crystals, possibly indicating an intrinsically negative surface under conditions apporaching thermodynamic equilibrium, due to differences in the free energies of formation of anion and cation vacancies in the surface–near region [*Kingery, 1974; Kliewer and Koehler, 1965*]. Above 450°C, however, $\mathbf{F}_\Delta$ turned strongly positive as it did in every CDA experiment conducted with these MgO crystals. In a narrow region around 500–550°C the steady state $\mathbf{F}_\Delta$ values remained undetermined due to creeping. $\mathbf{F}_\Delta$ stayed positive up to 950°C exhibiting a shallow maximum around 800°C.

According to eq. (9) it is best to measure $\mathbf{F}_\Delta$ at low bias voltages because, according to eq. (5), $\mathbf{F}^+$ and $\mathbf{F}^-$ are proportional to the square of the bias voltage plus a linear term. Low bias voltages bring out this linear term. In **Fig. 9a–c** we plot $\mathbf{F}^+$ and $\mathbf{F}^-$ for three selected temperatures from 0 to +45 V and −35 V, measured at 2 V increments.

The "as measured" data show a repulsive response under positive bias and, less pronounced, an extra attraction under negative bias. The linear terms are given by the sections parallel to the abscissa above the critical bias voltage. Below this critical voltage ($U_{crit.}$) the absolute values $|\mathbf{F}_0^+|$ and $|\mathbf{F}_0^-|$ increase linearly with U meaning that $\mathbf{P}_{surface}$ is constant from 0 to $U_{crit.}$. Above this threshold value the surface contribution recedes as $\mathbf{P}_{surface} \propto 1/U$. This means that the surface charge acts elastically like a spring which is pushed back into the bulk by the externally applied positive bias. Note that $U_{crit.}$ reaches values as high as +25 V. An internal electric field which pins positive charges to the MgO surface and can resist such a high externally applied field implies the presence of surface states which are energetically stable. The fact that such surface states can only be populated with charge carriers from within confirms our contention that the charge carriers in the MgO crystals under study are generated in the bulk.

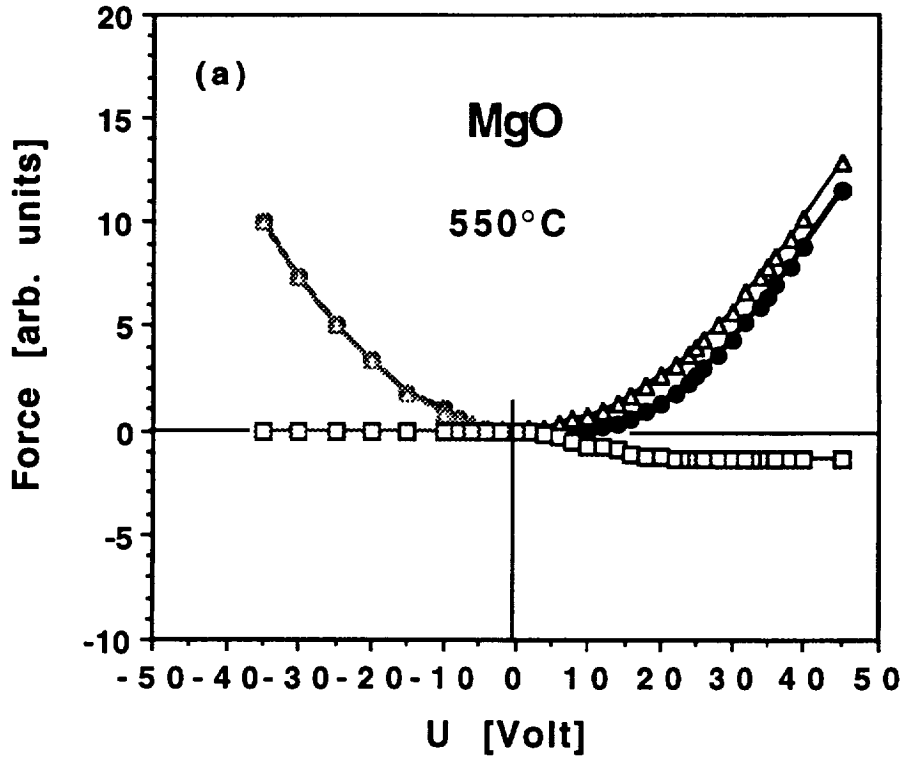
(a)
MgO
550°C
Force [arb. units]
U [Volt]
20
15
10
5
0
-5
-10
-50 -40 -30 -20 -10 0 10 20 30 40 50

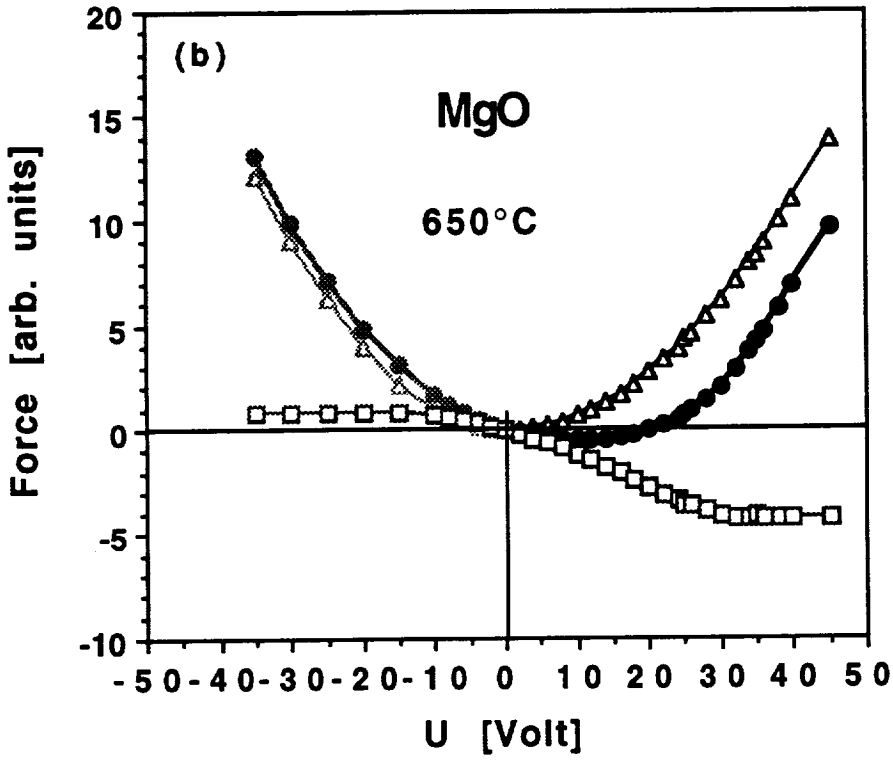
(b)
MgO
650°C
Force [arb. units]
U [Volt]
20
15
10
5
0
-5
-10
-50 -40 -30 -20 -10 0 10 20 30 40 50

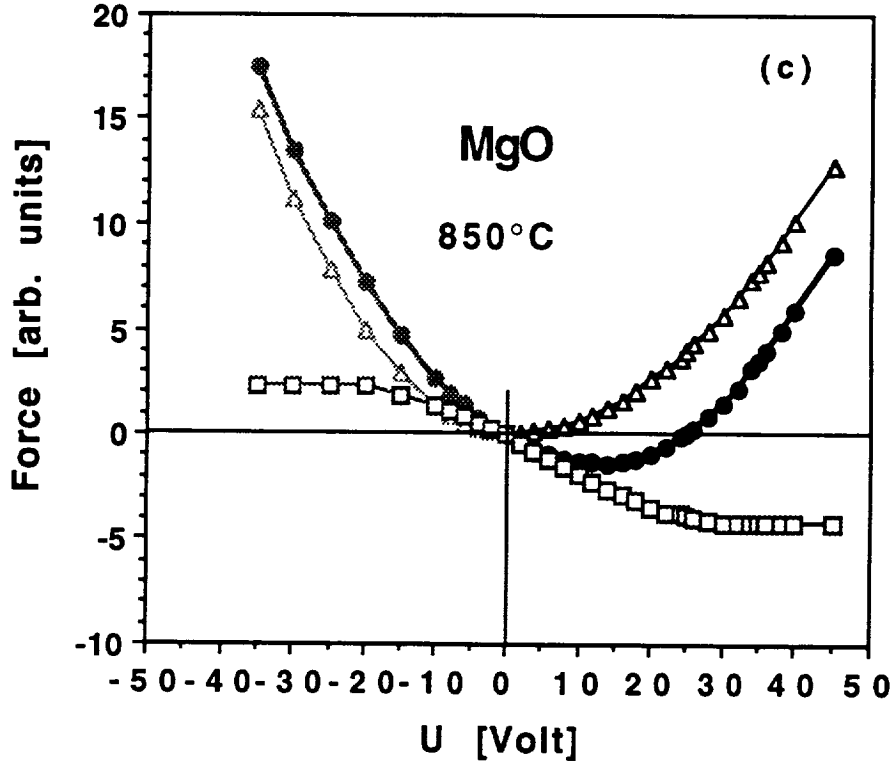

Fig. 9 Deconvoluted F^+ and F^- data at low bias voltages according to eq. (5). The solid circles are the "as measured" data. The open triangles represent the parabolic term which describes the ideal dielectric response, $F^{\pm} \propto U^2$. The open squares represent the linear term, $F_0^{\pm}$, arising from the presence of surface charges. Repulsion under positive bias indicates that the surface charge is positive. U_{crit} is the bias voltage above which the externally applied electric field overcomes the internal electric field.

Since the MgO crystal represents a closed system and is electrically decoupled from the outside by the highly insulating fused silica hang-down fiber overall charge neutrality must be maintained. We therefore conclude that the inside of the MgO crystal contain a negative charge which is equal to the sum of all positive surface charges. The positive charges which come to the surface above 500°C diffuse relatively rapidly as is demonstrated by the kinetic CDA curves in **Figs. 4a/b**. Since all CDA phenomena reported here are reversible at sufficiently slow cooling rates, the charge carriers must be able to retrodiffuse into the bulk. While the charge carrier diffusion towards the surface is probably caused by mutual repulsion in the interior, the retrodiffusion may be driven by the field gradient between the positive surface and the negative interior.

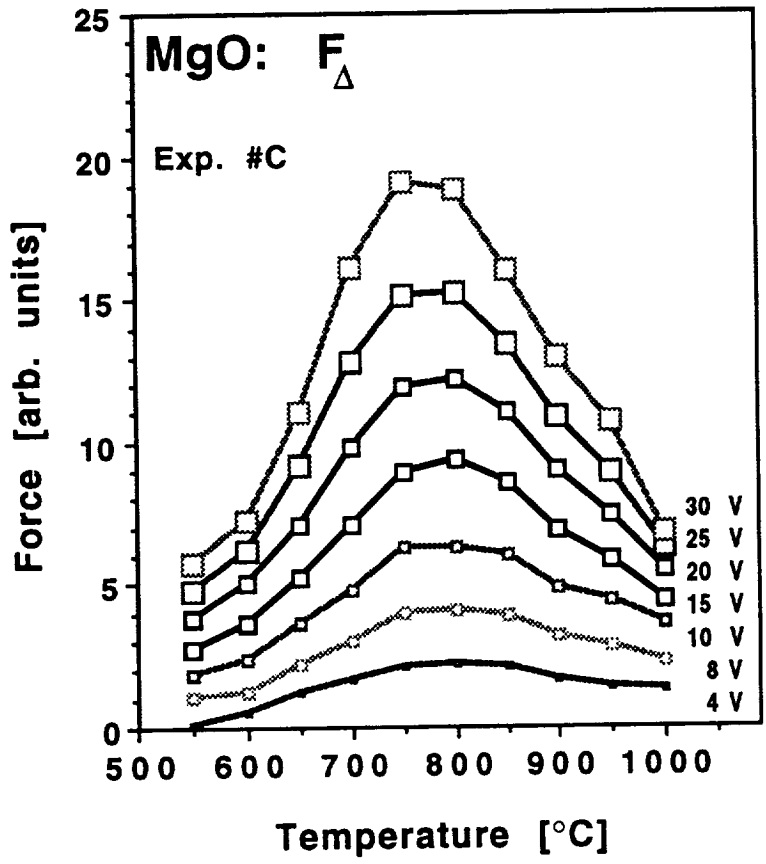

Fig. 10 Variation of F_Δ as a function of temperature between 550–1000°C. The maximum observed around 750–800°C indicates that the density of positive charge carriers at the surface peaks around this temperature.

Fig. 8 already indicated that F_Δ reaches a maximum around 800°C. In **Fig. 10** we focus on the temperature region 550–1000°C, plotting $F_\Delta(T)$ as measured in the 0 to ±30 V bias range in 2 V and 5 V incremental steps. The plot confirms that F_Δ is temperature dependent and reaches a maximum around 750–800°C. Prolonged exposure to temperatures above 800°C led to an irreversible loss of CDA response similar to the irreversible loss of the anomalously high d.c. conductivity that was shown for MgO in **Fig. 2** and for olivine in **Fig. 1**. The probable cause for this irreversibility will be discussed in more detail in Part II.

Conclusion

CDA has provided us with the means to show that, contary to widespread belief, the d.c. conductivity anomalies below 700–800°C in MgO cannot be due to surface damage or contamination either prior to or during the experiment. Instead the CDA data suggest that some peculiar charge carriers exist in the bulk of the MgO crystals under study. These charges are reversibly generated during heating and consumed during cooling. They carry a positive sign. The process is reversible upon cooling but becomes partly irreversible after the crystals have been heated for extended periods of time at temperatures exceeding 700–800°C, even in pure Ar. The strongest argument so far in favor of an indigenous source is based on the appearance of the positive surface charge in both temperature intervals of anomalously high d.c. conductivity, between 200–400°C and between 500–800°C. The uniqe features of CDA is its capacity to show that the surface charge is sustained by a strong internal electric field. Such an internal field implies that the charges originate in the bulk and are driven to the surface by some internal force.

This conclusion invites speculations about the nature of these charge carriers and how they were introduced into the nominally high purity MgO crystals. So far we know that these charge carriers are positive and mobile at temperatures at which ionic mobilities, for instance of Mg^{2+} or O^{2-} via vacancy hopping or by interstitial diffusion, are still extremely small in MgO [*Sempolinski and Kingery, 1980; Sempolinski et al., 1980*]. Only holes, e.g. defect electrons, can have sufficient mobility to explain the observations. Now, holes can exist on (i) the cation or (ii) the anion sublattice. In case (i) they would correspond to a transiently oxidized transition metal cation, for instance Fe^{3+} on a Mg^{2+} site. In case (ii) they would consist of O^- on an O^{2-} site and as such deserve the designation of "positive holes" [*Griscom, 1990; Henderson and Wertz, 1977*]. Given the low transition metal concentration in the MgO crystals under study it is unlikely that cation impurity–bound holes are responsible for the observed phenomena. Therefore, positive holes remain the only candidates. In Part II we shall present data obtained by other techniques which allow us to go beyond the as yet tentative assignment and unambiguously identify the charge carriers that are responsible for the electrical conductivity anomalies in MgO below 700–800°C.

Acknowledgements

This work was supported in part by the National Aeronautics and Space Administration through the Cooperative Agreement with the SETI Institute NCC 2-446 and the NASA Ames Research Center Directors' Discretionary Fund, by the NATO Grant RG.890479, and the European Economic Communities Contract EN 3C-0023-D. F.F. acknowledges receipt of a National Research Council Senior Associateship during the early part of the work.

References

Ashcroft, N.W., and N.D. Mermin, *Solid State Physics*, Holt–Saunders Internatl., Philadelphia, PA. and Tokyo, 1976.

Ballhaus, C., R.F. Berry, and D.H. Green, Oxygen fugacity controls in the Earth's upper mantle, *Nature*, 348, 437-440, 1990.

Beran, A., and A. Putnis, A model of the OH positions in olivine, derived from infrared-spectroscopic investigations, *Phys. Chem Minerals*, 9, 57-60, 1983.

Bradley, R.S., A.K. Jamil, and D.C. Munro, The electrical conductivity of olivine at high temperatures and pressures. *Geochim. Cosmochim. Acta*, 28, 1669-1678, 1964.

Buening, D. K., and P. R. Busek, Fe-Mg lattice diffusion in olivine., *J. Geophys. Res.*, 78, 6852-6862, 1973.

Butler, C.T., B.J. Sturm, and R.B. Quincy, Arc fusion growth and characterization of high-purity magnesium oxide single crystals, *J. Cryst. Growth*, 8, 197-204, 1971.

Chen, Y., M. M. Abraham, L. C. Templeton and W. P. Unruh, Role of hydrogen and deuterium on the formation of V- centers in magnesium oxide, *Phys. Rev. B*, 11, 811, 1975.

Constable, S., and A. Duba, Electrical conductivity of olivine, a dunite and the mantle, *J. Geophys. Res.*, 95, 6967-6978, 1990.

Deines, P., R. H. Nafziger, G. C. Ulmer and E. Woermann, *Temperature-oxygen fugacity tables for selected gas mixtures in the system C-H-O at one atmosphere total pressure*, Bull. Earth and Miner. Sci. Exp. Station. Pennsylvania State University, University Park, PA, 1974.

Duba, A., The electrical conductivity of olivine, *J. Geophys. Res.*, 77, 2483-2495, 1972.

Duba, A., J. N. Boland, and A. E. Ringwood, Electrical conductivity of pyroxene, *J. Geol.*, 81, 27-35, 1973.

Duba, A., H. C. Heard, and R. N. Schock, Electrical conductivity of olivine at high pressure and under controlled oxygen fugacity, *J. Geophys. Res.*, 79, 1667-1673, 1974.

Duba, A., and I. A. Nicholls, The influence of the oxidation state on the electrical conductivity of olivine, *Earth Planet Sci. Lett.*, 18, 59-64, 1973.

Duba, A., M. Young, and T. J. Shankland, Electrical conductivity of synthetic olivine to 1500°C: Product, Promise and Problems., *Eos*, 69, 1436, 1988.

Duba, A.G., and T.J. Shankland, Free carbon and electrical conductivity in the Earth's mantle, *Geophys. Res. Lett.*, 9, 1271-1274, 1982.

Freund, F., F. Batllo, and M.M. Freund. Dissociation and recombination of positive holes in minerals., *Spectroscopic Characterization of Minerals and Their Surfaces*, Ed. L.C. Coyne, S.W.S. McKeever and D.F. Blake. 310-329, American Chemical Society, Washinton, D.C, 1990.

Freund, F., and G. Oberheuser, Water dissolved in olivine: a single crystal infrared study, *J. Geophys. Res.*, 91, 745-761, 1986.

Freund, F., and H. Wengeler, The infrared spectrum of OH--compensated defect sites in C-doped MgO and CaO single crystals, *J. Phys. Chem. Solids*, 43, 129-145, 1982.

Freund, M.M. *Highly mobile holes in wide band gap oxide insulators*, Ph.D. Thesis. Swiss Federal Institute of Technology, Zürich, 1990.

Freund, M.M, F. Freund, and F. Batllo, Highly mobile oxygen holes in magnesium oxide, *Phys. Rev. Lett.*, 63, 2096-2099, 1989.

Gourley, T., and W.H. Runciman, Multiphonon infrared absorption spectra of magensium oxide and calcium oxide, *J. Phys. C.*, 6, 583-592, 1973.

Griscom, D.L. Electron spin resonance, *Glass: Science and Technology*, 151-251, 1990.

Henderson, B., and J. E. Wertz, *Defects in the Alkaline Earth Oxides*, Taylor & Francis, London, 1977.

Hirsch, L.M., Enhancing mantle conductivity, *Nature*, 347, 232-233, 1990.

Karato, S., The role of hydrogen in the electrical conductivity of the upper mantle, *Nature*, 347, 272-273, 1990.

Kathrein, H., and F. Freund, Electrical conductivity of magnesium oxide single crystals below 1200 K., *J. Phys. Chem. Solids*, 44, 177-186, 1983.

Kathrein, H., U. Knipping, and F. Freund, Atomic carbon in magnesium oxide, Part VI: Electrical conductivity., *Mat. Res. Bull.*, 15, 1393-1399, 1980.

Kingery, W. D., Plausible concepts necessary and sufficient for interpretation of ceramic grain boundary phenomena: I. Grain boundary characteristics, structure and electrostatic potential, *J. Amer. Ceram. Soc.*, 75, 1-8, 1974.

Kittel, C., *Introduction to Solid State Physics*, J. Wiley & Sons, New York, 1980.

Kliewer, K. L., and J.S. Koehler, Space charge in ionic crystals. I. General approach with application to NaCl, *Phys. Rev. A*, 140, 1226-1240, 1965.

Lehovec, K., Space-charge layer and distribution of lattice effects at the surface of ionic crystals, *J. Chem. Phys.*, 21, 1123-1128, 1953.

Marfunin, A.S., *Spectroscopy, Luminescence and Radiation Centers in Minerals*, 257-262, Springer Verlag, New York, 1979.

Miller, G. H., G. R. Rossman, and G. E. Harlow, The natural occurrence of hydroxide in olivine, *Phys. Chem. Minerals*, 14, 461-472, 1987.

Morin, F.J., J.R. Oliver, and R.M. Housley, Electrical properties of forsterite, Mg_2SiO_4: I, *Phys. Rev. B*, 16, 4434-4445, 1977a.

Morin, F.J., J.R. Oliver, and R.M. Housley, Electrical properties of forsterite, Mg_2SiO_4: II, *Phys. Rev. B*, 19, 2886-2894, 1977b.

Omura, K., K. Kurita, and M. Kumazawa, Experimental study of the pressure dependence of the electrical conductivity of olivine at high temperatures, *Phys. Earth Planet. Int.* , 57, 291-303, 1989.

Osburn, C.M., and R.W. Vest, Electrical properties of single crystals, bicrystals, and polycrystals of magnesium oxide, *J. Amer. Ceram. Soc.*, 54, 428-435, 1971.

Shankland, T.J., Transport properties of olivines. *The Application of Modern Physics to the Earth and Planetary Interiors,* Ed. S.K. Runcorn. NATO Advanced Study Institute, p. 175-190, Wiley Publ., New York, 1969.

Schock, R.N., and A. Duba. Point defects and the mechanisms of electrical conduction in olivine, *Point Defects in Minerals,* Ed. R.N. Schock. 88-96, Amer. Geophys. Union, Washington, D.C., 1985.

Schock, R. N., A. G. Duba, H. C. Heard and H. D. Stromberg, The electrical conductivity of polycrystalline olivine and pyroxene under pressure., *High Pressure Research: Applications in Geophysics.*, Ed. M. Manghnani and S. Akimoto. Academic Press, New York, 1977.

Schock, R. N. , A. G. Duba, and T. J. Shankland, Electrical conduction in olivine, *J. Geophys. Res.*, 94, 5829-5839, 1989.

Sempolinski, D.R., and W.D. Kingery, Ionic conductivity and magnesium vacancy mobility in magnesium oxide, *J. Amer. Ceram. Soc.*, 63, 664-669, 1980.

Sempolinski, D.R., W.D. Kingery, and H.L. Tuller, Electronic conductivity of single crystal magnesium oxide, *J. Amer. Ceram. Soc.*, 63, 669-675, 1980.

Shankland, T.J., and A.G. Duba, Standard electrical conductivity of isotropic, homogeneous olivine in the temperature range 1200-1500°C, *Geophys. J. Int.*, 103, 25-31, 1990.

Smyth, D., and R.L. Stocker, Point defects and non-stoichiometry in forsterite, *Phys. Earth Planet. Int.*, 10, 183-192, 1975.

Sockel, H. G., *Defect Structure and electrical conductivity of crystalline ferrous silicate,* Defects and Transport in Oxides. 341-354, Plenum Press, New York, 1974.

Sze, S.M., *Physics of Semiconductor Devices,* Wiley & Sons, New York, 1969.

Thorp, J. S., N. E. Rad, D. Evans and C. D. H. Williams, The temperature dependence of permittivity in magnesia and iron-magnesia single crystals, *J. Mater. Sci.*, 21, 3091-3096, 1986.

Wilkins, R.W.T, and W. Sabine, Water content of some nominally anhydrous silicates, *Amer. Mineral.*, 58, 508-516, 1973.

Electrical Conductivity Measurements under Minimum Perturbation Conditions

Part II: O^- Charge Carriers in Magnesium Oxide

Friedemann Freund*
Department of Physics, San Jose State University, San Jose, CA 95192

Abstract

Anomalously high electrical conductivity is observed in MgO single crystals (99.99% purity grade, <50 ppm transition metal impurities plus traces of OH^-, grown by arc fusion) below ≈800°C. This conductivity anomaly is widely believed to be a "dirt effect", caused by surface contamination. However, this conjecture cannot be upheld. Infrared studies show that OH^- in the bulk undergo changes in the exactly same temperature intervals in which the conductivity shows anomalies. Between 500–800°C H_2 molecules are being generated out of OH^-, implying an internal redox reaction: $OH^- + OH^- = H_2 + O_2^{2-}$. The appearance (disappearance) of mobile charge carriers upon heating (cooling) coincides with oxidation (reduction) of trace transition metal cations, measured by electron spin resonance spectroscopy. This is consistent with dissociation of peroxy defects, O_2^{2-}, into O^-. Magnetic susceptibility measurements indicate spin–decoupling of diamagnetic O_2^{2-} between 300–500°C into paramagnetic O^-. The O^- concentration was estimated to be of the order of 1000 ppm. Conversion of OH^- into H_2 plus O_2^{2-} is corroborated by a mass spectrometric study of MgO ex $Mg(OH)_2$ which releases molecular H_2 (2000–5000 ppm) above 400°C and atomic O above 600°C, consistent with disproportionation: $O_2^{2-} = O^{2-} + O$. All data jointly indicate that the electrical conductivity anomaly of MgO single crystals is not a "dirt effect", caused by surface contamination, but that it is due to the generation of O^- charge carriers which occurs in the bulk. The underlying reaction involves the redox conversion of lattice–bound OH^- into H_2 plus O_2^{2-}. These O_2^{2-} coexist with transition metal cations in lower oxidation states. If the H_2 molecules diffuse out, the MgO crystals retain O_2^{2-} defects, equivalent to interstitially bound excess oxygen, $MgO_{1+\delta}$. This is a solid state reaction by which crystals which originally grew under reducing conditions can become internally oxidized.

---

* also at the SETI Institute, c/o NASA Ames Research Center, MS 239-4, Moffett Field, CA 94035.

Introduction

Scientists have traditionally worked very hard at cleaning and perfecting the materials they want to study. Nature, however, has worked equally hard at evading scientists, and many studies of material properties have ended ungloriously in the file labeled "dirt effects". It has been known for some time that mantle–derived olivine crystals display a somewhat bothersome, anomalously high electrical conductivity below ≈700°C [*Duba, 1972; Duba et al., 1974; Duba and Nicholls, 1973; Schock et al., 1977; Sockel, 1974*]. It is reported that this anomalous behavior is poorly reproducible and disappears upon prolonged heating in reduced gases. This has led to the widespread belief that the anomaly is probably caused by contamination of some kind. At closer inspection it is found that conductivity anomalies are not unique to mantle–derived olivine crystals. They are also known from studies of other crystals, in particular synthetic MgO crystals where the conductivity enhancement covers many orders of magnitude up to ≈800°C [*Lempicki, 1953; Mansfield, 1953; Lewis and Wright, 1968; Lewis and Wright, 1970; Osburn and Vest, 1971; Kathrein and Freund, 1983*]. In MgO, like in olivine, the anomaly disappears upon prolonged heating to 700–800°C and has been reported to be poorly reproducible. It therefore appeared reasonable to assume that it had something to due with contamination, specifically surface contamination. Though there were enough hints to suggest that the situation might be more complicated, researchers have generally been reluctant to spend time and effort pursuing this enigmatic anomaly for fear that Nature may once more be successful in setting them up with a "dirt effect".

Part I [*Freund et al., 1991*] re–examined the anomalous conductivity behavior of MgO and found it worth a detailed study applying a new technique, Charge Distribution Analysis (CDA). In the course of this study two distinct temperature regions of anomalous conductivity behavior were identified, extending from 200 to 400°C and from 500 to 800°C. In both temperature regions the effect was caused by charge carriers that reside predominantly at the surface. However, these charge carriers were <u>not</u> related to some kind of surface contamination. CDA gave strong indications that they arose in the bulk and that their propensity for the surface is the result of an internal driving force.

While CDA was able to ascertain that these charge carriers were positive, it could not unambiguously identify their chemical nature. To meet this objective other techniques are needed. The following presentation is based on work which has mostly been carried out in my laboratory with students and collaborators whose names are acknowledged at the end. Work by other groups will be referenced sparsely. This is despite the fact that MgO has been studied intensively over many years [e.g. *Henderson and Wertz, 1977*]. However, most researchers have either passed over the temperature region where the electric conductivity anomalies occur or avoided making correlations between their specific results, obtained by other techniques, and the conductivity response.

Experimental

As in the CDA experiments described in Part I arc–fusion grown, nominally high purity MgO single crystals were used, obtained from W. & C. Spicer, Ltd., Cheltenham, England. They were of the same purity (4N = 99.99 %) or a somewhat lower purity grade (3N = 99.9 %) with typically 70–100 ppm Fe, 10–20 ppm Cr and <10ppm Mn as the crystals used in the d.c. and CDA studies [*Freund et al., 1991; Kathrein and Freund, 1983*]. Lesser purity grade crystals (99.5 %) were included, produced by Dynamit–Nobel AG, Troisdorf, Germany, in an industrial carbon arc production furnace. These crystals, designated below as DN–MgO, have a higher Ca, Al and Si content. The 4N–MgO crystals typically contain ≈10 ppm Mn, Cr, Ni and ≈30 ppm Fe plus Ca, Al and Si of about 10 ppm each. They are slightly yellowish–brown due to color centers [*Henderson and Wertz, 1977*] and often cloudy, due to submicron–sized cavities decorating dislocation lines and subgrain boundaries. All crystals, irrespective of their purity grade, contain OH^- impurities at concentrations in the 10–100 ppm range introduced by H_2O adsorbed to the MgO starting powder [*Abraham et al., 1971; Butler et al., 1971*]. Specpure grade MgO powder was obtained from Johnson Mathey Chemicals, Ltd., Batch # 3.51934, quoted to contain ≈3 ppm Fe, ≈1 ppm Ag, <1 ppm Ca and <1 ppm Cu.

For the infrared (IR) spectroscopic study a PERKIN–ELMER Model 225 grating spectrometer was used, modified to cover the range from 3000–4500 cm^{-1}. All spectra were recorded at liquid nitrogen temperature (≈80 K) after heating the samples either *in situ* or externally to temperatures up to 1000°C. A custom–built stainless steel cryostat was available for *in situ* treatments up to 550°C. The cryostat was contained in an ultrahigh vacuum chamber equipped with NaCl and sapphire single crystal windows and pumped to 5 x 10^{-8} torr base pressure by means of a turbomolecular pump. Screwed to the bottom of the cryostat was a Cu block with a rectangular opening. A ceramic block containing a pair of 100 W heating elements could be brought in mechanical contact with the Cu block by means of a linear motion drive. Cleaved MgO crystals of 10–20 mm thickness and ≈10 mm width were wrapped with 0.1 mm Au foil (for thermal contact) and placed inside the Cu block. They were heated repetitively in 20-25°C increments for 30 min and then either quenched by pouring liquid nitrogen directly into the hot cryostat after decoupling the heater block or cooled slowly by allowing the system to cool dynamically to room temperature before filling the cryostat with liquid nitrogen. To reach temperatures >550°C the crystals were externally heated in a tube furnace for 30 min, air–quenched to ambient temperature and subsequently mounted in the cryostat Cu block for cooling to 80 K.

The electron paramagnetic resonance (EPR) study was conducted with a BRUKER B–ER 414 spectrometer operating at 9.7 GHz. A 2 x 2 x 2 mm MgO crystal doped with 760 ppm Cr was used as a calibration standard. Cleaved 3N–MgO single crystals (3 x 3 x 12 mm) and coarsely crushed DN–MgO crystals (100–385 μm size fraction) were sealed in thin–walled fused silica tubes under high purity He (Air Liquide), heated for 5–30 min in 50°C incremental steps up to 1000°C and for 5 min down in the same temperature steps to 400°C. Each temperature treatment

was following by a rapid quench in liquid N_2. The EPR spectra were recorded at 77 K or room temperature. The repositioning of the samples in the resonance cavity was reproducible with ±1% relative intensity variation.

The magnetic susceptibility study was conducted with a EG&G Princeton Applied Research Vibrating-Sample Magnetometer (VSM) Model 4500, combined with a 5.4 KGauss Varian magnet, model V-2200A. The VSM was equipped with a high temperature sample holder (25–1000°C) made of boron nitride (BN) within a double–wall vacuum chamber. The interior sample chamber was evacuated and refilled with 5 torr He for thermal contact. The MgO single crystal was ground into a cylinder of 4.8 mm diameter and 15.6 mm height. It was mounted with a small amount ZrO_2-based high-temperature cement onto the BN rod, preheated to 980°C and cooled slowly. The data were collected during reheating at 4°C/min. The magnetic response of the BN sample rod with cement, as determined in a separate run, was subtracted from the data.

The mass spectroscopic data were collected in an all–glass, hydrocarbon–free ultrahigh vacuum (UHV) system, bakeable to 450°C, with a base pressure in the 10^{-10} torr range. The system used electromagnetically operated polished spherical stopcocks as valves and was pumped by two Hg diffusion pumps in tandem between liquid nitrogen traps. The sample was placed in a fused silica tube (4 mm i.d.), connected to the glass apparatus via a graded seal, and heated with a free–standing Pt coil in an outer glass chamber filled with Ar (to prevent diffusion of H_2 through the hot fused silica wall). The gases evolved from the sample were directed through selectable glass capillaries of known conductance into an Omegatron cyclotron resonance mass filter, built entirely of Pt–Ir alloy except for the ThO_2–covered tungsten wire for the electron source. Typically 30–70 μg specpure MgO powder samples were placed in the fused silica sample tube and outgassed for several hours at 1000°C. They were then hydroxylated and deuteroxylated to $Mg(OH)_2$ and $Mg(OD)_2$ respectively, using double–distilled H_2O and 99.7% D_2O (Merck Uvasol) at 355 torr equilibrium pressure. The hydroxides and deuteroxides thus obtained were very slowly decomposed to finely divided MgO containing a high concentration of residual OH^- and OD^- along with point defects. The pressure inside the UHV system was measured with a Bayart–Alpert gauge and the heating rate of the sample was controlled through an automated feed–back loop to keep the degassing rate within the dynamic range ($1:10^6$) of the Omegatron. After the main decomposition when the degassing rate decreased rapidly the Bayart–Alpert gauge was shut off to avoid decomposition at the hot wire. The purpose of this experiment was to determine small amounts of H_2/HD/D_2 and/or O_2/O in the presence of H_2O/HDO/D_2O vapor.

Results and Discussion

Infrared Spectroscopy of OH^- Impurities

OH^-–bearing point defects in MgO single crystals were studied by IR spectroscopy over a very wide temperature range using the experimental procedures outlined above [*Freund and Wengeler, 1982*]. The OH^- impurities cause two prominent groups of bands. One group is relatively strong and consists of three, sometimes four equispaced bands at 3297, 3312, 3327, and 3342 cm^{-1}. This "quadruplet" has been assigned to a defect where a single OH^- sits adjacent to an Mg^{2+} vacancy, V''_{Mg}, and compensates half of its charge. Using the Kröger [*1964*] defect denomination* this defect is written as $[OH^{\cdot} V''_{Mg}]'$. The second group is of lower intensity and consists of three bands at 3550, 3571, and 3566 cm^{-1}. This "triplet" has been assigned to a defect where two OH^- sit adjacent to an Mg^{2+} vacancy and fully compensate its charge, $[OH^{\cdot} V''_{Mg} {}^{\cdot}HO]^x$.

Fig. 1a/b shows a remarkable result. The intensity variations indicate that the number of OH^- at the defect sites varies considerably with temperature between 25°C and 950°C. The variations are fully reversible, indicating first that the crystals behave as a closed system and second, that a complex redistribution of OH^- defects takes place during heating and cooling which involves several internal reservoirs. Third, the relative intensities of the two groups are not in agreement with what one would predict from simple defect equilibria.

On the basis of minimum energy considerations, e.g. minimalization of the the local Coulomb potential, the fully compensated defects, $[OH^{\cdot} V''_{Mg} {}^{\cdot}HO]^x$ should be significantly more abundant that the half compensated defects, $[OH^{\cdot} V''_{Mg}]'$. Instead, the triplet in (**b**) is 5–10 times weaker than the quadruplet in (**a**). In addition the intensities of both groups vary significantly not only as a function of temperature but also as a function of the cooling rate. The latter is particularly pronounced between 200–400°C: slowly cooled crystals give higher intensities than rapidly cooled crystals. Now, the 200–400°C interval is the same which stood out in the conductivity measurements as a region of anomalous electrical conductivity behavior (see **Figs. 5/6** in Part I [*Freund et al., 1991*]). There are two possible conclusions: (i) the conductivity anomaly is directly related to OH^- defects, and (ii) the OH^- defects act as local probes for something else happening in the bulk which in turn is responsible to the conductivity anomaly.

---

* Superscript dot, prime, and cross indicate a positive, negative and neutral charge with respect to the ideal structure. V means vacancy. Subscripts characterize the lattice site except for O^{2-} sites which are omitted. Subscript i stands for interstitial. Square brackets delineate the point defect, generally omitting lattice points that are not essential.

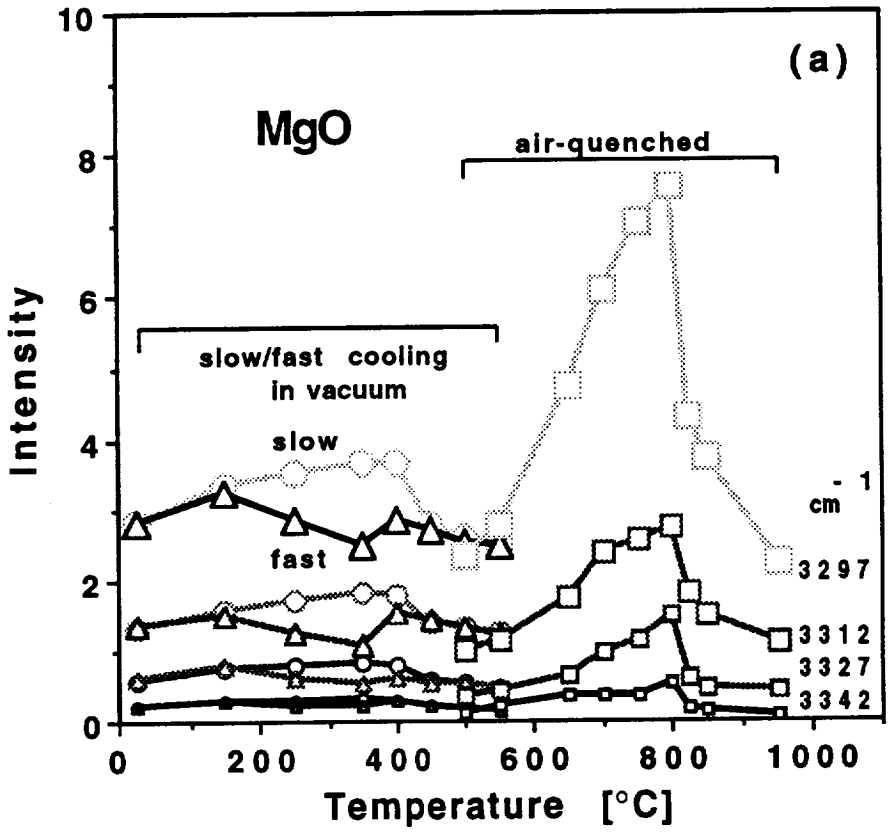

Fig. 1a: Intensity variations as a function of temperature of the quadruplet group, assigned to the O–H stretching vibration, ν_{OH}, of single OH^- associated with an Mg^{2+} vacancy. Each data point represents the IR intensity after the crystal had been heated to the indicated temperature and cooled. All IR measurements were done at 80 K [after *Freund and Wengeler, 1982*].

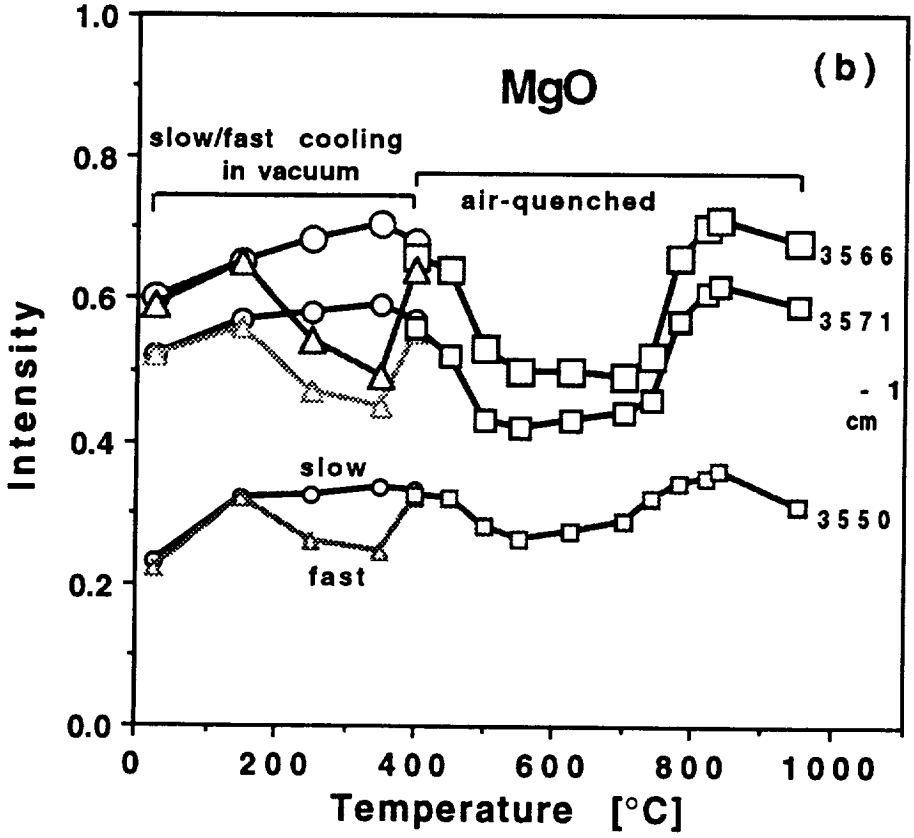

Fig. 1b: Intensity variations as a function of temperature of the triplet group, assigned to two OH^- associated with an Mg^{2+} vacancy. Each data point represents the IR intensity after the crystal had been heated to the indicated temperature and cooled. All IR measurements were done at 80 K [after *Freund and Wengeler, 1982*].

Turning to the T–dependent intensity variations we note that the trends are opposite: while the quadruplet intensity increases by a factor of 4 between 500–800°C, the triplet intensity decreases. This is against what one would predict on the basis of simple defect equilibria. If the number of $[OH^{\cdot} V''_{Mg}]'$ defects increases (because a "reservoir" in the bulk releases H^+), the number of $[OH^{\cdot} V''_{Mg} {}^{\cdot}HO]^x$ defects should increase as well. Instead they decrease.

The "reservoir" consists of H^+ on interstitial sites, $H_i^{\cdot}$, which manifest themselves in broad background absorption that extends from 3300–3700 cm^{-1} [*Freund and Wengeler, 1982*]. Around 500°C these $H_i^{\cdot}$ diffuse to existing Mg^{2+} vacancies and form additional OH^-–compensated cation vacancy defects:

$$[O^x V''_{Mg}]'' + H_i^{\cdot} = [OH^{\cdot} V''_{Mg}]' \qquad [1]$$

$$[O^x V''_{Mg} {}^xO]'' + 2\,H_i^{\cdot} = [OH^{\cdot} V''_{Mg} {}^{\cdot}OH]^x \qquad [2]$$

However, the fact that the intensity of the triplet assigned to the $[OH^{\cdot} V''_{Mg} {}^{\cdot}OH]^x$ defect decreases above 500°C suggests a concurrent second reaction by which these fully OH^-–compensated defects convert into another type of defect that bears no OH^-. This second reaction correlates with the appearance of a weak band around 4150 cm^{-1}. On the basis of partially deuterated MgO crystals this band has been assigned to the H–H stretching vibration, ν_{H-H}, of H_2 molecules occupying non–symmetrical defect sites [*Freund and Wengeler, 1982*].

This leads to the next question: how do $[OH^{\cdot} V''_{Mg} {}^{\cdot}HO]^x$ defects give rise to H_2 molecules ?

Fig. 2 illustrates the reaction by which, due to the perturbation of the local Coulomb potential at the Mg^{2+} vacancy site [*King and Freund, 1984*], the two OH^- are destabilized with respect to the valency state of oxygen. It is often not appreciated that oxygen has two ionization states, O^- and O^{2-}, of which only the first is thermodynamically stable, e.g. has a positive electron affinity [*Edlén, 1960*]. Upon addition of the first electron, $O + e^- = O^-$, the energy gained amounts to 1.4 eV. However, when the second electron is added, $O^- + e^- = O^{2-}$, the highly negative second electron affinity, –8.9 eV, comes to bear, making this reaction highly endothermal. At the same time, the lattice energy of a crystal like MgO, ≈40 eV/mole, primarily derives from the Coulomb interaction between the oppositely charged ions, Mg^{2+} and O^{2-}. By containing divalent O^{2-} interacting with divalent Mg^{2+} the system more than recovers the energy expended on the negative second electron affinity of the oxygen anions. Hence, MgO is stable. This overall stability of the structure does not necessarily mean that O^{2-} will be stable at every point in the crystal structure. A cation vacancy, for instance, represents a large perturbation of the local Coulomb energy. The possibility has to be considered that the O^{2-} becomes destabilized with respect to the O^- state. According to the IR data [*Freund and Wengeler 1982*] this destabilization indeed takes place when OH^- neighbor a Mg^{2+} vacancy: $OH^- = O^- + H$. Additional energy may be gained (i) by the recombination of two H to H_2:

$$[OH^{\cdot} V''_{Mg} {}^{\cdot}OH]^x = [O^{\cdot} (H_2)''_{Mg} {}^{\cdot}O]^x \qquad [3]$$

and (ii) by spin pairing of two O^-, leading to an O^- dimer, chemically equivalent to a peroxy anion, O_2^{2-}:

$$[O^{\cdot} (H_2)''_{Mg} {}^{\cdot}O]^x = [{}^{O}_{O}{}^{\cdot\cdot}(H_2)''_{Mg}]^x \qquad [4]$$

Some of the energy gain is expected to be counteracted by lattice strain in the neighborhood of the defect which arises from the short (≈1.5 Å) O–O bond [*Cremer, 1983*] and the necessity to accomodate the local contraction.

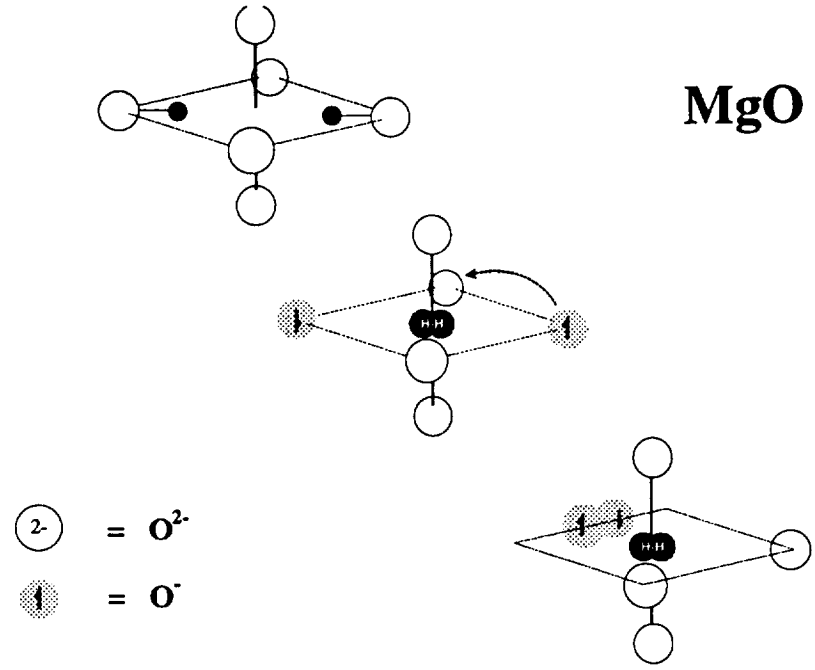

Fig. 2 Conversion of two OH^- associated with an Mg^{2+} vacancy defect into O_2^{2-} (peroxy) plus H_2.

In addition H_2 molecules can leave the cation vacancy site and diffuse away. If the crystals are small and/or the time is long, the H_2 molecules diffuse out, leaving behind peroxy–compensated Mg^{2+} vacancies:

$$[^{O^{\cdot\cdot}}_{O}(H_2)^{''}_{Mg}]^x = [^{O^{\cdot\cdot}}_{O}V^{''}_{Mg}]^x + (H_2)\Uparrow \qquad [5]$$

Identification of O^- by Magnetic Susceptibility Measurements

MgO is intrinsically diamagnetic, $\chi_{dia} = -10.8\ 10^{-6}$ emu/mole and its diamagnetism is independent of temperature [*Nagel et al., 1976*]. Protons will not change the magnetic susceptibility of MgO**. The O_2^{2-} anion, if it forms according to eq. [5] and **Fig. 2**, has 14 valence electrons and is diamagnetic. O^- states, however, have 7 electrons and an unpaired electron spin.

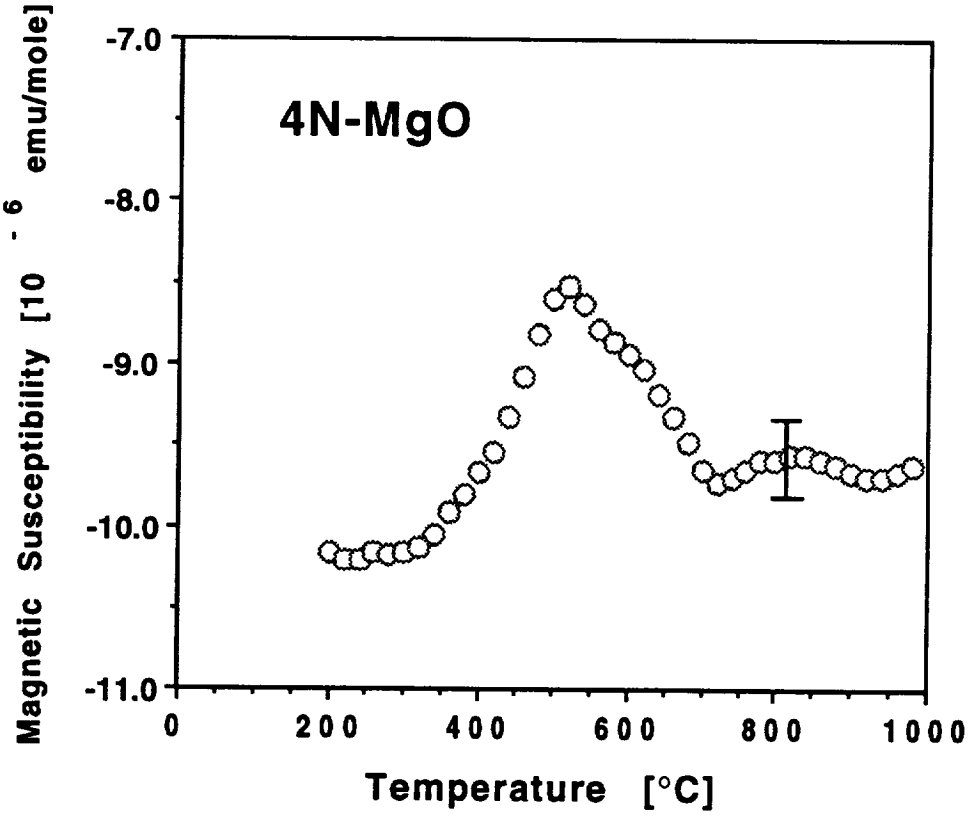

Fig. 3 Anomalous paramagnetic contribution observed during heating at 4°C/min of a nominally high purity MgO single crystals (99.99%, <50 wt.–ppm transition metal impurities). The error bar indicates the probable uncertainty of the measurements (after [*Batllo et al., 1991*]).

** The nuclear spin of the proton is orders of magnitude too small to be of interest here.

Fig. 3 shows the magnetic susceptibility χ of a 4N–MgO crystal between 180–980°C. The crystal was first heated to 900°C, cooled at 10°C and reheated to 980°C at 4°C/min while measurements were taken [*Batllo et al., 1991*]. The χ(T) curve was adjusted at 200°C to the intrinsic diamagnetism of MgO, corrected for the small transition metal impurities, <50 at.–ppm. **Fig. 3** shows a paramagnetic anomaly that starts above 300°C and reaches a maximum around 500°C, approximately +1.5 10^{-6} emu units above the base value. This rise in paramagnetism indicates the generation of unpaired spins in the MgO matrix. The few 3d transition metal impurities cannot explain this anomalous rise. Mg^{2+} cannot turn paramagnetic, for instance by auto–reduction to Mg^+ or auto–oxidation to Mg^{3+} because the +1 and +3 valency states of Mg are highly unstable. By default we are left with O^- as the only alternative paramagnetic species that may form thermally in the MgO matrix, for instance through dissociation of existing peroxy defects, O_2^{2-}.

Assuming that the Landé factor for O^- in the O^{2-} matrix of MgO is the same as for free O^-, the magnitude of the paramagnetic contribution χ_{para} at 500°C gives an O^- concentration of the order of 1000 at.–ppm [*Batllo et al., 1991*]. This value is significantly higher than the typical concentration of residual OH^- in arc–fusion grown MgO [*Abraham et al., 1971; Freund and Wengeler, 1982*], suggesting that a major fraction of OH^- originally contained in these MgO crystals has converted to O_2^{2-} defects as described by eqs. [3–5].

Next we have to address the question whether the observed paramagnetic anomaly supports the contention that O^- are the mobile charge carriers that are also responsible for the electric conductivity anomaly and positive surface charge determined by CDA [*Freund et al., 1991*]. For this we need to understand why the paramagnetism starts around 300°C and reaches its maximum around 500°C, whereas the large electric conductivity anomaly begins around 500°C and reaches its maximum near 800°C.

The paramagnetic anomaly is consistent with the prediction that two unpaired O^- are unstable at low temperatures because they undergo self trapping to form the diamagnetic peroxy defect, $^{\uparrow\downarrow}O_2^{2-}$ [*Batllo et al., 1991; King and Freund, 1984*]. By virtue of its short (≈1.5 Å) O–O bond [*Cremer, 1983*] the peroxy anion represents a small polaron, e.g. it is associated with a strong and highly localized lattice strain. The dissociation of $^{\uparrow\downarrow}O_2^{2-}$ into two paramagnetic O^- occurs in two sequential steps described by eqs. [6] and [7]: (i) decoupling the spins; (ii) dissociating into an O^- bound to the Mg^{2+} site plus an unbound O^- which delocalizes through O^{2-}/O^- valency fluctuations. This highly mobile, unbound O^- represents a large polaron, e.g. it is associated with lattice strain spread over a relatively large volume [*Freund, 1990*]:

$$[^{\uparrow\downarrow}_{O}O\cdots V''_{Mg}]^x = [^{\uparrow}O^{\cdot}\,V''_{Mg}\,^{\downarrow}O^{\cdot}]^x \qquad [6]$$

$$[^{\uparrow}O^{\cdot}\,V''_{Mg}\,^{\downarrow}O^{\cdot}]^x = [^{\uparrow}O^{\cdot}\,V''_{Mg}]' + {}^{\downarrow}O^{\cdot} \qquad [7]$$

The defects with two O^- and one O^- at the Mg^{2+} vacancy site are also known as V_0 and V^- centers, respectively [*Henderson and Wertz, 1977*]. The magnetic susceptibility data presented in **Fig. 3** are consistent with a 2–step dissociation by which V_0 centers start to form around 300°C according to eq. [6]. The maximum of the paramagnetic anomaly is reached when all O_2^{2-} have become V_0 centers. Above 500°C the V_0 centers dissociate into V^- centers plus unbound O^- according to eq. [7] without further increase in the number of spins. Since χ_{para} is proportional to 1/T, it is expected that $\chi(T)$ decreases above 500°C as shown in **Fig. 3**.

Evidence for O^- from Electron Paramagnetic Resonance Studies

If peroxy defects exist in the MgO crystals and dissociate according to eq. [7], releasing O^- as mobile charge carriers in the O^{2-} sublattice, EPR spectroscopy can be used in two ways: (i) to measure the concentration of quenched V^- centers or (ii) to measure the oxidation of transition metal cations according to:

$$Fe^{2+} + O^- = Fe^{3+} + O^{2-} \quad [8a]$$

$$Mn^{2+} + O^- = Mn^{3+} + O^{2-} \quad [8b]$$

$$Cr^{3+} + O^- = Cr^{4+} + O^{2-} \quad [8c]$$

Fe^{2+}, Mn^{2+} and Cr^{3+} represent the oxidation states in which these cation impurities are normally found in the MgO crystals. The oxidation states, Mn^{3+} and Cr^{4+}, are unstable with respect to disproportionation [*Henderson and Wertz, 1977*]. The presence of V^- centers in rapidly quenched CaO has been reported early [*Tomlinson and Henderson, 1969*] but no systematic study seem to have followed this lead. We used EPR to measure the appearance of the Fe^{3+} signal and disappearance of Mn^{2+} and Cr^{3+} signals as a result of oxidation [*Kathrein et al., 1984*].

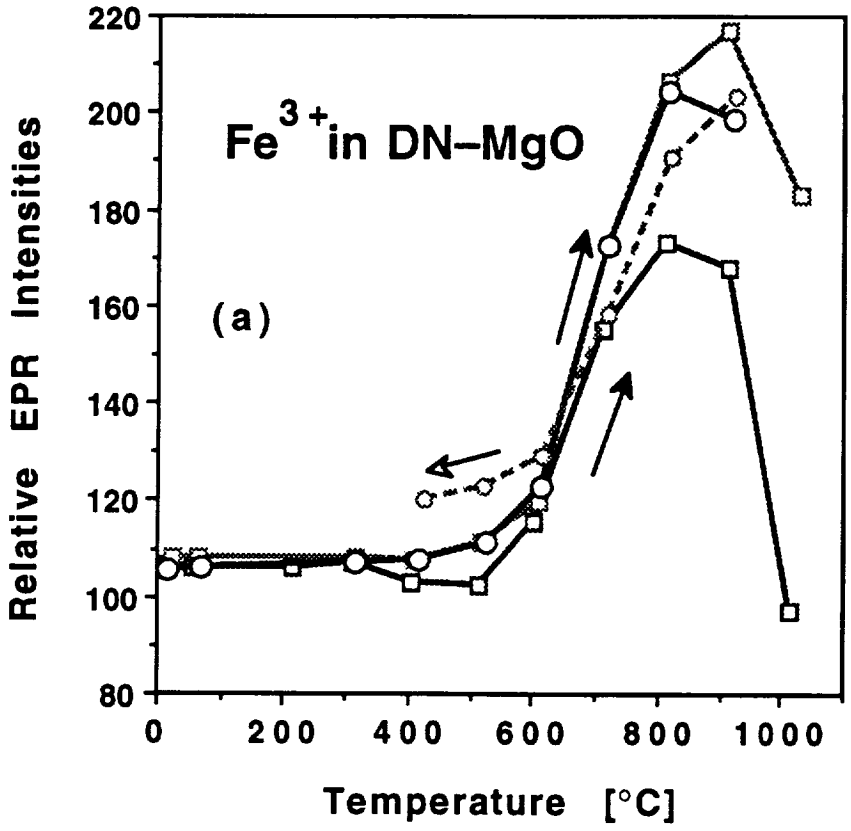
Fe3+ in DN–MgO
(a)
Relative EPR Intensities
Temperature [°C]
220
200
180
160
140
120
100
80
0
200
400
600
800
1000

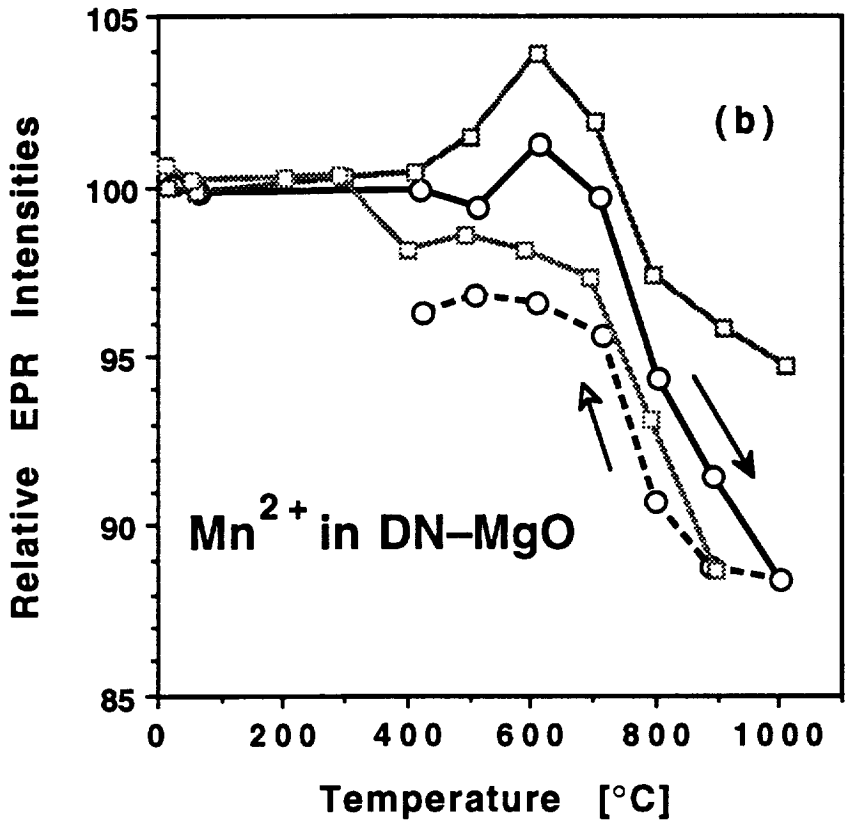
105
100
95
90
85
Relative EPR Intensities
(b)
Mn2+ in DN–MgO
0
200
400
600
800
1000
Temperature [°C]

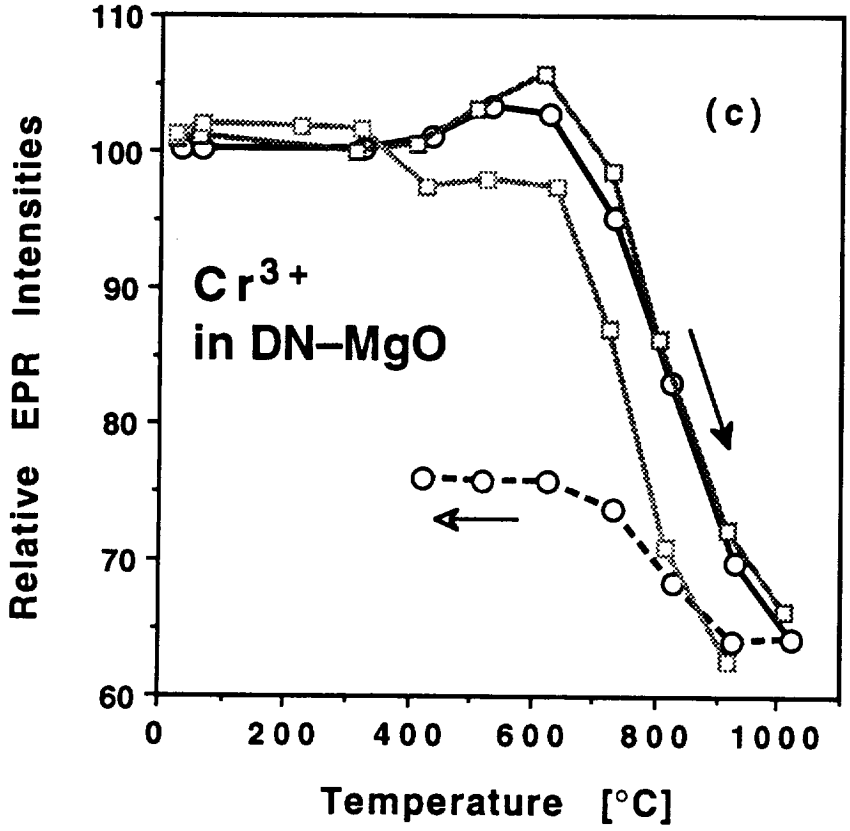

Fig. 4 Relative intensities of the EPR signals for three transition metal impurities (**a**) Fe^{3+}, (**b**) Mn^{2+}, and (**c**) Cr^{3+} in DN–MgO heated (solid lines) and cooled (dashed line) in steps under He, measured at 77 K (after [*Kathrein et al., 1984*]). The reversible increase of Fe^{3+} intensity and decrease of Mn^{2+} and Cr^{3+} intensities between 500–800°C indicates reversible redox reaction inside the MgO matrix.

Fig. 4a–c shows that the number of Fe^{3+} increases between 500–850°C and decreases between 850–1000°C. Upon cooling to 400°C with 5 min holding time at each temperature step the oxidation reverses, e.g. auto–reduction occurs. Likewise, the intensity of the Mn^{2+} and Cr^{3+} signals decreases upon heating to 1000°C and recovers upon stepwise cooling, also suggesting auto–reduction. The reversibility and the speed with which the reversibility is achieved is inconsistent with the proposition that gaseous O_2 may be involved in these redox reactions. Instead, the experimental data strongly suggest an internal process driven by O^- states that are thermally generated upon heating above 500°C and disappear upon cooling according to eqs. [8a–c]. The results are also in agreement with the magnetic susceptibility data presented above,

indicating that the internal redox reactions of the transition metal cations are coupled to the dissociation of the peroxy defects:

$$2\ Me^{n+} + O_2^{2-} \Leftrightarrow 2\ Me^{(n+1)+} + 2\ O^{2-} \qquad [9]$$

At low temperatures when the O^- are self–trapped and, hence, localized (see eq. [6]) transition metal cations in low oxidation states coexist with O_2^{2-} in the same MgO matrix. An Fe^{2+} impurity on a regular Mg^{2+} site represents neutral defect, $[Fe_{Mg}^{x}]^x$. Likewise, the V_0 center and the peroxy anion adjacent to a Mg^{2+} vacancy are neutral defects, $[O^{\cdot}V_{Mg}^{''}O]^x$ and $[{}^{O^{\cdot\cdot}}_{O}V_{Mg}^{''}]^x$, respectively. Between 500–800°C, when the V_0 centers or peroxy entities dissociate according to eq. [7] and release unbound O^-, some O^- are captured by the transition metal cations leading to their oxidation. An Fe^{3+} on a regular Mg^{2+} site represents a positive charge, $[Fe_{Mg}^{\cdot}]^{\cdot}$. The V^- center is the remnant of the peroxy defect after releasing an unbound O^- (see eq. [7]). It represents a negative charge, $[O^{\cdot}V_{Mg}^{''}]^{'}$. Therefore, the capture of an O^- state by any transition metal cation leaves two oppositely charged defects. Their long–range Coulomb interaction provides the force which, upon cooling, drives the auto–reduction of the transition metal cations, e.g. causes eq. [9] to procede from right to left.

Fig. 4a showed that, after the nearly two–fold increase between 500–800°C, the Fe^{3+} intensity decreases above 800°C, suggesting that there is yet another redox process at high temperatures. This is reminescent of the decrease of the anomalous electrical conductivity above 800°C as measured by d.c. techniques and of the positive surface charge as measured by CDA and expressed through F_Δ [*Freund et al., 1991*]. To illustrate the correlation between the EPR data for the O^-–driven Fe^{2+}/Fe^{3+} redox reaction and the d.c. conductivity data **Fig. 5** replots the d.c. conductivity of a 4N–MgO single crystal (in log Siemens units versus temperature in °C) and one of the EPR Fe^{3+} intensity curves from **Fig. 4a**.

Emission of H_2 Molecules and O Atoms

It would be certainly be of value to be able to provide an independent proof that OH^- defects in MgO are responsible for the *in situ* formation of H_2 plus O_2^{2-}. To address this question I turn to the last technique to be discussed here: the mass spectroscopic measurement of gas evolution from finely divided, ultrahigh purity MgO obtained by thermally decomposing $Mg(OH)_2$.

According to textbook knowledge the decomposition of $Mg(OH)_2$ should be a simple, straighforward reaction: $Mg(OH)_2 = MgO + H_2O$. However, the finely divided MgO first formed still contains residual OH^- balanced by Mg^{2+} vacancies. Its composition may be written as $Mg_{1-\delta}O_{1-2\delta}(OH)_{2\delta}$, with $\delta \ll 1$. At sufficiently high temperatures, however, the OH^- should be expelled as H_2O leaving stoichiometric MgO.

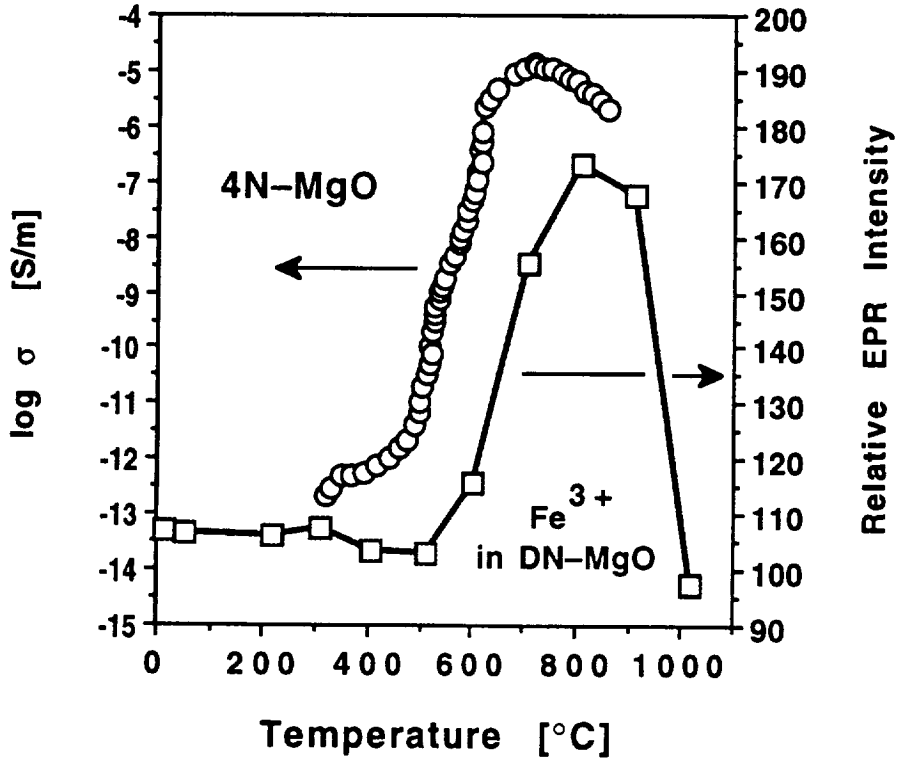

Fig. 5 Correlation between the electrical conductivity anomaly between 500–800°C as measured by d.c. techniques and the Fe^{3+} intensity variation as measured by EPR (after [*Kathrein and Freund, 1983; Kathrein et al., 1984*]) providing support that the anomalous rise of the d.c. conductivity and the internal oxidation of Fe^{2+} to Fe^{3+} have a common cause, viz. the generation of unbound O^- states.

The redox reaction given in eq. [5] indicates that H_2 molecules may form at OH^-–compensated Mg^{2+} vacancy sites. As long as the H_2 molecules remain in the MgO matrix the bulk composition remains unchanged, but the non–stoichiometric MgO should be written $Mg_{1-\delta}O_{1-2\delta}(O_2)_\delta(H_2)_\delta \equiv Mg_{1-\delta}O(H_2)_\delta$. The situation changes as the H_2 molecules diffuse out of the MgO crystals:

$$Mg_{1-\delta}O(H_2)_\delta = Mg_{1-\delta}O + \delta\, H_2 \Uparrow \qquad [10]$$

The cation–deficient MgO on the right hand side contains excess oxygen in the form of peroxy defects, O_2^{2-}. With $\delta \ll 1$ it may also be written as $MgO_{1+\delta}$. Under thermodynamic equilibrium conditions such MgO with excess oxygen can only be expected to form at a high O_2 pressure, never under reducing conditons and never in a vacuum [*Osburn and Vest, 1971; Wriedt, 1987*]. Obviously the $MgO_{1+\delta}$ will not be stable. Upon further heating it is expected to decompose by

releasing its excess oxygen just like any inorganic peroxide decomposes into oxide plus O_2 [*Cotton and Wilkinson, 1980*]. However, microscopically this decomposition reaction is a rather complicated process. It procedes by way of O^- diffusing to the surface and combining to O_2^{2-} which in turn release atomic O through disproportionation:

$$O^- + O^- = (O_2^{2-})_{surface} = O^{2-} + O\Uparrow \qquad [11]$$

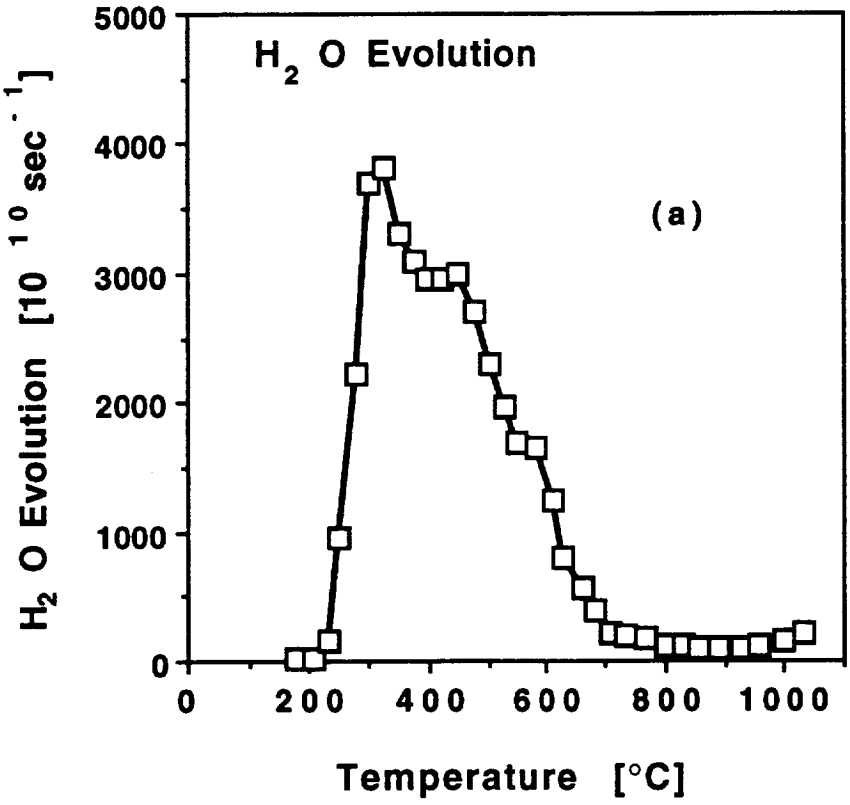

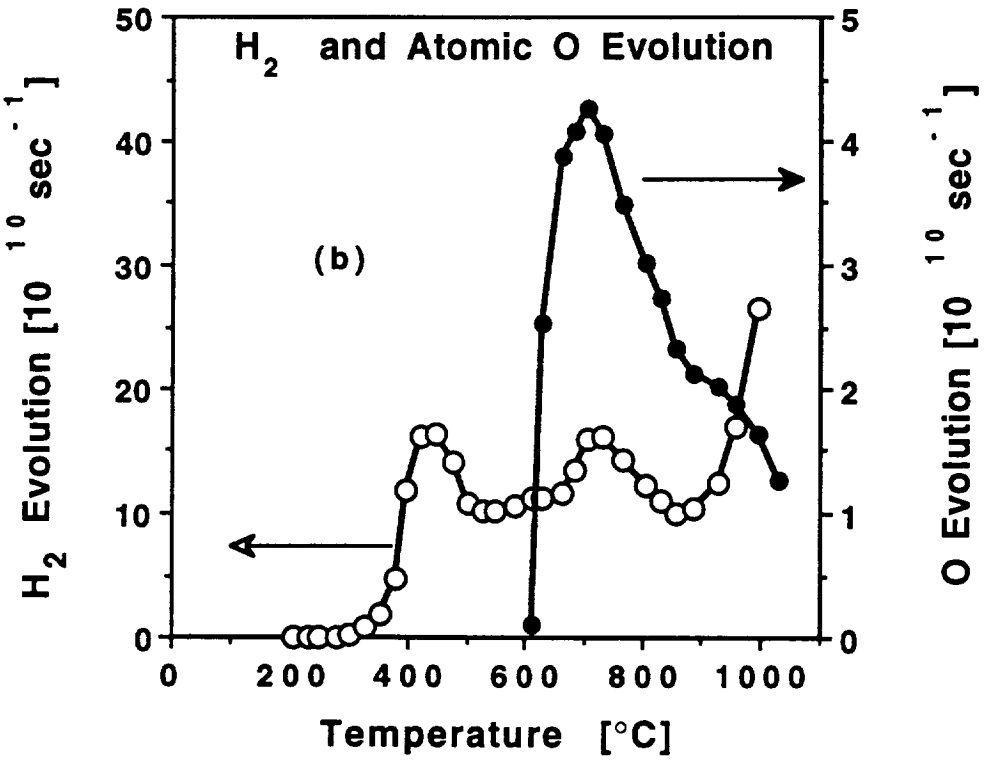

Fig. 6a/b Evolution of H_2O, H_2 and O during decomposition in vacuum of ultrahigh purity $Mg(OH)_2$ into MgO. Note that the intensity scales for H_2O, H_2 and O differ as 1000:10:1 (after [*Martens et al., 1976*]).

Fig. 6a/b shows the H_2O, H_2 and O evolution as measured mass spectroscopically starting from ultrapure $Mg(OH)_2$ and leading to finely divided MgO [*Martens et al., 1976*]. The H_2O evolution begins above 200°C and leads to a maximum near 300°C. Above 300°C cubic MgO forms, e.g. $Mg_{1-\delta}O_{1-2\delta}(OH)_{2\delta}$, with $\delta \ll 1$. At the same time H_2 molecules start to evolve. Above 600°C the H_2 evolution is joined by O evolution which reaches a maximum around 750°C and then decays. The H_2 evolution above 900°C comes from the hot fused silica sample tube. The H_2 evolution between 300–900°C as well as the O evolution above 600°C comes from the OH^-–containing MgO.

Fig. 6b dramatically illustrates the sequence of reactions described by eqs. [10] and [11]. The number of H_2 molecules evolved was found to vary between 2000–5000 ppm with respect to the number of OH^- contained in the original $Mg(OH)_2$, the higher value applying to deuterated samples [*Freund et al., 1982*]. This implies an equal number of peroxy defects. Using an independent approach, a wet-chemical titration technique, Tench and coworkers [*Praliaud et al.,*

1979] found highly oxidizing properties in MgO produced in the same way, through dehydration of high purity $Mg(OH)_2$ and determined the concentration of oxidizing centers to be 3.5×10^{19} g^{-1} MgO, equivalent to 2250 at.–ppm. This proves that dehydration can lead to oxidation, even in the absence of transition metal cations. The only way to balance the redox reaction is to let O^{2-} be oxidized to O^- while reducing protons to H_2. The 2250 at.–ppm value determined by titration is in good agreement with the range of peroxy concentrations obtained from the H_2 evolution of MgO shown in **Fig. 6b**. It corrobarates the 1000 ppm O^- concentration value derived from the magnetic susceptibility data shown in **Fig. 3**.

According to eq. [11] the O emission from the MgO surface irreversibly consumes O^-. This process is expected to affect the electrical conductivity and the CDA response, in particular $\mathbf{F}_\Delta$ which is an indicator of the O^- surface density. In the preceeding paper [*Freund et al., 1991*] we reported that the anomalously high electrical conductivity of MgO ended around 700–800°C when the log σ vs 1/T [K] curve joined the high temperature branch [*Sempolinski and Kingery, 1980*]. $\mathbf{F}_\Delta$ was was at a maximum around 750°C.

Fig. 7a combines the evolution of O atoms as measured from the MgO powder by mass spectrometry with $\mathbf{F}_\Delta(T)$ as measured with an MgO single crystal by CDA. Though the two experiments were carried out under very different conditions, the results closely match. The on–set of the O emission coincides with the built–up of the high positive surface charge. The maximum O emission rates lies within 50°C of the $\mathbf{F}_\Delta$ maximum. **Fig. 7b** combines the O evolution curve with the rising portion of the d.c. conductivity between 500–800°C (plotted as log σ versus T [°C]). Both plots support the arguments leading up to eq. [11], e.g. the conductivity anomaly of MgO below ≈800°C is caused by O_2^{2-} defects which generate mobile O^-. The increase of $\mathbf{F}_\Delta$ indicates an increase of O^- density at the surface, but O emission destroys O^- charge carriers and, hence, decreases $\mathbf{F}_\Delta$. Likewise the annihilation of O^- must also lead to a decrease of d.c. conductivity.

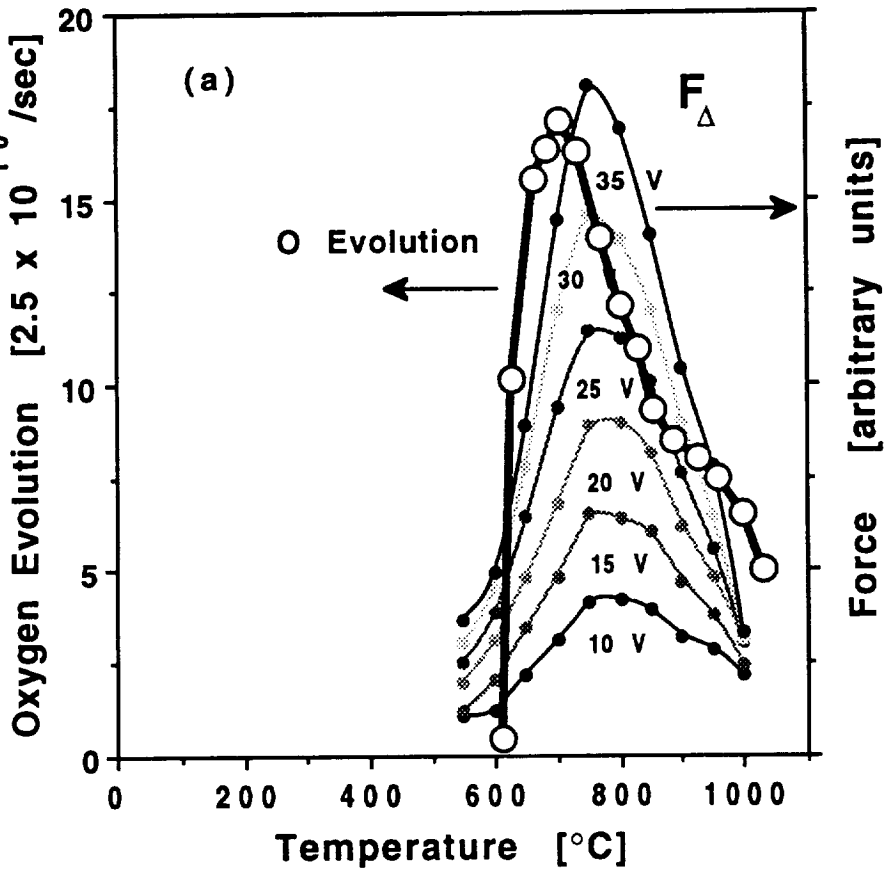

Fig. 7a Comparison between F_Δ above 500°C of a 4N–grade MgO single crystal with the atomic O evolution from ultrahigh purity MgO powder suggesting the decomposition of surface O^- into O^{2-} plus O (after [*Freund et al., 1991; Kathrein and Freund, 1983; Martens et al., 1976*]).

In vacuum, and in the absence of transition metal cations, the only way to irreversibly annihilate O^- charge carriers is by O atom emission according to eq. [11]. Obviously, the O emission can only take place from the MgO surface. Therefore, reduced gases which are brought in contact with the surface and are oxidized by O^- will have the same effect: they irreversibly annihilate O^- charge carriers. The gases of interest are H_2 and CO, and their "cleansing action" can be described in simple chemical terms as:

$$O^- + O^- + H_2 = O^{2-} + H_2O \Uparrow \quad [12a]$$

$$O^- + O^- + CO = O^{2-} + CO_2 \Uparrow \quad [12b]$$

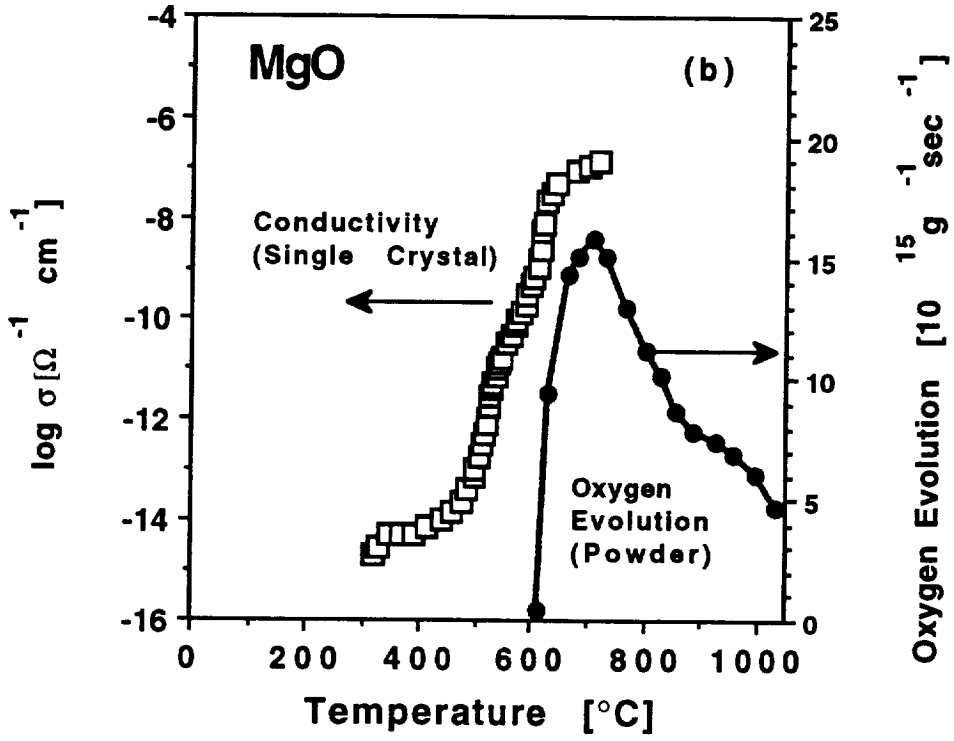

Fig. 7b Comparison between the d.c. conductivity anomaly above 500°C of a 4N–grade MgO single crystal with the atomic O evolution from ultrahigh purity MgO powder suggesting the decomposition of surface O^- into O^{2-} plus O (after [*Freund et al., 1991; Kathrein and Freund, 1983; Martens et al., 1976*]).

Conclusion

There are three important conclusions to be drawn from the data presented here and in Part I [*Freund et al., 1991*]. The first conclusion pertains to the cause of the anomalous electrical conductivity of MgO crystals below ≈800°C. The cause is not extraneous as has been widely assumed until now but indigenous, pointing at defects or impurities that exist in the bulk of the crystals under study. The mobile charge carriers have been recognized as positive holes, equivalent to defect electrons on the O^{2-} sublattice, chemically O^- states. At low temperatures, below ≈300°C, they are localized, spin–paired and diamagnetic, probably consisting of O_2^{2-} defects at cation vacancy sites. Above 500°C the O_2^{2-} defects dissociate and release delocalized, highly mobile O^- into the O^{2-} sublattice. The fact that these O^- have a strong propensity to come to the surface must not be mistaken for a sign of surface contamination. This raises the possibility

that a similar anomalous conductivity behavior observed in structurally and compositionally more complex crystals such as mantle–derived olivine may also have an indigenous cause.

The second conclusion pertains to the origin of the O^- charge carriers. The IR data presented here strongly support the contention that OH^-–compensated Mg^{2+} vacancies are sites where OH^- pairs undergo an internal redox reaction and become converted into molecular H_2 plus O_2^{2-}. This reaction consumes lattice–bound OH^- which are obvious signs of dissolved H_2O component. Therefore, the OH^- concentration that can be measured by IR spectroscopy is not representative of the total H_2O content. If H_2 molecules diffuse out, the only "memory" of the earlier H_2O content consists of O_2^{2-} defects. In the case of the MgO crystals studied here the total amount of H_2O incorporated during crystal growth appears to have been significantly larger (by a factor 5–10) than the current OH^- content suggests*. This suggests that the conjecture *OH^- content equal dissolved H_2O content*, hitherto taken for granted in all discussions concerning dissolved "water" in minerals, may need revision.

The third conclusion has potentially even more far–reaching implications. It pertains to the over–all redox state of the MgO crystals under study. The single crystals were grown in the chemically reducing environment of a carbon arc furnace where the atmosphere is dominated by CO/CO_2 with traces of H_2O [*Abraham et al., 1971; Butler et al., 1971*]. The powder was obtained by dehydrating $Mg(OH)_2$ in the intrinsically reducing environment of very high vacuum. In both cases the defect stoichiometry of nominally high purity, transition metal free crystals should be characterized by oxygen vacancies, equivalent to an excess of Mg [*Yamaka and Sawamoto, 1954; Mitoff, 1959; Osburn and Vest, 1971*]. Instead our experimental data indicate that the MgO contains excess O in form of peroxy defects and have the approximate composition $MgO_{1+\delta}$. Being equivalent to interstitial O atoms peroxy defects are the epitome of highly oxidizing conditions [*Wriedt, 1987*]. The amount of excess O appears to be substantial, of the order of 1000 ppm in the arc fusion grown single crystals and 2000 ppm in MgO powder obtained from $Mg(OH)_2$.

Fig. 8 shows an isobaric section through the three–component phase diagram Mg–O_2–H_2. The diagram is divided into a *reduced* region delineated by Mg–H_2–H_2O–MgO and an *oxidized* region delineated by MgO–H_2O–O_2. Also included are compounds MgH_2, H_2O_2 and MgO_2 and $Mg(OH)_2$ [*Cotton and Wilkinson, 1980*]. MgO straddles the boundary between the reduced and oxidized phase regions. As shown schematically in the enlarged portion below MgO is oxygen–deficient, if heated under low O_2 partial pressures [*Mitoff, 1959; Osburn and Vest, 1971*] or in the presence of Mg vapor [*Yamaka and Sawamoto, 1954*]. It is oxygen–rich, if heated in O_2, equivalent to an MgO–MgO_2 solid solution [*Wriedt, 1987*]. The phase region extends towards $Mg(OH)_2$, due to the known solubility of H_2O component. Though the extent of isobaric solid solution formation along the three axes is unknown the shaded area outlines a probable scenario. The upper open circle is representaive for non-stoichiometric MgO as expected to crystallize under reducing conditions (excess H_2 or Mg) in the presence of H_2O. The line joining MgO–$Mg(OH)_2$

* Assuming that H_2O is the only gas the dissolution of which leads to peroxy defects.

represents compositions $Mg_{1-\delta}O_{1-2\delta}(OH)_{2\delta}$. The bold straight arrow pointing downwards delineates the path which the system $Mg_{1-\delta}O_{1-2\delta}(OH)_{2\delta}$ would take after internal conversion of OH^- into H_2 plus O_2^{2-} by loosing H_2. The endpoint lies on the abscissa and represents the "water-free" composition $Mg_{1-\delta}O_{1-2\delta}(O_2)_\delta \approx MgO_{1+\delta}$.

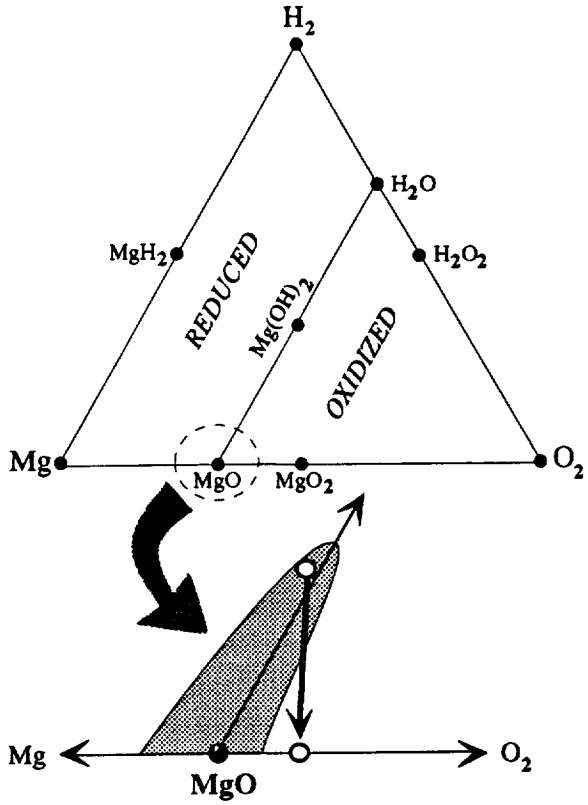

Fig. 8 $Mg–O_2–H_2$ phase diagram with the non–stoichiometry region for MgO redrawn and enlarged in the lower half (schematic). The shaded area outlines the compositional variability of MgO crystallizing in the presence of H_2O under reduced and oxidized conditions. The open circle in the shaded area represents $Mg_{1-\delta}O_{1-2\delta}(OH)_{2\delta} \Leftrightarrow Mg_{1-\delta}O_{1-2\delta}(O_2)_\delta/(H_2)_\delta$ obtained under reducing conditions with conversion of OH^- to H_2 plus O_2^{2-}. The open circle on the abcissa represents the composition $Mg_{1-\delta}O \approx MgO_{1+\delta}$ which would be achieved by complete conversion of OH^- and loss of H_2.

Fig. 8 illustrates that, while the representative point for the initial non–stoichiometric MgO lies in the "reduced" region, it can cross the dividing line between "reduced" and "oxidized" and settle in the "oxidized" region. It needs to be stressed is that such a transition would be achieved without exposing MgO to oxidizing conditions but solely by way of the internal conversion reaction discussed above, $2\ OH^- \Leftrightarrow H_2 + O_2^{2-}$, followed by out–diffusion of H_2. If the isobaric solubility for H_2O is larger than the solubility for O_2, the excess O in the MgO structure in form of peroxy

defects can exceed the solubility limit for O_2 at the same pressure. This possibility is illustrated in **Fig. 8** by placing the representative point for $MgO_{1+\delta}$ outside the shaded region.

So far MgO has been used as a model substance to study this internal reaction sequence. Chemically and structurally more complex minerals such as olivine do not lend themselves to some of the techniques applied here. However, given the fundamental nature of the reaction steps discussed above, it cannot be ruled out that traces of dissolved H_2O component in olivine and other minerals will undergo a similar internal conversion, followed by out–diffusion of H_2. The petrological consequences of such a process could reach far beyond the concern about electrical conductivity behavior emphasized here. Until now it has been common practice to judge the redox state of minerals from their transition metal equilibria as reflected, for instance, by the Fe^{2+}/Fe^{3+} ratio measured at 20°C. This Fe^{2+}/Fe^{3+} ratio is then used to derive the conditions under which these minerals have formed. The results presented here show that the Fe^{2+}/Fe^{3+} ratio is not a unique, not even a reliable indicator of the internal redox state. Crystals that originally formed under highly reducing conditions may acquire the sigmum of an oxidized condition without concomitant adjustment of the ratio of Fe^{2+}/Fe^{3+} and other transition metal cations.

Acknowledgements

Different parts of this work were supported by the Deutsche Forschungsgemeinschaft and the National Aeronautics and Space Administration through the Cooperative Agreement with SETI Institute NCC 2-446. It is my pleasure to acknowledge the collaboration of my former students in Germany who contributed to this study, in particular Reinhard Martens, Heinz Wengeler, and Hendrik Kathrein, and of my former colleague Horst Gentsch of the University of Essen who provided access to his mass spectrometer. François Batllo of the Univerisity of Dijon, France, and Kiumars Parvin of the San Jose State University contributed to the magnetic measurements which were in part supported by the National Science Foundation Grant No. DMR-8507478, NATO Grant RG.890479, and European Economic Communities Contract EN 3C-0023-D. F.F. acknowledges receipt of a National Research Council Senior Associateship during a part of this work.

References

Abraham, M.M., C.T. Butler, and Y. Chen, Growth of high-purity and doped alkaline earth oxides; Part I: Magnesium oxide and calcium oxide., *J. Chem. Phys.*, 55, 3752-3756, 1971.

Batllo, F., R. C. LeRoy, K. Parvin, F. Freund and M. M. Freund, Positive hole centers in magnesium oxide – correlation between magnetic susceptibility, dielectric anomalies and electric conductivity., *J. Appl. Phys. (in print)*, 1991.

Butler, C.T., B.J. Sturm, and R.B. Quincy, Arc fusion growth and characterization of high-purity magnesium oxide single crystals, *J. Cryst. Growth*, 8, 197-204, 1971.

Cotton, F. A. , and G. Wilkinson, *Advanced Inorganic Chemistry*, Wiley, New York, 1980.

Cremer, D., *General and theoretical aspects of the peroxide group*, The Chemistry of Functional Groups, Peroxides. p. 1-79, Wiley, New York, 1983.

Duba, A., The electrical conductivity of olivine, *J. Geophys. Res.*, 77, 2483-2495, 1972.

Duba, A., H. C. Heard, and R. N. Schock, Electrical conductivity of olivine at high pressure and under controlled oxygen fugacity, *J. Geophys. Res.*, 79, 1667-1673, 1974.

Duba, A., and I. A. Nicholls, The influence of the oxidation state on the electrical conductivity of olivine, *Earth Planet Sci. Lett.*, 18, 59-64, 1973.

Edlén, B, Electron affinities of oxygen, *J. Chem. Phys.*, 33, 98, 1960.

Freund, F., M.M. Freund, and F. Batllo, Electrical conductivity measurements under minimum perturbation conditions. Part I: Charge Distribution Analysis of magnesium oxide single crystals, *J. Geophys. Res.*, in submission, 1991.

Freund, F., and H. Wengeler, The infrared spectrum of OH^--compensated defect sites in C-doped MgO and CaO single crystals, *J. Phys. Chem. Solids*, 43, 129-145, 1982.

Freund, F., H. Wengeler, and R. Martens, A hydrogen-deuterium fractionation mechanism in magnesium oxide., *Geochim. Cosmochim. Acta*, 46, 1821-1829, 1982.

Freund, M.M. *Highly mobile holes in wide band gap oxide insulators*, Ph.D. Thesis. Swiss Federal Institute of Technology, Zürich, 1990.

Henderson, B., and J. E. Wertz, *Defects in the Alkaline Earth Oxides*, Taylor & Francis, London, 1977.

Hirsch, L.M., Enhancing mantle conductivity, *Nature*, 347, 232-233, 1990.

Kathrein, H., and F. Freund, Electrical conductivity of magnesium oxide single crystals below 1200 K., *J. Phys. Chem. Solids*, 44, 177-186, 1983.

Kathrein, H., F. Freund, and J. Nagy, O^-- ions and their relation to traces of H_2O and CO_2 magnesium oxide: an EPR study., *J. Phys. Chem. Solids*, 45, 1155-1163, 1984.

King, B.V., and F. Freund, Surface charges and subsurface space charge distribution in magnesium oxide containing dissolved traces of water, *Phys. Rev. B*, 29, 5814-5824, 1984.

Kröger, F.A., *The Chemistry of Imperfect Crystals*, North-Holland, Amsterdam, 1964.

Lempicki, A., The electrical conductivity of magnesia single crystals at high temperatures, *Proc. Phys. Soc.. London*, 66B, 281-283, 1953.

Lewis, T.J., and A.J. Wright, The electrical conductivity of magnesium oxide at low temperatures, *Brit. J. Appl. Phys.*, 1, 441-447, 1968.

Lewis, T.J., and A.J. Wright, The electrical conductivity of magnesium oxide at high fields, *J. Phys. D.*, 3, 1329-1339, 1970.

Mansfield, R., The electrical conductivity and thermoelectric power of magnesium oxide, *Proc. Phys. Soc. London*, 66B, 612-614, 1953.

Marfunin, A.S., *Spectroscopy, Luminescence and Radiation Centers in Minerals*, p. 257-262, Springer Verlag, New York, 1979.

Martens, R., H. Gentsch, and F. Freund, Hydrogen release during the thermal decomposition of magnesium hydroxide to magnesium oxide, *J. Catal.*, 44, 366-372, 1976.

Mitoff, S.P., Electrical conductivity of single crystal of MgO, *J. Chem. Phys.*, 31, 1261-1269, 1959.

Nagel, S., M. Maschke, and A. Baldereschi, Pseudopotential calculations of the electronic valence charge density and the optical dielectric constant of sodium chloride and magnesium oxide., *Phys. Stat. Sol. B*, 76, 629-632, 1976.

Osburn, C.M., and R.W. Vest, Electrical properties of single crystals, bicrystals, and polycrystals of magnesium oxide, *J. Amer. Ceram. Soc.*, 54, 428-435, 1971.

Praliaud, H., S. Coluccia, A. M. Deane and A. J. Tench, Oxidizing properties of magnesium oxide formed by thermal decomposition of magnesium hydroxide, *Chem. Phys. Lett.*, 66, 44-47, 1979.

Schock, R. N., A. G. Duba, H. C. Heard and H. D. Stromberg, The electrical conductivity of polycrystalline olivine and pyroxene under pressure. *High Pressure Research: Applications in Geophysics*, Ed. M. Manghnani and S. Akimoto, Academic Press, New York, 1977.

Sempolinski, D.R., and W.D. Kingery, Ionic conductivity and magnesium vacancy mobility in magnesium oxide, *J. Amer. Ceram. Soc.*, 63, 664-669, 1980.

Sockel, H. G., *Defect structure and electrical conductivity of crystalline ferrous silicate*, Defects and Transport in Oxides. p. 341-354, Plenum Press, New York, 1974.

Tomlinson, A.C., and B. Henderson, *J. Phys. Chem. Solids*, 33, 1793, 1969.

Wriedt, H.A., The magnesium-oxygen system, *Bull. Alloy Phase Diagrams*, 8, 227-233, 1987.

Yamaka, E., and K. Sawamoto, Electrical conductivity of magnesium oxide single crystals, *Phys. Rev.*, 95, 848-850, 1954.

Electrical Conductivity Measurements under Minimum Perturbation Conditions

Part III: Peroxy in Olivine

Rodney C. LeRoy*, François Batllo°, Minoru M. Freund+ and Friedemann Freund++
Department of Physics, San Jose State University, San Jose, CA 95192

Abstract

Mantle–derived olivine crystals exhibit an anomalously high electric conductivity up to ≈700°C when heated for the first time. This anomaly is commonly believed to be a "dirt effect", due to extraneous surface contamination, to polishing damage of the surface or to vapor–deposited amorphous carbon in the stability field of graphite. Using a new technique, Charge Distribution Analysis or CDA which measures contact–free the dielectric polarization in an electric field gradient at 0 Hz, the conductivity anomaly can be shown to be correlate with the appearance of highly mobile, positive charge carriers that are reversibly generated in the bulk between 450–550°C. They give rise to a surface charge, supported by an internal electric field which disappears upon cooling. The positive sign of the charge carriers suggests that they consist of holes. However, they are not holes on the cation sublattice, e.g. transient Fe^{3+} states due to oxidation, but holes on the O^{2-} sublattice, e.g. O^- states. Their reversible appearance during heating/cooling cycles suggests that the O^- states are generated from indigenous peroxy defects, probably peroxy links, $O_3Si/^{OO}\backslash SiO_3$, which coexist with Fe^{2+} in the olivine structure. The peroxy defects dissociate thermally between 450–550°C, causing the observed conductivity anomaly. The O^- charge carriers diffuse to the surface, causing the positive surface charge. At the same time they are susceptible to oxidation by reduced gases at ≥700°C, e.g. $CO + 2\ O^- = CO_2 + O^{2-}$. At the same time the O^- can internally oxidize Fe^{2+} to Fe^{3+} as if the olivine became oxidized by traces of O_2 in the ambient atmosphere. By analogy to MgO where cation vacancy bound OH^- pairs undergo an internal redox reaction to H_2 plus O_2^{2-}, it is proposed that the peroxy defects in olivine derive from traces of dissolved fluid phase components, notably H_2O, and that the O^- charge carriers are an integral part of the defect structure which the olivine crystals acquire in the upper mantle.

---

* Present address: Department of Physics, University of California, Davis, CA 95616.
° Permanent address: Réactivité des Solides, Université de Bourgogne, 21004 Dijon, France.
+ Department of Physics, University of California, Berkeley, CA 94720.
++ Mailing address: NASA Ames Research Center, MS 239-4, Moffett Field, CA 94035.

Introduction

Olivine is by far the major mineral of upper mantle rocks and therefore continues to occupy a central place in geophysical research. Understanding its defect structure and the role of impurities is essential to understanding the behavior of rocks under upper mantle conditions. Given the tremendous amount of effort that has been devoted to the experimental study of olivine from a variety of standpoints it appears unlikely that anything fundamentally new may remain to be discovered. Yet, in this paper we shall present evidence that olivine crystals from upper mantle rocks contain some intriguing charge carriers, highly mobile and evasive, which have resisted recognition until now.

The electrical conductivity of olivine has been measured with great care, both at ambient pressure (0.1 MPa) and at high pressures, under a wide range of oxygen fugacities [*Constable and Duba*, 1990, *Duba et al.*, 1974, *Duba and Nicholls*, 1973, *Duba et al.*, 1988, *Schock et al.*, 1977, *Schock et al.*, 1989, *Shankland*, 1981, *Sockel*, 1974]. As a result of these studies various charge carriers and conductivity mechanisms have been identified which influence or control the behavior of olivine in the high temperature (HT) region, above approximately 800°C. At the same time these studies have also laid open a striking anomaly in the conductivity behavior in the lower temperature (LT) region, below approximately 800°C. **Fig. 1** in Part I [*Freund et al.*, 1991] contained typical electrical conductivity data of olivine and olivine–rich rocks at oxygen fugacities of the upper mantle, all obtained at 0.1 MPa pressure. In the HT region, above ≈800°C, Arrhenius plots with constant slopes suggest a simple relation between conductivity σ and absolute temperature T: $\sigma_{i,j} = \sum_{i,j} \sigma_0 \exp [-E/kT]$, where σ_0 are pre-exponential factors and E activation energies for the charge carriers i,j, while k is the Boltzmann constant. In the LT region, below ≈800°C, the conductivity behavior was more complex. Each time an olivine sample is heated for the first time there appears to be a peculiar enhancement fo the conductivity, often by several orders of magnitude. This anomalous behavior must have annoyed many researchers. It is reportedly irreproducible in the sense that the high conductivity wanes during extended treatment in reducing CO/CO_2 gas atmospheres at temperatures around 700°C and disappears above 800°C. The waning and eventual disappearance has led to the belief that the high conductivity is a "dirt effect", probably caused by surface contamination during sample handling, by structural disorder introduced into the surface layer through the sample preparation, for instance during polishing, or by the deposition of a thin layer of amorphous carbon, vapor–deposited from the CO/CO_2 atmosphere by way of the disproportionation reaction $CO_2 = C + O_2$ in the stability field of graphite [*Constable and Duba*, 1990].

As illustrated in **Fig. 2** of Part I the same electrical conductivity anomaly occurs when cleaved, synthetic MgO single crystals are heated in a pure Ar [*Freund et al.*, 1991]. Therefore, disproportionation of CO_2 can be dismissed as the culprit. By judiciously selecting the right experimental conditions, the anomaly can be shown to be quite reproducible. The remainder of Part I was dedicated to describing a new technique Charge Distribution Analysis or CDA which has made it possible to show that, far from being erratic, the on–set of the electrical conductivity

C-2

anomaly in MgO and the stepwise increase of the static dielectric constant correlates with the appearance of a positive surface charge, supported by an internal electric field. These surface charges and their internal support field cannot be explained by mere surface contamination. Instead they require indigenous charge carriers that originate in the bulk – charge carriers which appear to have "fallen through the cracks" of prior investigations.

This brash conclusion was underscored in Part II by presenting results from several studies of MgO obtained with independent techniques, selected to illuminate different aspects of the enigmatic charge carriers which appear to be associated with the anomalous conductivity [*Freund*, 1991]. At the end of Part II a strong case could be made that the charge carriers in question are electronic defects on the O^{2-} sublattice, commonly referred to as positive holes or O^- states.

From a solid state physics viewpoint O^- are defect electrons in wide band gap insulating oxides. They occupy energy levels near the O 2p–dominated valence band. If their wave functions spread out over a large lattice volume, causing large polarons, the O^- may become highly mobile charges of positive sign [*Freund et al.*, 1989]. They carry electric current without mass transport. If the O^- are localized, forming small polarons, they are electrically inactive though they may still be detected because of their unpaired spin. From a solid state chemistry viewpoint O^- states are radicals, paramagnetic and intrinsically unstable [*Henderson and Wertz*, 1977, *Marfunin*, 1979]. They are oxidants which may oxidize transition metal cations from low to higher oxidation states. If two O^- undergo self–trapping and pair their spins, they become invisible to all known physical techniques. They form dimers, O_2^{2-}, conveniently called peroxy entities, they become diamagnetic and non–reactive. Formally an O_2^{2-} corresponds to an interstitial oxygen atom, $O_2^{2-} = O^{2-} + O$.

In Part III we return to olivine – a mineral which is more complicated than MgO, both structurally and chemically. The striking similarity between olivine from the upper mantle and synthetic MgO crystals in their respective anomalous conductivity behavior below 700–800°C raises an interesting question. After having corroborated by independent techniques that the conductivity anomaly in MgO is <u>not</u> a "dirt effect" but caused by indigenous O^-, we must be open to the possibility that the same enigmatic charge carriers exist in olivine. Unfortunately, because of their high Fe^{2+} content, olivine crystals from the upper mantle do not lend themselves to some of the powerful techniques presented in Part II through which we could unambiguously identify the charge carriers in MgO as O^- states [*Freund*, 1991]. For olivine Charge Distribution Analysis (CDA) remains an option. With its unique capability to study electrical and dielectric properties under minimum perturbation conditions we can learn something about the charge carriers of olivine which control the anomalous conductivity behavior.

Experimental

The CDA experiments were performed in an asymmetrical capacitor arrangement using two similar PERKIN–ELMER Thermogravimetric Analyzers TSG–1 and TGS–2 with a CAHN and a PERKIN–ELMER microbalance respectively. The TGS–1 had a small furnace, Pt wire wound on a cup–shaped alumina ceramic body, 6 mm internal diameter and 12 mm high, depicted in **Fig. 1**, while the furnace of the TGS–2 measured 10 mm internal diameter and 18 mm high. The Pt winding was bifilar and the furnace was a.c. operated using one half period of the sine wave for power and the other for measuring the resistance and, hence, the temperature. The furnace was surrounded by a 0.1 mm Au foil serving to equalize temperature gradients and as the counterelectrode. The sample was placed on a loop made of 0.1 mm diameter fused silica, suspended from the microbalance via a fused silica wire. The bias electrode was approximately circular, 4 mm diameter of Ni or Au, and introduced laterally above the sample. The critical sample–bias electrode distance could not be accurately controlled but was adjusted to 0.2–0.3 mm. Bias electrode and counterelectrode were connected to the ± output and ground respectively, of a KEITHLEY 240A digital voltage source (±1100V). The contribution from the fused silica support loop to the force measurement under CDA consitions was considered negligible.

All CDA measurements were performed at 0.1 MPa pressure in high purity 20-40 ml/min high purity N_2 (99.99 %, <5 vppm O_2, <10 vppm H_2O) during stepwise heating and cooling programs to be detailed below. Heating and cooling between incremental and decremental steps were usually fast, 20 or 40°C/min as noted in each case, in order to minimize exposure to the potentially detrimental effects of the unbuffered N_2 atmosphere. For some test runs slower heating and cooling rates were used, 1-10°C/min. The samples were allowed to thermally equilibrate at each temperature step prior to the application of the bias voltages. An equilibrium time of about 5 min was generally found sufficient. The ± bias voltages were applied in preselected increments, usually in 10–20 V.

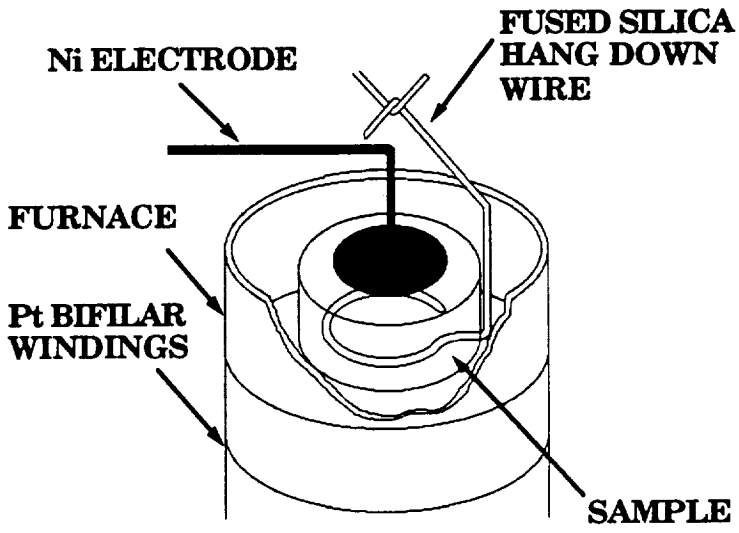

Fig. 1: Cut-away section of bias electrode–sample–counter–electrode assembly in the TGS–1.

It should be emphasized that, from the out–set, the CDA runs with olivine were not intended to simulate the temperature, pressure and oxygen fugacity conditions appropriate for the upper mantle but to duplicate our previous experiments with MgO single crystals as described in Part I. The purpose of the study was to collect as much information about olivine as possible in the temperature interval where the electrical conductivity anomaly is most pronounced, e.g. below 800°C. We exerted no control of the oxygen partial pressure but instead chose the same high purity N_2 gas as in the MgO runs. Though the stated <5 vppm O_2 content of N_2 atmosphere lies outside the thermodynamic stability range of olivine, even if oxidation would take place, it will be kinetically hindered at the relatively low temperatures. The heating times were kept to a minimum, typically 30–45 min, and heating never exceded 800°C. Tests were performed as described below to assess the reversibility of the observed CDA response. As long as the CDA response was reversible, it was assumed that the olivine crystals represented a closed system with no detectable oxidation by the traces of O_2 in the unbuffered N_2 atmosphere. The chance of oxidation was also kept to a minimum by the fact that the single crystals used in this study provided a minimum surface area across which oxidation could occur. We noted that crystals heated for 2 hrs or more to 750–800°C tended to acquire a brownish surface hue, indicative of incipient oxidation [*Iishi*, 1989].

Olivine single crystals from San Carlos, Arizona, USA, were available as large rounded pebbles, optically slightly turbid. Thin sections revealed a polygonized substructure of misoriented subgrains separated by dislocation walls, indicative of a high degree of disorder and/or mechanical deformation in the mantle. Occasionally small veinlets were filled with finely divided matter, probably due to metasomatic alternation. Microscopic inspection of two thin sections of random orientation revealed no visible fluid inclusions though the possibility remains that occasional fluid inclusions were missed during the survey [*Pasteris and Wanamaker*, 1988, *Roedder*, 1984]. No infrared (IR) signals characteristic for fluid or gaseous CO or CO_2 were observed. A large single crystal measuring 5.5 x 8.6 x 9.5 mm was cut and polished on all sides. The IR absorption spectrum recorded through its 8.6 mm thickness showed no detectable ν_{OH} absorption band in the 3700-3300 cm^{-1} range. This indicates a vanishingly small concentration of residual OH^- impurities – a result that is not inconsistent with the wide OH^- concentration range down to nil as reported by Miller et al. [*Miller et al.*, 1987] for many olivine crystals from different locations and definitely less than the ≈20 at.ppm OH^- determined by Mackwell and Kohlstedt [*Mackwell and Kohlstedt*, 1990] in a hydrothermally treated olivine single crystal from the same San Carlos locality.

The 5.5 x 8.6 x 9.5 mm single crystal was cut into eight pieces, each measuring 4.5 x 4 x 2.5 mm, using a thin–blade, water–cooled, slowing rotating diamond saw. The edges were rounded off on SiC sanding paper to approximate a somewhat cylindrical shape. The pieces were cleaned in methanol or chlorinated hydrocarbon solvents and in distilled water. No traces of solvent residues could be detected by IR after drying. The crystals were placed on the fused silica loop with their polished sides facing the bias electrode. The effect of reversing the samples and placing them on the fused silica loop with the rough sides towards the bias electrode was not specifically studied, but it is known both from theory (see Part I) and prior experience with irregularly shaped samples [*Freund et al.*, 1990] that the force measured is a function of the volume integral over the region containing the sample. Hence, the measurements are position–sensitive only to the extent that the volume integral changes.

Results

Our first task was to carry out a careful reversibility test up to 600°C. During experiment #j4 the following heating/cooling protocol was adhered to: (i) a fresh olivine crystal was loaded on the fused silica loop and dried *in situ* at 120°C for 1 hr; (ii) the sample was cooled to ambient temperature (24°C) and then reheated at a rate of 20°C/min to 100°C and on to 600°C in 100°C increments with approximately 30 min hold time at each temperature step during which plus and minus bias voltages were applied sequentially in 20 V increments up to ±100 V; (ii) the sample was cooled in one sweep to 400°C at a cooling rate of 20°C/min and the ± bias voltages were applied as before; (iii) the sample was reheated to 600°C at 20°C/min; (iv) the sample was cooled at 20°C/min from 600°C in one sweep to 300°C; (v) the sample was reheated a third time to 600°C

at 20°C/min; (vi) the sample was cooled to 200°C and then to 100°C, interrupted by application of the ± bias voltages; (vii) the sample was heated a fourth time to 600°C at 20°C/min; and finally, (viii) the sample was cooled to 100°C at 20°C/min. Total duration of run #j4 was >10 hrs with ≈2 hrs accumulative exposure time to 600°C.

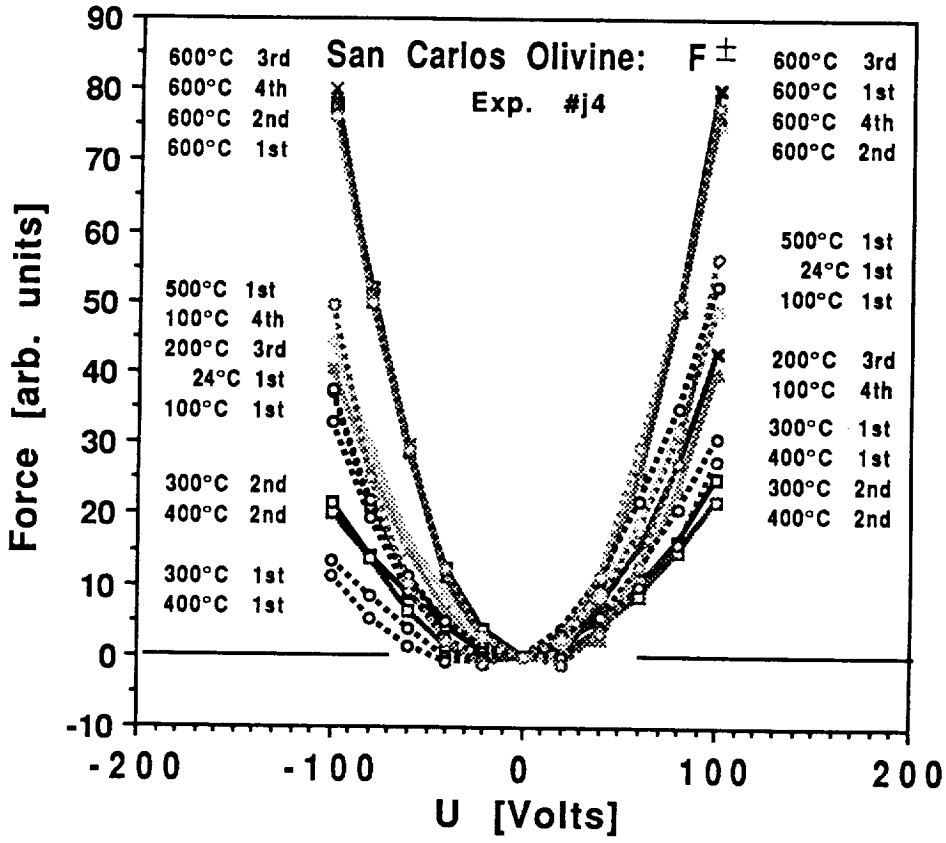

Fig. 2: F^+ and F^- as a function of voltage, measured during four consecutive heating/cooling cycles up to 600°C to demonstrate the reproducibility of the CDA measurements. 1st cycle: circles and dashed lines; 2nd cycle: squares; 3rd cycle: crosses; 4th cycle: triangles. The labels refer to the sequence of the ±100 V data.

In **Fig. 2** all F^+ and F^- values obtained during exp. #j4 are compiled in a force versus voltage plot. The ordinate is in arbitrary units. As expected from the CDA theory presented in Part I the response to increasing bias voltages gives rise to a series of approximately parabolic curves. If

the olivine crystal behaved as an ideal dielectric with a static dielectric constant ε_{static} that is essentially temperature–independent [*Cygan and Lasaga*, 1986], the response would be exactly parabolic, $\mathbf{F}^{\pm} \propto U^2$, and all curves would coincide. The variable steepness of the parabolas reflects a variations in $\varepsilon_{static}(T)$. Deviations from the exact parabolic shape reflect field–variant contributions, $\mathbf{P}_{surface}$, due to surface charges. The surface charges are very sensitive to the cooling rate and cause some significant changes in the $\mathbf{F}^+$ and $\mathbf{F}^-$ values between 100–500°C. The excellent reproducibility (interpreted as absence of irreversible oxidation) is demonstrated by the fact that even after four heating/cooling cycles the $\mathbf{F}^{\pm}$ values at 600°C agreed within ±5%.

In **Fig. 3** the same $\mathbf{F}^{\pm}$ values are used to calculate $\mathbf{F}_{\Sigma}$, e.g. the field–invariant part of the dielectric response which is proportional to ε_{static}. These F_{Σ} values are plotted as a function of T for the four consecutive heating/cooling cycles*. At all temperatures except at 400°C where the reproducibility lies within ±10% the reproducibility is better than ±5%, indicating that the surface contributions were self–cancelling for $\mathbf{F}^+$ and $\mathbf{F}^-$. At 600°C the F_{Σ} values coincide nearly perfectly. This is a strong indication that the olivine underwent no noticeable chemical changes during the heating and cooling cycles due to oxidation. This lends credence to the presumption that the olivine crystals under study can be safely heated repeatedly to at least 600°C without suffering oxidation, even though the ambient N_2 atmosphere was unbuffered. Other experiments similar to #j4 but not shown in detail here were extended to temperatures above 600°C. They indicated a progressive deterioration of the reproducibility above 700°C, suggesting the beginning of oxidation.

* Due to an internal normalization routine the ordinate force units are different than those of **Fig. 2.**

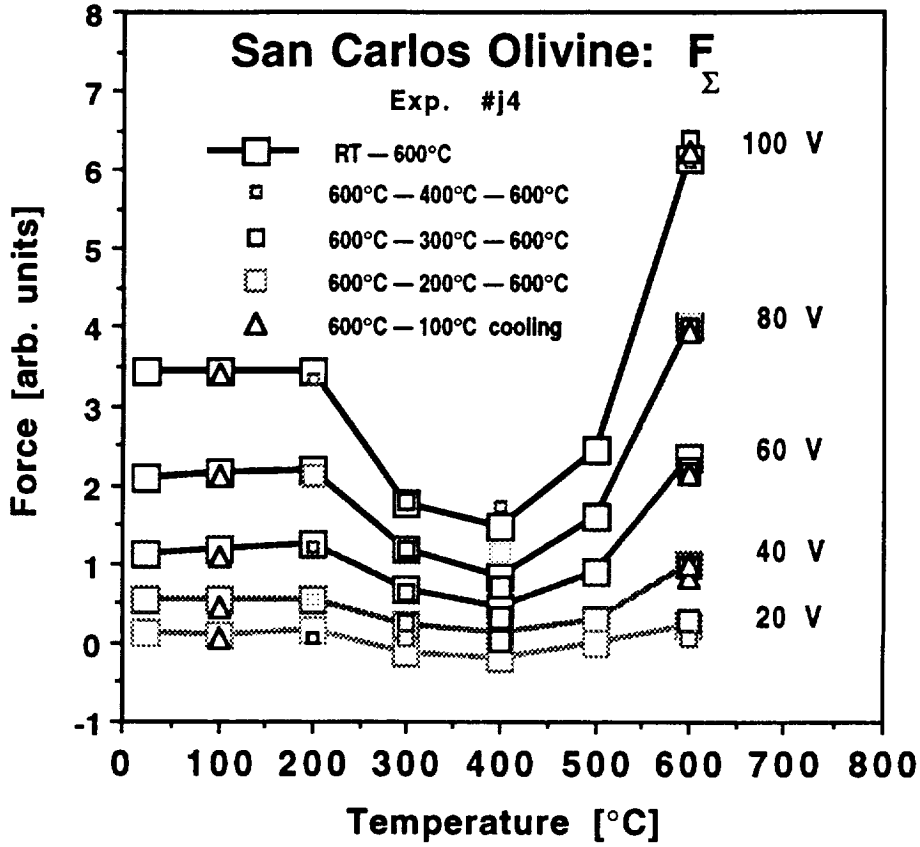

Fig. 3: F_Σ for the four consecutive heating/cooling cycles plotted as a function of temperature. The F_Σ values are reproducible within better than ±5% at 600°C, indicating that the sample did not suffer irreversible changes due to oxidation.

According to **Fig. 3**, during the first heating run, F_Σ was slightly high at 24, 100 and 200°C, lower between 300–500°C and increased again between 400–600°C. Upon cooling the shape of the $F_\Sigma(T)$ curve was reproduced, including the enhanced values at 200 and 100°C**. Most noteworthy is the stepwise F_Σ increase between 450-600°C which was fully reversible within ±5%, even at cooling rates as fast as 20°C/min. Since ε_{static} of an ideal dielectric must be essentially temperature–independent [*Ashcroft and Mermin*, 1976] this stepwise F_Σ increase

** In other experiments with slower cooling rates no enhancement of the F_Σ values upon cooling below 300–400°C were observed, indicating that the lower temperature portion of the $F_\Sigma(T)$ curves shown in **Fig. 3** is affected by the rapid cooling. The reason is that some mobile charge carriers generated at 600°C are easily frozen upon rapid cooling, causing residual polarization.

signals the appearance of mobile charge carriers which increase the dielectric polarizability of the olivine through their $\mathbf{P}_{space}$ contribution. The reproducibility suggests (i) that during reheating approximately the same number of mobile charge carriers is generated and (ii) that the charge carriers disappear upon cooling or become immobilized through a trapping process. The $\mathbf{F}\Sigma(T)$ reproducibility remained within ±10% limits upon heating to 700°C and deteriorated slightly after exposing the olivine crystals to temperatures above 700°C for extended periods of time, typically 2–4 hrs.

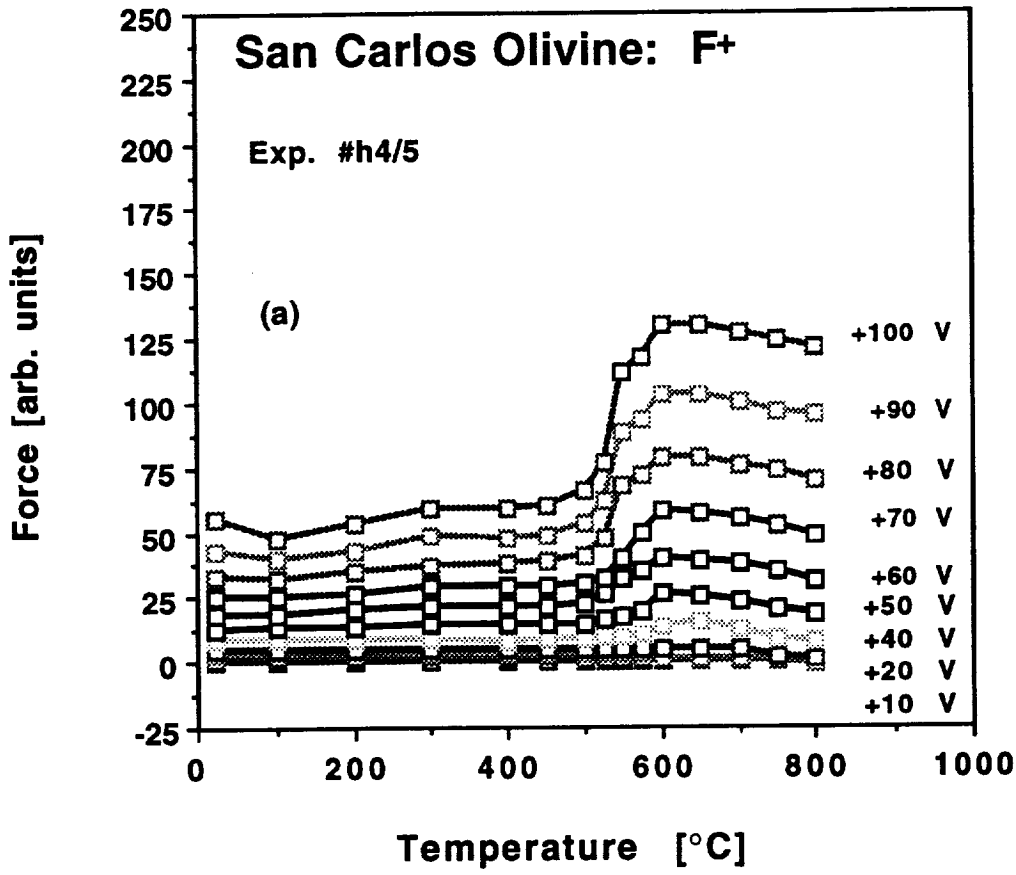

Fig. 4a: F^+ as a function of temperature during stepwise heating to 800°C.

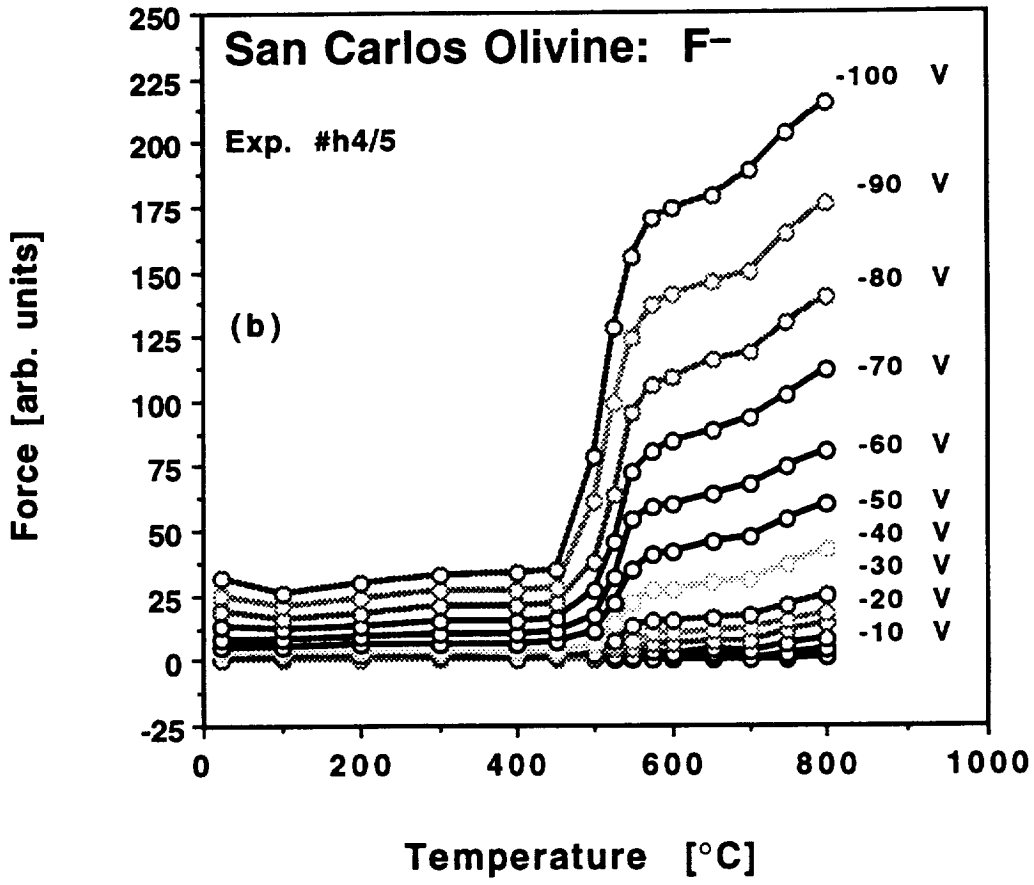

Fig. 4b: F^- as a function of temperature during stepwise heating to 800°C.

After having gained confidence that heating in the unbuffered N_2 atmosphere was benign up to 600°C, acceptable to 700°C and even higher, provided the time of exposure was kept short, we performed stepwise heating experiments up to 800°C without intermittent cooling. The experiments were repeated in nearly the identical way, using a fresh sample. **Fig. 4a/b** shows the result of the most complete run of the series, experiment #h4/5, featuring 15 temperature steps. The sample was first dried *in situ* at 120°C, cooled to 24°C and heated in 100°C steps up to 400°C, in 50°C steps from 400-500°C, in 25°C steps from 500-600°C and to 800°C in 50°C steps, the heating rate between steps always being 40°C/min. After holding the temperature for 5 min the bias voltages were applied in 5 V increments up to ±30 V and in 10 V increments to ±100 V.

The $F^{\pm}$ values were measured continuously but the values used for **Fig. 4a/c** represent those 2 min after application of the bias voltages. Since each temperature step required ≈60 min to complete the sequence of F^+ and F^- measurements, the total duration of run #h4/5 was >18 hrs with >6 hrs exposure to temperatures >600°C. After completing the heating cycle the sample was cooled fast (40°C/min) from 800–600°C and slowly (2°C/min) from 600–24°C while maintaining the flow of N_2. Thereafter the $F^{\pm}$ values were remeasured and were found to agree with those of the first heating run to with approximately ±20%, except below 150°C where the agreement was less than 50%.

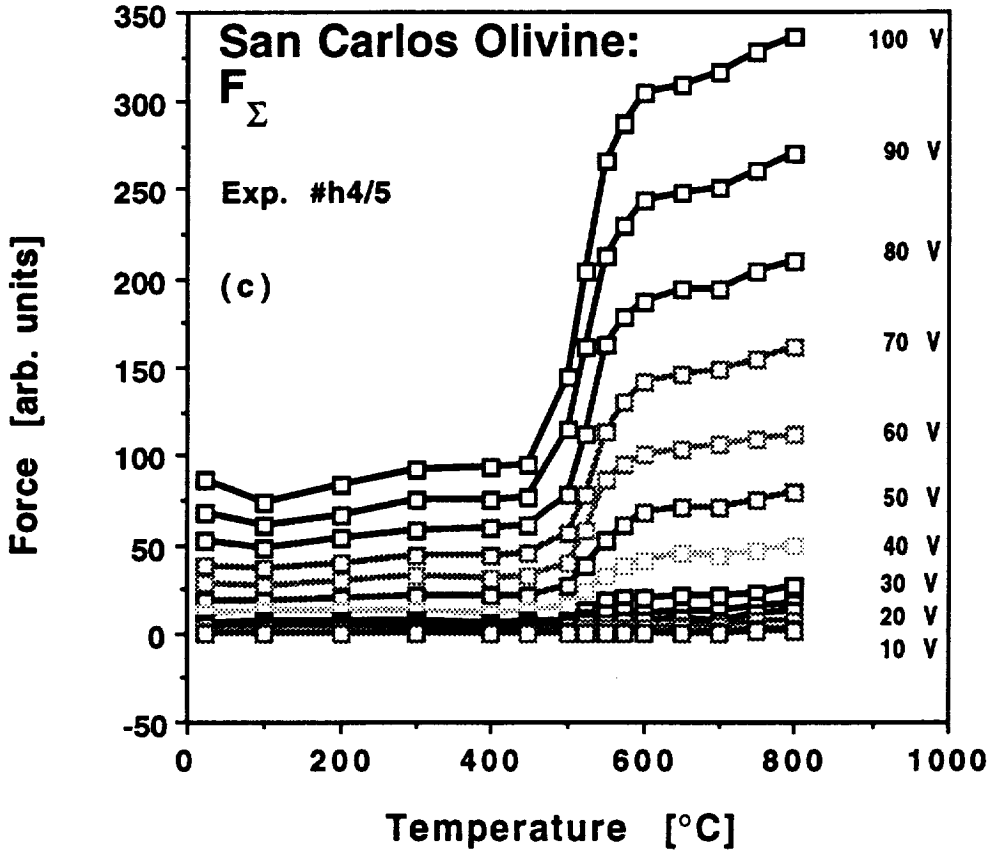

Fig. 4c: F_Σ as a function of temperature during stepwise heating to 800°C.

As shown in **Fig. 4a/b** F^+ and F^- were nearly constant from 24-450°C but rose sharply between 450-600°C. F^- continued to rise between 600–800°C, while F^+ fell off slightly. $F_\Sigma(T)$, depicted in **Fig. 4c**, shows a stepwise increase between 450–600°C, similar to the F_Σ increase in MgO in the same temperature interval (see Part I). Such a stepwise increase can only be caused by the

appearance of mobile charge carriers that are capable of diffusing in the externally applied electric field gradient. Above 600°C F_Σ tended to level out, possibly indicating saturation of charge carriers. This tendency of F_Σ to reach a plateau was repeatedly observed in similar experiments, sometimes even a trend towards a decrease, but upon prolonged heating $F_\Sigma(T)$ continued to rise moderately from 700–800°C as shown in **Fig. 4c**.

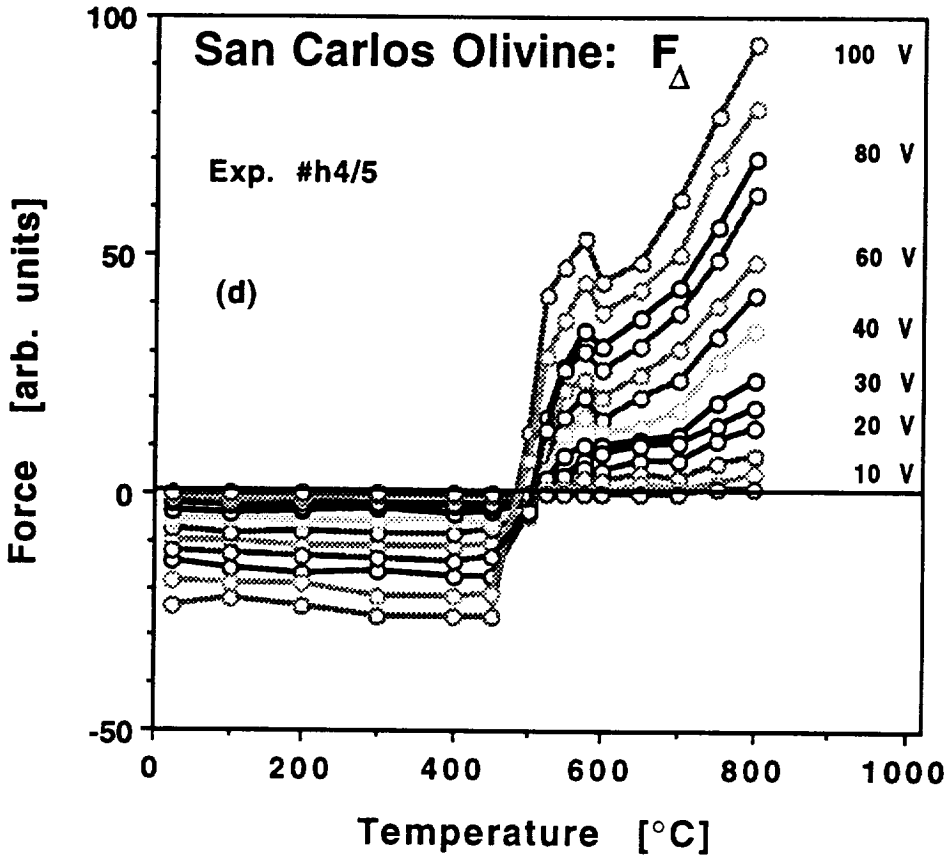

Fig. 4d: F_Δ as a function of temperature during stepwise heating to 800°C.

$F_\Delta(T)$ is depicted in **Fig. 4d**. We recall that F_Δ reflects the field–variant contribution, due to $P_{surface}$, and that its sign gives the sign of the surface charge layer. Below 450°C the surface charge of fresh, previously unheated olivine crystals was weakly but consistently negative or near–zero. Between 450-575°C F_Δ always changed sharply to positive and remained positive up to 800°C. The minimum in the $F_\Delta(T)$ curve in **Fig. 4d** between 600–650°C may be a artefact of the data acquisition routine, caused by different response times of the F^+ and F^- after application of the bias voltage. If F^+ and F^- values recorded 5 or 10 min after application of the the bias voltage were used to calculate F_Δ, the amplitude of the minimum would diminish. We did not

observe a decrease of $\mathbf{F}_\Delta$ above 750°C similar to that reported for MgO (see Part I). Through repetitive heating/cooling cycles it was ascertained that $\mathbf{F}_\Delta$ always tended to be slightly negative or zero between 100–450°C and always became strongly positive above 450–550°C. Upon cooling at <10°C/min the positive $\mathbf{F}_\Delta$ values reverted to near zero or even became negative again. Upon quenching at fast cooling rates, >20°C/min, the $\mathbf{F}_\Delta$ values remained positive as mentioned above. If heating was carried out beyond 700°C, the reversibility was lost and $\mathbf{F}_\Delta$ remained positive.

Next we conducted an experiment to demonstrate the internal electric field associated with the positive surface charge above 500°C. In **Figs. 5a** and **5b** $\mathbf{F}^+$ values obtained during run #H3 are plotted as a function of U and U^2 respectively. (For the sake of clarity not all data contained in **Fig. 5a** are replotted in **Fig, 5b**.) The sample was pretreated in a similar way as for run #h4/5, e.g. dried *in situ* for a few hours around 100°C. After this there was essentially zero surface charge. The sample was then heated in 50°C or 25°C increments to 800°C and positive bias voltages were applied in 2 V or 4 V increments to +20 V, ending with +25 V. All $\mathbf{F}^+$ used for these plots were obtained ≤2 min after application of the bias voltages. The $\mathbf{F}^+(U)$ and $\mathbf{F}^+(U^2)$ curves for the temperature interval 100–500°C are represented by the dotted bold lines. They are nearly perfect parabolas, passing through the origin. All $\mathbf{F}^+$ values within this range were attractive, indicating an essentially zero surface charge and confirming the observations of run #h4/5. The $\mathbf{F}^+(U)$ curves obtained between 550–650°C were no longer simple parabolas passing through the origin. Their linearly extrapolated $\mathbf{F}^+$ vs U^2 graphs shown in **Fig. 5b** intersect the ordinate at negative values. Between 675–800°C the $\mathbf{F}^+$ became clearly repulsive at low bias voltages, indicated by negative force values. Their linearly extrapolated $\mathbf{F}^+$ vs U^2 graphs intersect the ordinate at ever larger negative values.

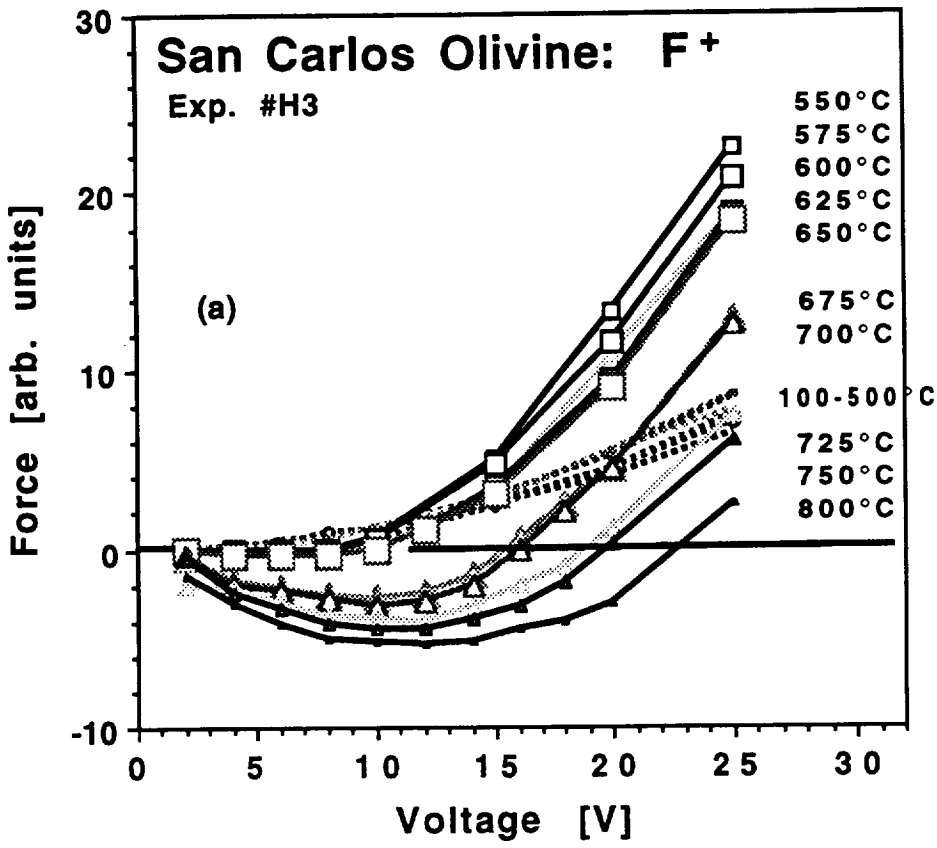

Fig. 5a: F^+ measured under low positive bias during stepwise heating plotted as a function of U. The dotted lines represent data up to 500°C, near–perfect parabolas passing through the origin.

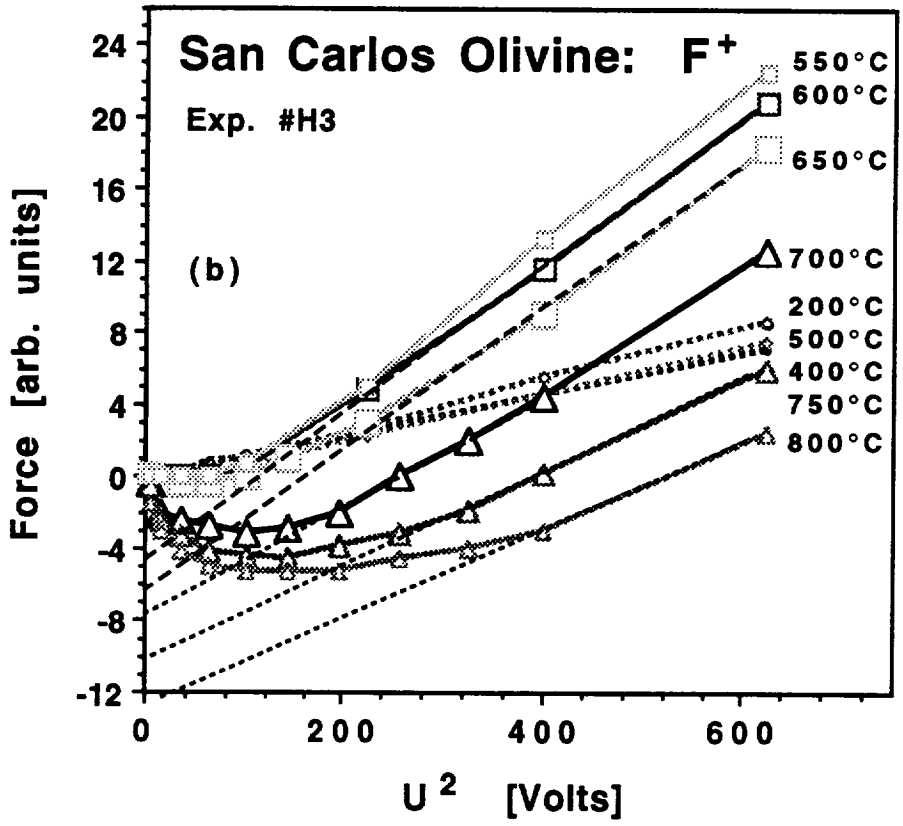

Fig. 5b: F^+ measured under low positive bias during stepwise heating plotted as a function of U^2. The dotted lines are the extrapolated parabolic components measured above 550°C. Some data from (**a**) are omitted in (**b**) for the sake of clarity.

We deconvoluted the F^+ values of **Fig. 5a/b** according to $F^+ = F_0^+ + aU^2$ (see eq. [5] in Part I) where aU^2 describes the ideal dielectric and F_0^+ arises from the charge at the sample surface. The deconvoluted curves are shown in **Fig. 6**. Up to 500°C $F_0^+ \approx 0$, indicating essentially zero surface charge as already mentioned. Between 550–800°C the positive surface charge gives rise to a repulsive term (marked in the lower half of **Fig. 6** by bold lines). U_{crit} as marked by the short vertical ticks indicates the critical voltage up to which the surface charge withstands the externally applied bias voltage. In other words it is the externally applied electric field up to which the surface charge acts as an electrostatic mirror. Above U_{crit} the surface charge is pushed back into the bulk. When the external bias is removed, the positive charge returns to the surface within a very short time, typically <10 sec at 600–650°C. The to–and–from migration of charges between surface and bulk is a fully reversible process as long as no oxidation takes place. In

keeping with the qualitative nature of the measurements presented here the force values in **Fig. 6** are given in arbitrary units. Theoretically it can be shown that $|F_0^+|$ is proportional to the surface charge density [*Freund et al.*, 1989]. In MgO single crystals, assuming a surface layer thickness of 15 nm, the charge carrier density was estimated to be of the order of 10^{21} cm^{-3}. No attempt was made with the present CDA set–up to quantify the surface charge density data for the olivine crystals.

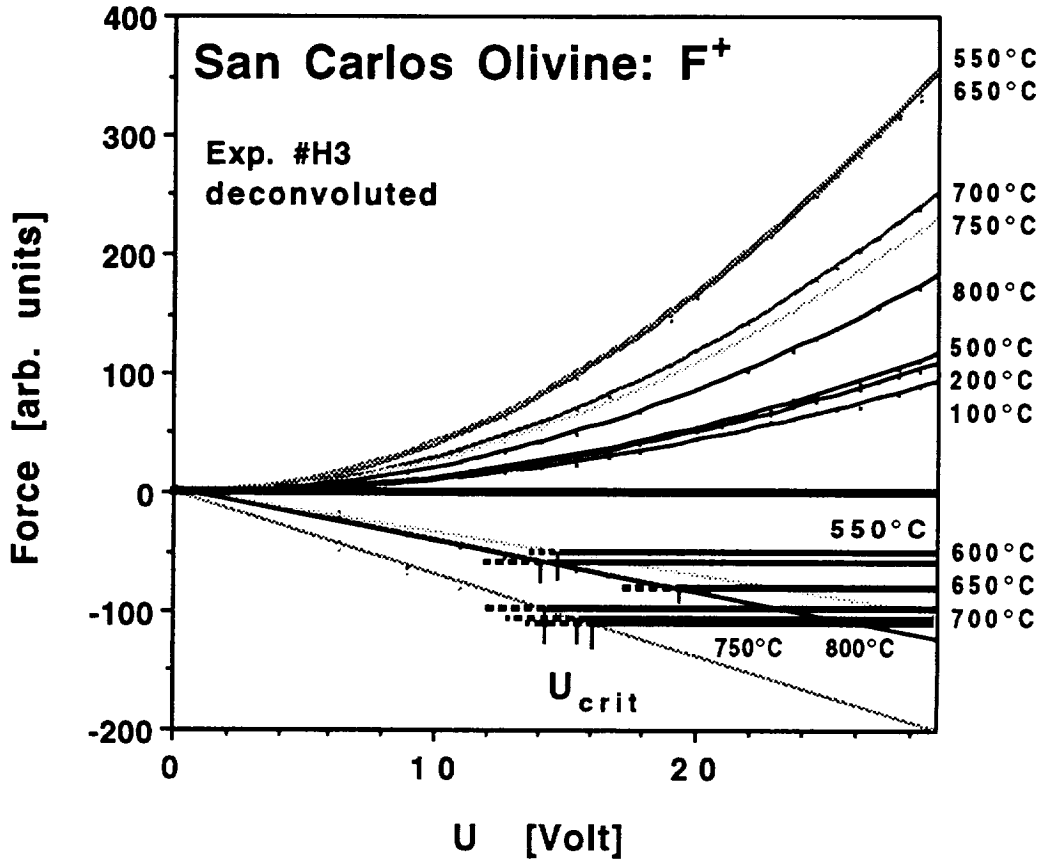

Fig. 6: Same data as shown in **Fig. 5a**, deconvoluted according to $F^+ = F_0^+ + aU^2$.

In closing the results section we note that the data presented in **Figs. 2–6** comprise only a fraction of the experiments which we carried out with olivine to ascertain the reproducibility of the phenomena to a degree of certainty comparable to that of the CDA study MgO as described in Part I [*Freund et al.*, 1991]. We also carried out a preliminary experiment during which we added about 5 vol.-% H_2 for 10-15 min to the N_2 stream close to 700°C. We observed an immediate decrease of the F^+ and F^- response. The rapidity of the changes indicated that a surface reaction had taken place. After the H_2 pulse F^+ and F^- did not fully recover, indicating an at least in part

irreversible reactions. A more complete study of the effects of H_2 and other reduced gases on the CDA response of olivine will be presented in a separate report.

Discussion

The main advantage of the CDA technique is that, by measuring contact–free under minimum perturbation conditions, it provides insights into charge generation and mobilization processes which cannot be achieved by any other single method. By way of the dielectric polarization at 0 Hz CDA detects mobile charge carriers without external carrier injection or extraction. In particular, CDA has the capability (i) of detecting the appearance and disappearance of charges in the bulk, (ii) of detecting the appearance and disappearance of surface charges, and (iii) of determining the sign and strength of the internal fields which support the surface charges.

The CDA data of olivine presented in this first report are still qualitative. We have not yet developed the mathematical tools to calculate the concentration of mobile charge carriers by finite element analysis. However, the reality of the observed physical phenomenon cannot be denied. The measurement of the dielectric polarization, contact–free in an electric field gradient of reversible polarity at 0 Hz, is a sufficiently simple technique that a number of conclusions can be drawn. The measurements clearly indicate that charge carriers are generated in the olivine crystals upon heating to 450–550°C, that these charge carriers are highly mobile and positive, and that they persist to higher temperatures, at least 700°C, possibly higher. They reversibly disappear upon cooling. These charge carriers are <u>not</u> the product of extraneous contamination. The most cogent argument against surface contamination stems from the fact that a surface charge develops which is supported by a strong internal electric field and that this surface charge vanishes when the mobile bulk carriers disappear. There is no physical process by which an internal electric field could support an surface charge layer, unless the charges which appear at the surface originate in the bulk of the crystal. The internal elecric field signals that something inside the crystal "pushes" the charge carriers to the surface and maintains them there, even against an externally applied counterfield of considerable strength. Neither a layer of "dirt", deposited onto the surface through amorphous carbon vapor deposition, nor defects introduced into the surface through polishing and other structurally damaging treatments can explain the presence of such an internal field.

The existence of surface charge layers on predominantly ionic crystals has long been predicted on thermodynamic grounds [*Kliewer and Koehler*, 1965, *Lehovec*, 1953]. They are a consequence of the fact that the free energies of formation for different families of point defects differ slightly at the surface and in the bulk. As a result, intrinsic defects such as cation and anion vacancies are present in different stoichiometric proportions near the surface than in the bulk. This creates charge imbalance even under thermodynamic equilibrium conditions. The surface charges can be exacerbated by the extrinsic defects and impurities, in particular by the segregation of aliovalent impurities. Such a segregation will always occur when the impurity concentration in the bulk exceeds the solubility limit [*Kingery*, 1974a/b]. However, the appearance and disappearance of

the positive surface charge in olivine between 450–550°C does not fall into this category of aliovalent impurity segregation. First, the temperature is too low and the reversible changes too rapid for atomic or ionic diffusion as we know it. The observations rather suggest electronic charges moving to and from the surface without attendant mass transport. Second, the surface charge is supported by an internal field, even against an externally applied counterfield. Such an internal field can only be generated, if the charges originate in the bulk and internal forces cause them to diffuse to the surface.

Positive charge carriers have already been observed in olivine at 1300°C through thermoelectric effect measurements in the stability region of olivine [*Schock et al.*, 1989]. It was suggested that these charge carriers consist of holes that are reversibly generated by the oxidation of Fe^{2+} to Fe^{3+} via gas phase O_2 according to the reaction:

$$8\,Fe^{x}_{Mg} + 2\,(O_2)_{gas} \Leftrightarrow 8\,Fe^{\bullet}_{Mg} + 4\,O^{x}_{O} + 2\,V^{''}_{Mg} + V^{''''}_{Si} \qquad [1]$$

In keeping with the non–stoichiometry of olivine as a function of oxygen fugacity [*Duba et al.*, 1974, *Duba and Nicholls*, 1973], eq. [1] is written as a reversible reaction. It postulates that, upon oxidation, the concentration of Fe^{3+} increases together with the concentration of Mg^{2+}, Fe^{2+} and of Si^{4+} vacancies [*Nakamura and Schmalzried*, 1983, *Sockel*, 1974]. Eq. [1] has been formulated for temperatures well above the temperature region which we have covered in our CDA experiments. At 1300°C diffusional processes involving cation vacancies and oxygen incorporation are most certainly activated, allowing the olivine structure to adjust to a changing oxygen fugacity within short time by $(Mg,Fe)^{2+}$ and Si^{4+} vacancy formation. It is quite possible that the charge carriers responsible for the sign of the thermoelectric effect at 1300°C do indeeed consist of defect electrons on the cation sublattice as postulated by Schock et al. [1989], e.g. of holes that form Fe^{3+} hopping from Fe^{2+} to Fe^{2+} site.

At 450–550°C, however, it is very unlikely that holes could be generated by the same processes as described in eq. [1], e.g. by incorporating gas phase O_2 into the bulk of mm–sized olivine single crystals and concomitant formation of $(Mg,Fe)^{2+}$ and Si^{4+} vacancies. Even if we assume for a moment that Fe^{2+} would become oxidized despite kinetically unfavorable factors by O_2 in the unbuffered N_2 atmosphere, and that $(Mg,Fe)^{2+}$ and Si^{4+} vacancies would form in accordance to eq. [1], we still have to explain the reversibility observed by CDA. Since the CDA experiments were carried out in N_2 containing ≥5 vppm O_2, the ambient P_{O_2} was many orders of magnitude above the oxygen fugacity prevailing in the upper mantle [*Nitsan*, 1974]. As a result any oxidation of the olivine at 450–550°C, if it occurs through reaction with the gas phase O_2, can only be unidirectional. This means that each successive heating of the olivine crystals to 600°C should have led to progressively more oxididation. Instead, as depicted in **Fig. 2**, the CDA data show a nearly perfect reproducibility of the field–invariant part of the dielectric polarization, $\mathbf{F}_{\Sigma}(T)$. Since $\mathbf{F}_{\Sigma}$ responds to the charge carrier concentration in the bulk, we conclude that the number of holes generated within the crystal during repetitive cycling up to at least 600°C was

constant and that the holes cannot be due to Fe^{2+} oxidation through traces of O_2 in the N_2 atmosphere.

If the appearance of hole–type charge carriers in olivine cannot be blamed on extraneous O_2, we are left with only one alternative: In the *as received* state, e.g. as delivered by the upper mantle and retrieved in the field, the olivine crystals must contain a hidden reservoir of hole–type charge carriers. One of the characteristic features of this reservoir is that, upon thermal activation through repetitive heating and cooling cycles, charge carriers are reversibly released and consumed. We therefore now direct our attention to solid state processes by which hole–type charge carriers may be reversibly generated. Since there exist no known structural or magnetic phase transitions in olivine between 450-600°C and no mixing/unmixing of the forsterite–fayalite solid solution [*Brown*, 1980], and since the $(Mg,Fe)^{2+}$ sublattice cannot be the source on the basis of the arguments just presented, the only alternative is that the hidden reservoir lies in the O^{2-} sublattice. The holetype charge carriers which become mobile are then, by definition [*Henderson and Wertz*, 1977, *Marfunin*, 1979], positive holes, e.g. O^- states. They acquire their mobility not by hopping from cation to cation sites but by entering acceptor levels near the O2p–dominated valence band.

During an earlier single crystal IR study of San Carlos olivine [*Freund and Oberheuser*, 1986] two observations were made which are relevant here. First, two groups of IR absorption bands due to OH^- impurities were observed. With respect to their relative position and intensities they resembled the OH^- impurity bands in MgO which had been assigned to single OH^- and to OH^- pairs at cation vacancy sites, $[OH^{\cdot} V''_{Mg}]^{\prime}$ and $[OH^{\cdot} V''_{Mg} {}^{\cdot}HO]^{x}$. As in MgO the bands assigned to OH^- pairs had a lower intensity than the bands assigned to single OH^- defects. This was in conflict with the expectation that OH^- pair defects, associated with divalent cation vacancies, should be more abundant. Second, a weak, but distinct IR band was observed in the 4150 cm^{-1} region which indicated the presence of H_2 molecules in the olivine structure. By analogy to MgO it was therefore suggested that the OH^- pair defects in olivine had been used up by a redox reaction to form H_2 molecules plus peroxy entities as OH^- pair defects in MgO (see eqs. [3/4] in Part II).

While there is only one substitutional mode for H_2O into MgO, in the olivine structure H_2O may substitute for either (Mg,Fe)O or SiO_2 component. The substitution for SiO_2 is arguably improbable, given the fact that olivine crystals in upper mantle rocks is generally associated with SiO_2–richer phases such as pyroxenes. Therefore, they are more likely (Mg,Fe)O–deficient than SiO_2–deficient as had been suggested by Beran and Putnis [1983]. If dissolution of δ H_2O in olivine occurs by substituting for δ(Mg,Fe)O, the structural formula becomes:

$$(Mg,Fe)_2\,SiO_4 + \delta\,H_2O \Leftrightarrow (Mg,Fe)_{2-\delta}\,SiO_{4-2\delta}(OH)_{2\delta} + \delta\,(Mg,Fe)O \quad [2]$$

If OH^- pairs in olivine, like their equivalent in MgO, underwent a redox conversion to H_2 plus peroxy and if these H_2 molecules subsequently diffused out of the olivine crystals, we have:

$$(Mg,Fe)_{2-\delta}\,SiO_4/(H_2)\delta \Rightarrow (Mg,Fe)_{2-\delta}\,SiO_4 + \delta\,H_2\Uparrow \qquad [3]$$

where the slash on the left hand side indicates that the H_2 molecules at first still reside in the olivine structure. After they diffused out the remaining, peroxy–bearing olivine would have the non–stoichiometry shown on the right hand side. If $\delta \ll 1$, this simplifies to $(Mg,Fe)_2SiO_{4+\delta}$ representing an olivine with excess oxygen contained in the structure in form of peroxy entities and balanced by a certain concentration of cation vacancies, primarily among Mg^{2+} and Fe^{2+}.

It should be noted that the actual oxygen content of natural minerals is never determined analytically. The reason is that oxygen is always assumed to be in the –2 oxidation state. Therefore, the contention that mantle–derived olivine may be slightly oxygen–rich, due to the sequence of redox and diffusional steps described by eqs. [2] and [3], cannot be supported by quoting chemical analyses from the literature. If $\delta \ll 1$, it is questionable whether the precision of current analytical techniques suffices to ascertain a small deviation from $(Mg,Fe)_2SiO_4$ towards $(Mg,Fe)_2SiO_{4+\delta}$. The task is made even more difficult by the fact that any small increase of the Fe^{3+} concentration would also be reflected in a deviation of the bulk stoichiometry towards $(Mg,Fe^{2+},Fe^{3+})_2SiO_{4+\delta}$. In order to chemically analyze for the alleged peroxy content one would have to determine both the oxygen to cation ratio and the Fe^{2+}/Fe^{3+} ratio. The latter may be possible by means of Mössbauer spectroscopy. It has been noted that the Fe^{2+}/Fe^{3+} ratios as determined from Mössbauer spectra are often inconsistent with the Fe^{2+}/Fe^{3+} ratios as determined by conventional wet–chemical techniques or as calculated from microprobe data [*Dyar et al.*, 1989]. During wet–chemical analysis any peroxy entities which exist in a mineral will be acid–hydrolyzed and used up to oxidize Fe^{2+}, thus resulting in a high apparent Fe^{3+} content. Mössbauer spectroscopy, by contrast, would measure the Fe^{2+}/Fe^{3+} ratio irrespective of whether or not peroxy coexist in the mineral matrix. A possible way to assess the peroxy content would be to heat a given olivine crystal in a small fused silica tube, sealed under vacuum, up to a temperature at which all peroxy would be consumed by the oxidation of Fe^{2+} to Fe^{3+}, followed by an acurate Mössbauer determination of the Fe^{3+} content retained in the olivine structure or used to form other phases:

$$Fe^{x}_{Mg} + O^{\bullet}_{O} \Rightarrow Fe^{\bullet}_{Mg} + O^{x}_{O} \qquad [4]$$

A major uncertainty of such a procedure rests with the assumption that the olivine crystals do not contain any other oxidizeable components such as traces of amorphous carbon lining the walls of fluid inclusion cavities and/or dislocations [*Green and Guegen*, 1983] which would also potentially react with O^- to give CO and CO_2.

While MgO is highly ionic, the bonding within the SiO_4 tetrahedra in olivine is strongly covalent and every oxygen belongs to an SiO_4 tetrahedron. If there is formation of peroxy entities in olivine, they will probably be quite different from the peroxy anion, O_2^{2-}, believed to exist in the MgO structure. The exact structure of the peroxy entities in olivine is unknown, but by analogy to other cases general features may be outlined. For the substitutional mode described by eq. [2] the

two most likely OH^-–compensated cation vacancy defects contain one or two OH^-. Since all O are bound to Si, they are of the form $O_3Si–OH\ V''_{Mg}$ and $O_3Si–OH\ V''_{Mg}\ HO–SiO_3$, where V''_{Mg} stands for a divalent cation vacancy* . A likely peroxy configuration is one that can be described as peroxy link:

$$O_3Si–OH\ \ HO–SiO_3 \Leftrightarrow O_3Si/^{OO}\backslash SiO_3 + H_2 \qquad [5]$$
$$V''_{Mg} \qquad\qquad V''_{Mg}$$

Peroxy links between SiO_4 tetrahedra, $O_3Si/^{OO}\backslash SiO_3$, have been discussed as a possible defect in vitreous SiO_2, beside the alternative configuration $O_3Si\backslash^{O}_{O}/SiO_3$. They are believed to be the source defects for the peroxy radicals, $O_3Si/^{OO\bullet}$, which are produced by low temperature (77 K) γ– or x–irradiation [*Friebele et al.*, 1979]. Shelby [1980] reported on a large increase of Si–OH when molecular H_2 was allowed to diffuse into initially OH–poor fused silica and ascribed it to a reaction similar to eq. [5] reversing from right to left.

Miller et al. [*Miller et al.*, 1987] who sampled olivine crystals from a worldwide distribution of localities failed to observe the very weak IR band of H_2 molecules. On the basis of this negative evidence they dismissed the possibility that OH^- pairs could undergo a redox conversion into H_2 plus peroxy entities. Unfortunately, the absence of H_2 molecules is not a strong argument against eq. [3] because H_2 molecules are not only intrinsically IR–inactive but can also diffuse out of the olivine crystals under study, removing the evidence of former OH^- and leaving peroxy entities as the only memory. We recall that the olivine crystals studied here show no IR band attributable to OH^- impurities. Hence, according to conventional wisdom, these olivine crystals would have to be classified as OH^-–free, suggesting that they come from an anhydrous portion of the upper mantle. If we admit on the basis of the evidence presented above that the same crystals contain peroxy entities and that these elusive defects may have formed according to eq. [5], our outlook changes.

As in the case of O_2^{2-} in MgO, peroxy defects in olivine become detectable only after they dissociate into O^-. Peroxy links are expected to dissociate as follows:

$$O_3Si/^{OO}\backslash SiO_3 \Leftrightarrow O_3Si/^{O\bullet}\ ^{\bullet O}\backslash SiO_3 \qquad [6]$$
$$V''_{Mg} \qquad\qquad V''_{Mg}$$

The two radicals on the right hand side may also be written as $[SiO_4]^\bullet$ or $[SiO_4]^{3-}$ with the hole delocalizing over the $[SiO_4]^{4-}$ tetrahedra [*Marfunin*, 1979] and possibly beyond. Propagation of the positive hole can then occur in a similar manner as for O^- states in MgO, e.g. by delocalizing on energy levels near the O 2p–dominated valence band [*Freund et al.*, 1989]. In the case of MgO, because of its intrinsic diamagnetism, we could follow the spin decoupling which precedes

* Footnote: Here we do not use the strict Kröger defect nomenclature because the result would be rather unyielding, given the complexity of the structural unit considered.

the dissociation $O_2^{2-} = O^- + O^-$ by magnetic measurements [*Batllo et al.*, 1990] and compare them to the CDA data. In the case of the olivine crystals the high concentration of Fe^{2+} and other transition metal cations prevents magnetic measurements from being a useful diagnostic tool and we have to rely on CDA for obtaining the necessary information.

The fact that highly mobile charge carriers appear in olivine upon heating to 450°C, generate a positive surface charge, reach saturation between 550–600°C, and disappear upon cooling is strikingly similar to MgO. Since we can be sure that the charge carriers in MgO are positive holes, e.g. O^- states propagating through the O^{2-} sublattice via some sort of O^{2-}/O^- valency fluctuations on energy levels near the O 2p–dominated valence band, we suggest that the positive charge carriers in olivine are of the same nature. We conclude that the mantle–derived olivine crystals under study contain the equivalent of the peroxy defects in MgO, probably peroxy links as described by eqs. [5/6] or some other similar configuration of self–trapped O^- dimers. These peroxy entities probably derive from solute H_2O (and possibly other fluid phase components [*Freund*, 1987]) that became incorporated into the olivine structure during crystallization in the high pressure–high temperature environment of the upper mantle.

There is a distinct difference to MgO, however, with respect to $\mathbf{F}_\Delta$ and its temperature dependence. In the case of MgO we noted (in Part I) that $\mathbf{F}_\Delta$ reached a maximum around 750°C and then decreased upon further heating. In Part II we presented evidence that the $\mathbf{F}_\Delta$ decrease correlates with the emission of atomic O from the MgO surface. If O is emitted from the top surface layer by O^- disproportionating according to reaction $O^- + O^- \Rightarrow O^{2-} + O\Uparrow$, two positive charges which had been transported by the O^- from the bulk to the surface become permanently fixed in the form of an anion vacancy, $V_O^{\bullet\bullet}$. In order to balance this fixed charge and reduce $\mathbf{F}_\Delta$ an aliquot number of Mg^{2+} vacancies, $V_{Mg}^{''}$, have to diffuse outwards from the bulk to the surface. In the case of MgO it is known that cations become diffusively mobile around 750–800°C by a vacancy hopping mechanism [*Sempolinski and Kingery*, 1980]. Consequently, annealing of $V_{Mg}^{''}$ is the most likely process that accounts for the reduction of F_Δ above 750°C in MgO. In the case of olivine, as shown in **Fig. 4d**, we do not observe a clear maximum in the $\mathbf{F}_\Delta(T)$ curve but only a transient feature followed by a further rise beyond 750°C. Concurrently the $\mathbf{F}_\Delta(T)$ reversibility is lost. In some experiments we noted a brownish hue on the olivine surface, indicating the onset of oxidation. Whether or not this oxidation ≥750°C is caused by Fe^{2+} reacting with extraneous gas phase O_2 in the unbuffered N_2 atmosphere or by Fe^{2+} reacting with indigenous O^- is yet unclear. In both cases $\mathbf{F}_\Delta$ is expected to become even more positive through the formation of Fe^{3+} on (Mg,Fe^{2+}) lattice sites.

At the beginning, in Part I, we pointed out that the electrical conductivity of olivine widely believed to be relevant to the upper mantle is the conductivity experimentally determined after the anomaly ≤700°C has been removed. The removal is achieved by heating the mantle–derived olivine crystals in CO/CO_2 or H_2/CO_2 gas mixtures until their electrical conductivity values come down to the low level characteristic for 0.1 MPa conditions. This procedure is justified by the conjecture that the conductivity anomaly is nothing but a "dirt effect", caused by extraneous

contamination. Now we know that the anomaly is due to indigenous O^- charge carriers. To the best of our current understanding these O^- charge carriers and their parent defects, the peroxy entities, represent a "memory" of a solute H_2O content, e.g. of an eariler OH^- content. IR spectroscopy in inapplicable because H_2 molecules and peroxy are intrinsically IR–inactive. Any attempt to use Raman spectroscopy would probably fail because of the relatively low H_2 and peroxy concentration. Electron paramagnetic resonance spectroscopy cannot used either because mantle–derived olivine crystals typically contain a much too high Fe^{2+} content.

By heating mantle–derived olivine to 700°C in CO/CO_2 or H_2/CO_2 at 0.1 MPa and thus removing their conductivity anomaly, the crystals loose their indigenous O^-–type charge carriers. Thus, their natural state is altered. The experimentally measured conductivity may no longer reflect the "true" conductivity which the same crystals would display, if they still had their full complement of O^-. One may argue that 700°C is too low a temperature to be of significance because, in the upper mantle, temperatures are likely to exceed 1000°C. However, this argument is fallacious because it is based on the assumption that the O^- charge carriers must disappear around 700°C. In reality, the annihilation of O^- around 700°C is probably an artefact of the experimental set–up used in any conductivity measurement: the O^- charge carriers are only consumed because the samples possess a free surface across which the O^- react with the CO/CO_2 or H_2/CO_2 gases. In the laboratory set–up the system is not closed. In the upper mantle, however, the olivine crystals will not possess a free surface (unless $CO/CO_2/H_2O$ fluids freely percolate around each grain). Therefore, to the extent that the upper mantle can be considered a closed system, the possibility has to be taken into consideration that O^- charge carriers persist beyond the 700°C threshold annihilation temperature.

Very little is known about the effect of pressure on the stability of O^- and on the stability of their parents defects, the peroxy entities. Given the fact that the O^-–O^- peroxy bond is short, typically ≈1.5 Å [*Cremer*, 1983] compared to 2.8–3.0 Å for most O^{2-}–O^{2-} distances in silicates, pressure is expected to delay peroxy dissociation and, hence, the generation of O^- charge carriers to higher temperatures [*Freund*, 1987]. Unless there are competitive mechanisms by which O^- can be consumed, for instance by oxidizing Fe^{2+} to Fe^{3+} and incorporating these Fe^{3+} into phases such as spinel or orthopyroxenes which accommodate or require Fe^{3+} in their respective crystal structures, the range over which O^- charge carriers might exist under upper mantle pressure conditions may extend into the 1000–1200°C region.

So far we only studied the O^- charge carrier generation at 0.1 MPa pressure during heating. From the available evidence we conclude that the O^- derive from peroxy parents. We recognize that the olivine crystals under study have a complex history in the pressure–temperature–time (P–T–t) space. At which point in the P–T–t space the peroxy parents have been introduced is unknown. They may have formed in the mantle, e.g. before the olivine crystals were brought up to the surface of the earth by volcanic activity. They may have formed during ascent while the olivine crystals underwent decompression and cooling. They may have formed after cooling. Each scenario would lead to different consequences with respect to the conductivity behavior of olivine

in the upper mantle. As long as the P–T–t pathway of the peroxy formation reaction is unknown, the field remains open to speculation.

One question, however, can be answered with some degree of confidence: The long–standing controversy concerning the sensitivity of olivine to oxidation in unbuffered environments. Many researchers have observed that olivine crystals readily show signs of oxidation when heated in any gas environment where the oxygen fugacity lies outside the thermodynamic stability range of the olivine phase [*Nitsan*, 1974]. As tell–tale signs for beginning oxidation color changes are reported and the precipitation of minute crystals of iron oxides at the surface and along dislocation lines [*Duba and Nicholls*, 1973, *Durham and Goetze*, 1977]. If one is unaware of the possible presence of peroxy entities in olivine, the conclusion appears unavoidable that traces of O_2 in the gas or traces of H_2O in microcracks are the oxidants and that only a prolonged exposure to reducing CO/CO_2 or H_2/CO_2 gases will correct the situation. However, if mantle–derived olivine crystals contain peroxy entities in their structure, due to solute H_2O component, followed by the redox reaction and loss of H_2 by diffusion as discussed above, the outlook changes: Crystals containing peroxy defects are susceptible to an internal oxidation according to eq. [4]. Such an internal oxidation occurs in the absence of any trace of O_2 in the gas phase. Even if one were able to produce an Ar or N_2 atmosphere with only a few O_2 molecules per liter, equivalent to $P_{O_2}<10^{-20}$ as required by the linear extrapolation of the thermodynamic data pertinent to the high temperature stability of olivine, the olivine crystals under study would still oxidize from within.

Acknowledgements

This work was supported in part by the National Aeronautics and Space Administration through the Cooperative Agreement with the SETI Institute NCC 2-446 and the NASA Ames Research Center Directors' Discretionary Fund, by NATO Grant RG.890479, and by European Economic Communities Contract EN 3C-0023-D. F.F. acknowledges receipt of a National Research Council Senior Associateship during the early part of the work.

References

Ashcroft, N.W., and N.D. Mermin, *Solid State Physics,* Holt–Saunders Internatl., Philadelphia, 1976.

Batllo, F., R.C. LeRoy, K. Parvin, F. Freund, and M.M. Freund. Positive hole centers in magnesium oxide — correlation between magnetic susceptibility, dielectric anomalies and electric conductivity., *J. Appl. Phys. (in print).*

Beran, A. , and A. Putnis. A model of the OH positions in olivine, derived from infrared-spectroscopic investigations, *Phys. Chem Minerals*, 9, 57-60, 1983.

Brown, G. E., *Olivine and silicate spinels,* in: *Reviews in Mineralogy*. Ed. ed. R.H. Ribbe, p. 275-381, Washington, D. C., Amer. Mineral. Soc., 5 1980.

Constable, S., and A. Duba. Electrical conductivity of olivine, a dunite and the mantle, *J. Geophys. Res.*, 95, 6967-6978, 1990.

Cremer, D., *General and theoretical aspects of the peroxide group,* in: *The Chemistry of Functional Groups, Peroxides*. Ed. ed. S. Patai, p. 1-79, Wiley & Sons, Publ., New York, 1983.

Cygan, R.T., and A.C. Lasaga. Dielectric and polarization behavior of forsterite at elevated temperatures, *Amer. Mineral.*, 71, 758-766, 1986.

Duba, A., H. C. Heard, and R. N. Schock. Electrical conductivity of olivine at high pressure and under controlled oxygen fugacity, *J. Geophys. Res.*, 79, 1667-1673, 1974.

Duba, A., and I. A. Nicholls. The influence of the oxidation state on the electrical conductivity of olivine, *Earth Planet Sci. Lett.*, 18, 59-64, 1973.

Duba, A., M. Young, and T. J. Shankland. Electrical conductivity of synthetic olivine to 1500°C: Product, Promise and Problems., *Eos*, 69, 1436, 1988.

Durham, W. B. , and C. Goetze. Plastic flow of oriented single crystals of olivine, I. Mechanical data, *J. Geophys. Res.*, 82, 5755-5770, 1977.

Dyar, M.D., A.V. McGuire, and R.D. Ziegerl. Redox equilibria and crystal chemistry of coexisting minerals from spinel lherzolite mantle xenoliths, *Amer. Mineral.*, 74, 969-980, 1989.

Freund, F. Electrical conductivity measurements under minimum perturbation conditions. Part II: O^- charge carriers in magnesium oxide., *J. Geophys. Res.*, in submission, 1991.

Freund, F. Hydrogen and carbon in solid solution in oxides and silicates, *Phys. Chem. Minerals*, 15, 1-18, 1987.

Freund, F., M.M. Freund, and F. Batllo. Electrical conductivity measurements under minimum perturbation conditions. Part I: Charge Distribution Analysis of magnesium oxide, *J. Geophys. Res.*, in submission, 1991.

Freund, F., G.C. Maiti, F. Batllo, and M. Baerns. O^- identified at high temperatures in CaO-based catalysts for oxidative methane dimerization, *J. Chim. Phys. (France)*, 87, 1467-1477, 1990.

Freund, F. , and G. Oberheuser. Water dissolved in olivine: a single crystal infrared study, *J. Geophys. Res.*, 91, 745-761, 1986.

Freund, M.M, F. Freund, and F. Batllo. Highly mobile oxygen holes in magnesium oxide, *Phys. Rev. Lett.*, 63, 2096-2099, 1989.

Friebele, E. J., D. L. Griscom, M. Stapelbroek, and R.A. Weeks. Fundamental defect centers in glass: The peroxy radical in irradiated high-purity fused silica, *Phys. Rev. Lett.*, 42, 1346-1349, 1979.

Green, H.W., and Y. Guegen. Deformation of peridotite in the mantle and extraction by kimberlite: A case history documented by fluid and solid precipitates in olivine, *Tectonophys.*, 92, 71-92, 1983.

Henderson, B., and J. E. Wertz, *Defects in the Alkaline Earth Oxides*, Taylor & Francis, London, 1977.

Iishi, K. Synthesis of laihunite by heating Fe-Mn olivine in air, *N. Jb. Mineral. Monatshefte*, 1989, 245, 1989.

Kingery, W. D. Plausible concepts necessary and sufficient for interpretation of ceramic grain boundary phenomena: I. Grain boundary characteristics, structure and electrostatic potential, *J. Amer. Ceram. Soc.*, 75, 1-8, 1974a.

Kingery, W. D. Plausible concepts necessary and sufficient for interpretation of ceramic grain boundary phenomena: II. Solute segregation, grain-boundary diffusion and general discussion., *J. Amer. Ceram. Soc.*, 75, 74-83, 1974b.

Kliewer, K. L., and J.S. Koehler. Space charge in ionic crystals. I. General approach with application to NaCl, *Phys. Rev. A*, 140, 1226-1240, 1965.

Lehovec, K. Space-charge layer and distribution of lattice effects at the surface of ionic crystals, *J. Chem. Phys.*, 21, 1123-1128, 1953.

Mackwell, S. J. , and D. L. Kohlstedt. Diffusion of hydrogen in olivine: Implications for water in the mantle, *J. Geophys. Res.*, 95, 5079-5088, 1990.

Marfunin, A.S., *Spectroscopy, Luminescence and Radiation Centers in Minerals*, p. 257-262, Springer Verlag, New York, 1979.

Miller, G. H., G. R. Rossman, and G. E. Harlow. The natural occurrence of hydroxide in olivine, *Phys. Chem. Minerals*, 14, 461-472, 1987.

Nakamura, A., and H. Schmalzried. On the nonstoichiometry and point defects of olivine, *Phys. Chem. Minerals*, 10, 27-37, 1983.

Nitsan, U. Stability field of olivine with respect to oxidation and reduction., *J. Geophys. Res.*, 79, 706-711, 1974.

Pasteris, J.D., and B.J. Wanamaker. Laser Raman microprobe analysis of experimentally re-equilibrated fluid inclusions in olivine: Some implications for mantle fluids, *Amer. Mineral.*, 73, 1074-1088, 1988.

Roedder, E. Fluid Inclusions, in: *Reviews in Mineralogy*, Mineral. Soc. Amer., Washington., 12, 503, 1984.

Schock, R.N., A.G. Duba, H.C. Heard, and H.D. Stromberg, *High Pressure Research: Applications in Geophysics*. Ed. M. Manghnani and S. Akimoto. Academic Press, New York, 1977.

Schock, R. N. , A. G. Duba, and T. J. Shankland. Electrical conduction in olivine, *J. Geophys. Res.*, 94, 5829-5839, 1989.

Sempolinski, D.R., and W.D. Kingery. Ionic conductivity and magnesium vacancy mobility in magnesium oxide, *J. Amer. Ceram. Soc.*, 63, 664-669, 1980.

Shankland, T.J., *Evolution of the earth*. Ed. R.J. O'Connell and W.S. Fyfe. American Geophysical Union Geodynamics Series, Vol. 5 ,p. 256-263, Amer. Geophys. Union, Washington, D.C., 1981.

Shelby, J.E. Reaction of hydrogen with hydroxyl-free vitreous silica, *J. Appl. Phys.*, 51, 2589-2593, 1980.

Sockel, H. G., *Defect Structure and electrical conductivity of crystalline ferrous silicate,* in: *Defects and Transport in Oxides*. Ed. M. S. Seltzer and R. I. Jaffe, p. 341-354, Plenum Press, New York, 1974.

VI List of Publications Describing Further Work Performed

1. LeRoy, R.C., *et al., Electrical conductivity measurements under minimum perturbation conditions. Part III: Peroxy in olivine.* J. Geophys. Res., 1991. in print.

2. Freund, F., *Electrical conductivity measurements under minimum perturbation conditions. Part II: O^- charge carriers in magnesium oxide.* J. Geophys. Res., 1991. in print.

3. Freund, F., M.M. Freund, and F. Batllo, *Electrical conductivity measurements under minimum perturbation conditions. Part I: Charge Distribution Analysis of magnesium oxide single crystals.* J. Geophys. Res., 1991. in print.

4. Batllo, F., *et al., Dissociation of O_2^{2-} defects into paramagnetic O^- in wide band gap insulators: A magnetic susceptibility study of magnesium oxide.* J. Appl. Phys., 1990. **67**: p. 588-596.

5. Batllo, F., *et al., Positive hole centers in magnesium oxide — correlation between magnetic susceptibility, dielectric anomalies and electric conductivity.* J. Appl. Phys., 1991. **69**: p. in print.

6. Freund, M.M., F. Freund, and F. Batllo, *Highly mobile oxygen holes in magnesium oxide.* Phys. Rev. Lett., 1989. **63**: p. 2096-2099.

7. Freund, F., F. Batllo, and M.M. Freund, *Dissociation and recombination of positive holes in minerals.*, in *Spectroscopic Characterization of Minerals and Their Surfaces,* L.C. Coyne, S.W.S. McKeever, andD.F. Blake, Editor. 1989, Amer. Chem. Soc.: Washinton, D.C. p. 310-329.

8. Freund, F., *et al., O- identified at high temperatures in CaO-based catalysts for oxidative methane dimerization.* J. Chim. Phys., 1990. **87**: p. 1467-1477.

9. Freund, F. and M.M. Masuda, *Highly mobile oxygen hole-type charge carriers in fused silica.* J. Mater. Res., 1991. **8**: p. 1619-1622.